

Diurnal Variation of the Tropospheric Energy Budget

By
Gary S. Foltz

Department of Atmospheric Science
Colorado State University
Fort Collins, Colorado

Supported by: NSF Grant OCD 75-01424
Principal investigator: William Gray
November 1976

Colorado
State
University

Department of
Atmospheric Science

Paper No. 262

DIURNAL VARIATION OF THE
TROPOSPHERIC ENERGY BALANCE

by

Gary S. Foltz

Department of Atmospheric Science

Colorado State University

Fort Collins, Colorado

November, 1976

Atmospheric Science Paper No. 262

TABLE OF CONTENTS

	Page
ABSTRACT	iii
1. INTRODUCTION	1
1.1 Basis for Present Study.	1
1.2 Approach	2
2. OBSERVED DIURNAL TEMPERATURE VARIATION FROM THE CONVENTIONAL RADIOSONDE NETWORK	8
2.1 Previous Research on Diurnal Temperature Variations.	8
2.2 Description of 12-hour Data Set.	12
2.3 Determination of Mean Temperature Difference	18
2.4 Layer of Consideration	21
2.5 Plotting and Analysis of the Temperature Difference Data	23
3. EXPECTED TROPOSPHERIC ENERGY GAIN/LOSS FROM RADIATION . .	39
3.1 Cloud-Free Radiational Model Results for Short Wave Radiation (SW).	39
3.2 Cloud-Free Radiational Model Results for Long Wave Radiation (LW).	42
3.3 Summary	45
4. DIURNAL VARIATION OF TROPOSPHERIC REQUIRED WARMING. . . .	48
4.1 Computational Procedures	48
4.2 Results	60
5. DAILY REQUIRED WARMING IN THE TROPICS AS DETERMINED FROM SPECIAL TROPICAL EXPERIMENTS	61
5.1 GATE Experiment.	61
5.2 Atlantic Trade-Wind Experiment (ATEX)	67
5.3 Line Islands Experiment.	74
5.4 Operations Redwing and Hardtack.	74
5.5 The Barbados Oceanographic and Meteorological Experiment (BOMEX)	76
5.6 Summary	77
6. SUMMARY	82
6.1 Results and Conclusions.	82

TABLE OF CONTENTS

	Page
7. SUGGESTED PHYSICAL MECHANISM FOR DIURNAL CYCLE OF REQUIRED WARMING - By William M. Gray.	91
ACKNOWLEDGEMENTS	101
BIBLIOGRAPHY	102
APPENDIX A	106
APPENDIX B	110
APPENDIX C	115
APPENDIX D	125
APPENDIX BIBLIOGRAPHY.	141

ABSTRACT

The tropospheric energy balance is examined in an effort to ascertain the diurnal variation of its components. The mean local diurnal temperature change in the 850-300 mb layer was observationally determined utilizing upper air data collected at 142 Northern Hemisphere radiosonde stations. Temperature data from GATE, ATEX, BOMEX, LIE Experiments, and Operations Redwing and Hardtack in the Tropical West Pacific were also analyzed. Diurnal radiative cooling values are computed for specific geographical regions and the magnitude of the required diurnal warming for each region is determined. Required warming is composed of a variety of atmospheric processes such as cloud induced temperature change, surface to air sensible heat transfer, horizontal advection, and vertical motion, etc.

A large morning maximum and late afternoon-early evening minimum of tropospheric required warming is found for all data sets, at all latitudes, in all seasons, and for both oceanic and land areas. These morning vs. late afternoon required warming differences are of magnitudes of 2-3 to one. It is hypothesized that the subsidence warming contribution to the diurnal variation of required warming dominates the other components. Increased morning subsidence and weaker afternoon-early evening subsidence is apparently a generally operating phenomenon in the troposphere.

1. INTRODUCTION

1.1 Basis for Present Study

This study was undertaken as a result of recent papers documenting a large diurnal cycle in oceanic heavy convective rainfall (Ruprecht and Gray, 1974; Jacobson and Gray, 1976). Ruprecht and Gray reported a pronounced morning maximum (07-12 Local Time) and evening minimum (19-24 Local Time) in heavy convective rainfall from tropical cloud clusters in the Western Pacific. The maximum was about twice as large as the minimum. Composited rawinsonde data of tropospheric divergence from these cloud clusters support the 2 to 1 difference in heavy rainfall. Jacobson later performed a more detailed statistical analysis of hourly rainfall records at a number of islands and atolls in the Western Pacific and further verified that the morning maximum and early evening minimum of heavy convective rainfall described in the earlier study was quite pronounced. The morning rainfall maximum was found at nearly all stations in all seasons examined. The weaker intensity precipitation showed much less of a diurnal cycle. This morning maximum of deep cumulus convection has also been found at many tropical land stations and during the winter season at many middle latitude land locations when direct surface heating from solar energy absorption is not dominant. The hypothesized mechanism for this diurnal cycle (Gray, 1976) is day vs. night differences in cloud versus clear region net radiational cooling. This paper attempts to investigate further the character of the above tropospheric diurnal cycle by studying the nature of the tropospheric diurnal radiational cooling cycle.

It has been well documented by several authors (Dopplick, 1970; Rogers, 1967; London, 1957) that the troposphere is continually cooling

at a rate of about 1-1.5°C/day. This radiational loss must be balanced by a compensating warming mechanism. It has been generally accepted (London, 1952; Sellers, 1965; and others) that this heat loss is balanced in a global sense primarily by latent heat of condensation (70-80%) and by surface to air sensible heat transfer through conduction (20-30%). Over the oceans however, the ratio of condensation to sensible heat gain is generally on the order of 10 or 20 to one.

How regular is the required warming process which must necessarily balance the net radiational cooling? Does it proceed at the same rate through the course of an entire day or does it vary in-phase or out-of-phase with the net radiational cooling? An examination of a 3-year Northern Hemispheric data set and special tropical project upper air data will be presented in order to ascertain the character of the diurnal variation, if any, in the atmospheric warming response to the troposphere's net radiational cooling.

1.2 Approach

The following estimate (Sellers, 1965) indicates the typically assumed magnitude of the daily energy sources and sinks occurring in the global troposphere:

$$\begin{aligned} \text{Net Radiation Cooling} &= \text{Rainfall Heating} + \text{Sensible Heat Gain} \\ \iint_{P A} R \cdot \frac{\partial A}{g} \frac{\partial P}{g} &= \iint_{P A} L (RF) \frac{\partial A}{g} \frac{\partial P}{g} + \iint_{P A} S.H. \frac{\partial A}{g} \frac{\partial P}{g} \quad (1.1) \end{aligned}$$

$$\sim -1.2^{\circ}\text{C/day} \quad = \quad \sim .9^{\circ}\text{C/day} \quad + \quad \sim .3^{\circ}\text{C/day}$$

where

P = the range of pressure found in the troposphere (~ 800 mb)

A = surface area of the globe

R = net radiative cooling

RF = rainfall

L = latent heat of condensation

S.H.= sensible heat

The troposphere's energy loss from radiation cooling must be compensated for by an equivalent amount of condensation and heating or sensible temperature flux.

For many years meteorologists have attempted to understand the nature of the global mean heat budget. London (1952) performed extensive calculations utilizing mean temperature and humidity profiles and mean cloudiness distributions for the Northern Hemisphere in 10° latitudinal belts in an effort to determine the net radiational cooling profile of the atmosphere. His findings were essentially the same as represented in equation (1.1). Several other scientists (London, 1957; Davis, 1963; Dopplick, 1970; others) have also studied this problem and further refined London's calculations. However, the time resolution of the balancing process between net radiative cooling and condensation and sensible heat transfer has only been extensively examined for a time scale of several days, months, seasons or years. It appears that only Hastenrath and Steinberg (1971) have attempted a thorough investigation of the diurnal variability of the tropospheric heat budget from 3-hour resolution radiosonde data obtained in the West Pacific.

In order to determine the diurnal variation of the various components in the tropospheric energy balance the following approach has been taken. From the time derivative of the first law of thermodynamics and the Eulerian expansion of $\frac{dT}{dt}$, the local temperature change for a single pressure level can be represented as

$$\frac{\partial T}{\partial t} = \frac{1}{C_p} \frac{dQ}{dt} - \vec{V} \cdot \nabla_h T + \omega (\Gamma_d - \Gamma) \quad (1.2)$$

where

T - Temperature

t - Time

Q - Diabatic heat sources and sinks

\vec{V} - Horizontal wind velocity

ω - Vertical velocity

Γ_d - Dry adiabatic lapse rate $(\partial T / \partial p)_d$

Γ - Environmental lapse rate $(\partial T / \partial p)$

C_p - Specific heat at constant pressure for dry air

To define the energy balance for a tropospheric layer between P_1 and P_2 , equation 1.2 must be integrated through these levels:

$$\int_{P_1}^{P_2} \frac{\partial T}{\partial t} dp = \frac{1}{C_p} \int_{P_1}^{P_2} \frac{dQ}{dt} dp - \int_{P_1}^{P_2} (\vec{V} \cdot \nabla_h T) dp + \int_{P_1}^{P_2} \omega (\Gamma_d - \Gamma) dp \quad (1.3)$$

For the purposes of this study the mean values for the layer P_1 to P_2 will be utilized so that Eq. (1.3) in the finite difference form for a specific time interval becomes

$$\overline{\Delta T}_{\text{observed}} = \overline{\Delta Q} - \overline{\text{ADV}} + \overline{\text{VM}} \quad (1.4)$$

where

- $\overline{\Delta T}$ - Observed change in mean local temperature between levels P_1 and P_2
- $\overline{\Delta Q}$ - Diabatic heat source (sink) for layer
- $\overline{\text{ADV}}$ - Temperature change due to horizontal advection for layer
- $\overline{\text{VM}}$ - Vertical motion induced sensible temperature change for layer

A close examination of the diabatic heat source or sink term reveals that

$$\overline{\Delta Q} = \overline{\text{LH}} + \overline{\text{SH}} + \overline{\text{SW}} + \overline{\text{LW}} \quad (1.5)$$

where

- $\overline{\text{LH}}$ - Warming (cooling) due to latent heat energy
- $\overline{\text{SH}}$ - Warming (cooling) due to turbulent transfer of sensible heat into the layer
- $\overline{\text{SW}}$ - Warming due to atmospheric absorption of short wave radiation
- $\overline{\text{LW}}$ - Cooling due to atmospheric irradiation of long wave radiation

Equation (1.4) can now be expanded to show the various constituents of the tropospheric energy balance equation.

$$\overline{\Delta T} = \overline{\text{LW}} + \overline{\text{SW}} + \overline{\text{SH}} + \overline{\text{ADV}} + \overline{\text{LH}} + \overline{\text{VM}} \quad (1.6)$$

This equation can be expressed as

$$\overline{\Delta T} = \overline{SW} + \overline{LW} + \overline{RW} \quad (1.7)$$

where

$$\overline{RW} = \overline{SH} + \overline{LH} + \overline{ADV} + \overline{VM} \quad (1.8)$$

\overline{RW} is the sum of all the required non-radiation warming necessary to balance Eq. (1.7) over any specified time period. It should be noted that all four components of the required warming term are dependent on atmospheric motion. $\overline{\Delta T}$ can be determined from standard radiosonde data, and \overline{SW} and \overline{LW} can be calculated from radiation models or determined from observational data (Cox and Hastenrath, 1971; Cox, Vonder Haar, Hanson, and Suomi, 1974; others). Therefore \overline{RW} can be solved for as a residual quantity.

The procedure which will be followed in determining the diurnal variation of the troposphere's energy balance is as follows:

1. From an extensive radiosonde data set determine the average hourly variation of the mean temperature, $\overline{\Delta T}$ in the middle tropospheric layer (generally 850-300 mb except over elevated regions where the 700-300 mb layer is examined).
2. Utilizing mean seasonal soundings computed from the same data set determine hourly variations of total solar heating, \overline{SW} , and infrared cooling, \overline{LW} , through the day. These values are obtained from radiation models and observational radiation data.
3. Ascertain the diurnal variation of required tropospheric warming, \overline{RW} , necessary to balance the observed diurnal variations in temperature and radiative cooling.
4. Discuss the relative contribution of the components of \overline{RW} from Eq. (1.8) in an effort to determine the physical process(es) responsible for the diurnal variation in required warming.

Newly obtained data from the GATE project for the summer of 1974 and data from other special tropical experiments is examined. It is the

intent of this study to establish the diurnal cycle, if any, in the tropospheric energy balance.

2. OBSERVED DIURNAL TEMPERATURE VARIATION FROM THE CONVENTIONAL RADIOSONDE NETWORK

2.1 Previous Research on Diurnal Temperature Variations

Early studies of the diurnal variations of temperature and other atmospheric parameters (Ballard, 1933; Hergesell, 1922) in the free atmosphere were confined to the lower two or three km due to the types of instrumentation available at that time. More recently, most studies of the diurnal temperature variation in the free atmosphere have dealt with the layers above the tropopause. In the stratosphere, the atmosphere responds directly to the solar radiational cycle and diurnal temperature changes are relatively large. Day to night temperatures can vary by as much as 4°C in the middle and upper stratosphere. The situation in the troposphere is much more complex. Here the diurnal variations are much smaller in magnitude and more difficult to directly measure. There have been some previous studies on the diurnal variability of lower stratospheric and tropospheric temperature which bear on this subject. Most studies of the lower stratosphere have attempted to determine the diurnal variation of temperature from operational radiosonde data (Kay, 1951; Finger, Mason, and Teweles, 1964; Sparrow, 1967; Finger and McInturff, 1968). These studies have been hampered by instrument error due to solar radiation absorption by the temperature sensor. Kay (1951) and Sparrow (1967) were unable to completely separate the real variations from the instrument errors in their data and simply stated that some degree of inherent error is included in their results. Finger et al. (1964) and Finger et al. (1968) made attempts to eliminate the error due to solar radiation (see Appendix C for a discussion of their method). Teweles and Finger (1960) have also specifically studied solar radiationally

induced instrument error in various types of radiosondes. They attempted to develop an error correction scheme for data collected in the stratosphere during the daylight hours. While the results of these papers, in regard to the stratospheric diurnal variation of temperature, are not directly applicable to this study, the methods used to eliminate the solar absorption instrument error and to analyze the observations are very relevant.

The early studies utilizing radiosonde data (Wulf, Hodge, and Obloy, 1946; Riehl, 1947) were concerned with determining the diurnal variation of temperature and pressure in the troposphere. However, in later years, the main purpose of tropospheric studies (Harris, 1959; Harris, Finger and Teweles, 1962; Carlson and Hastenrath, 1970; Wallace and Patton, 1970; Hastenrath, 1972) has been to use diurnal temperature, pressure, and wind measurements to increase the understanding of diurnal and semi-diurnal tidal oscillations. Although the purpose here is not the study of atmospheric tides, the data collected for those studies is very pertinent to this effort. Table 2.1 lists the previous studies of the diurnal variations of temperature in the troposphere utilizing various local time intervals. The magnitudes of the diurnal variations and times of maximum temperature for four of the studies are shown in Fig. 2.1.

It should be noted that prior to 1960 the operational radiosonde employed a duct-type temperature sensing element which was quite susceptible to solar radiation error in the upper troposphere and stratosphere. However, in mid-1960, a new sonde (series X) was introduced which had an externally mounted thermistor. This considerably reduced the solar radiation induced error. In addition, the military sonde AN/AMT-4A, with outrigger-type construction, has been utilized at all military radiosonde stations since 1956. It was also used during the nuclear testing projects

TABLE 2.1

Studies Concerning Diurnal Variations of Temperature in the Troposphere

Source	Data Source (s)	Time Resolution of Measurements	Location (s)	Diurnal Range of Mean 850-300 mb Temperature	Time of T _{max}	Time of T _{min}
Wulf, Hodge Obloy(1946)	U.S. Weather Bureau Operational Soundings 1 Jan. 1942-1 July 1942	Observations taken at approximately 1100 and 2300 local time	Stations located near the 75th meridian in the U.S.	Temperature Difference of approximately 1.0°C	Always warmer at 1100 than 2300	
Riehl (1947)	Radiosonde data 1 Oct.-30 Nov. 1944	Observations taken every 3 hours	San Juan, P.R. Antigua	1.78°C (includes Large Amount of Instrument Error)	1400LT	2300LT
Harris (1959)	Standard Military Radiosonde Observations, June, July, Aug. 1956 and 1957	Combined two series of 6-hourly observations made 3 hours out of phase and obtained 3-hour resolution	Washington D.C.	0.5°C	1300LT	0100LT
Harris Finger & Teweles (1962)	Standard Military Radiosonde Observations 1 Apr. 1956-31 Mar. 1958	Performed same procedure as Harris (1959) and obtained 3-hour resolution	Terceira, Azores (38°N, 27°W)	0.4°C (summer)	1500LT	0300LT
Carlson and Hastenrath (1970)	Upper Air Data Collected During Nuclear Testing Project During Apr.-July 1956 & Apr. July 1958	Performed same procedure as Harris (1958) and obtained 3-hour resolution	Eniwetok atoll (11°N, 162°E)	0.5°C	1500LT	0300LT

TABLE 2.1 (cont'd)

Source	Data Source (s)	Time Resolution of Measurements	Locations (s)	Diurnal Range of Mean 850-300 mb Temperature	Time of T_{max}	Time of T_{min}
Wallace and Patton (1970)	Standard Radiosonde Observations July-Aug. 1957 to 1964	12-hour observations: 02 to 07 LT vs. 14 to 19 LT	105 N. American Radiosonde Stations	0.7°C (12-hour Temperature difference)	1600 (00GMT)	0400 (12GMT)
Hastenrath (1972)	Upper-Air data collected during nuclear testing project. Apr-July 1956 and Apr-July 1958	Performed same procedure as Harris (1959) to obtain 3-hour resolution	8 Western Pacific Radiosonde stations	0.6°C	1500LT	0300LT

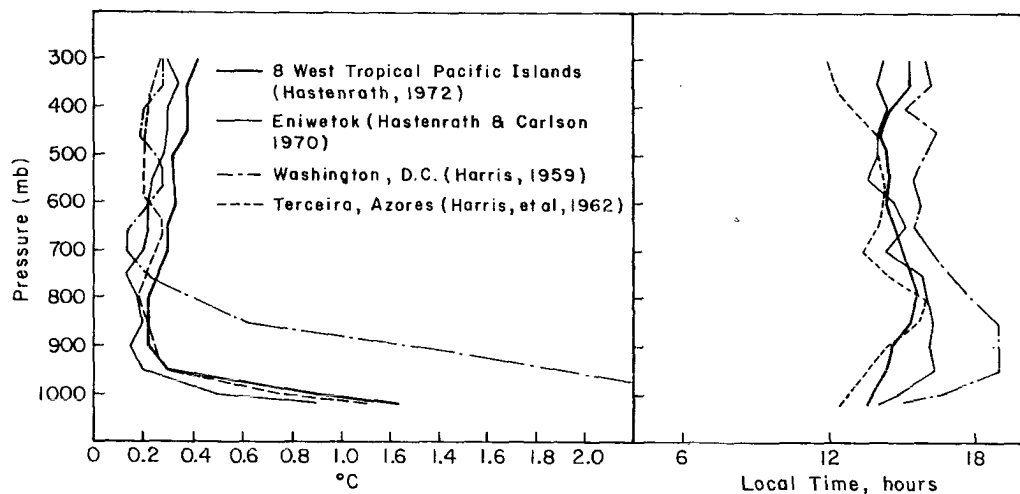


Fig. 2.1. Diurnal variations of temperature at Eniwetok, after Carlson, *et al.* (1970), Washington, DC after Harris (1959), Terceira, Azores after Harris, *et al.* (1962), and 8 West Pacific stations after Hastenrath (1972). Amplitude of daily variation in $^{\circ}\text{C}$ (left figure) and time of maximum temperature in hours (right figure).

in 1956 and 1958. This instrument was also a great improvement over the previous military sondes as far as reducing the radiational error.

Without exception, the results of all studies using data collected by radiosondes employing an externally mounted thermistor are consistent with the findings of this paper.

2.2 Description of 12-hour Data Set

Previous studies of the diurnal variability of various atmospheric parameters have typically relied on data collected during short term scientific experiments (ATEX, BOMEX, Line Islands Experiment, GATE, Marshall Islands Nuclear Project, etc.) or on information obtained by combining two series of 6 or 12 hour interval sounding data sets. Radiosonde measurements taken on different schedules before and after the change from 0300 and 1500GMT (also sometimes 0900 and 2100GMT) to 0000 and 1200GMT (also sometimes 0600 and 1800GMT) standard radiosonde observation time on 1 June 1957 have often been used. This procedure gives a 3 or 6 hour time resolution. Obviously, this type of data is the most desirable for discerning diurnal variations. Its availability is limited, however.

Since most radiosonde observations are made only at 00GMT and 12GMT, a procedure had to be established for utilizing this vast 12 hour interval data source. The data sample for this part of the study was collected at 142 upper air stations located in an area extending westward from 20°W longitude to 120°E longitude and from the equator northward to 85°N latitude (Fig. 2.2). As this data set was limited in its time resolution (12 hours), stations located within a 10° latitudinal band, e.g. $30\text{--}40^{\circ}\text{N}$, were examined in relation to the local time of their radiosonde ascents.

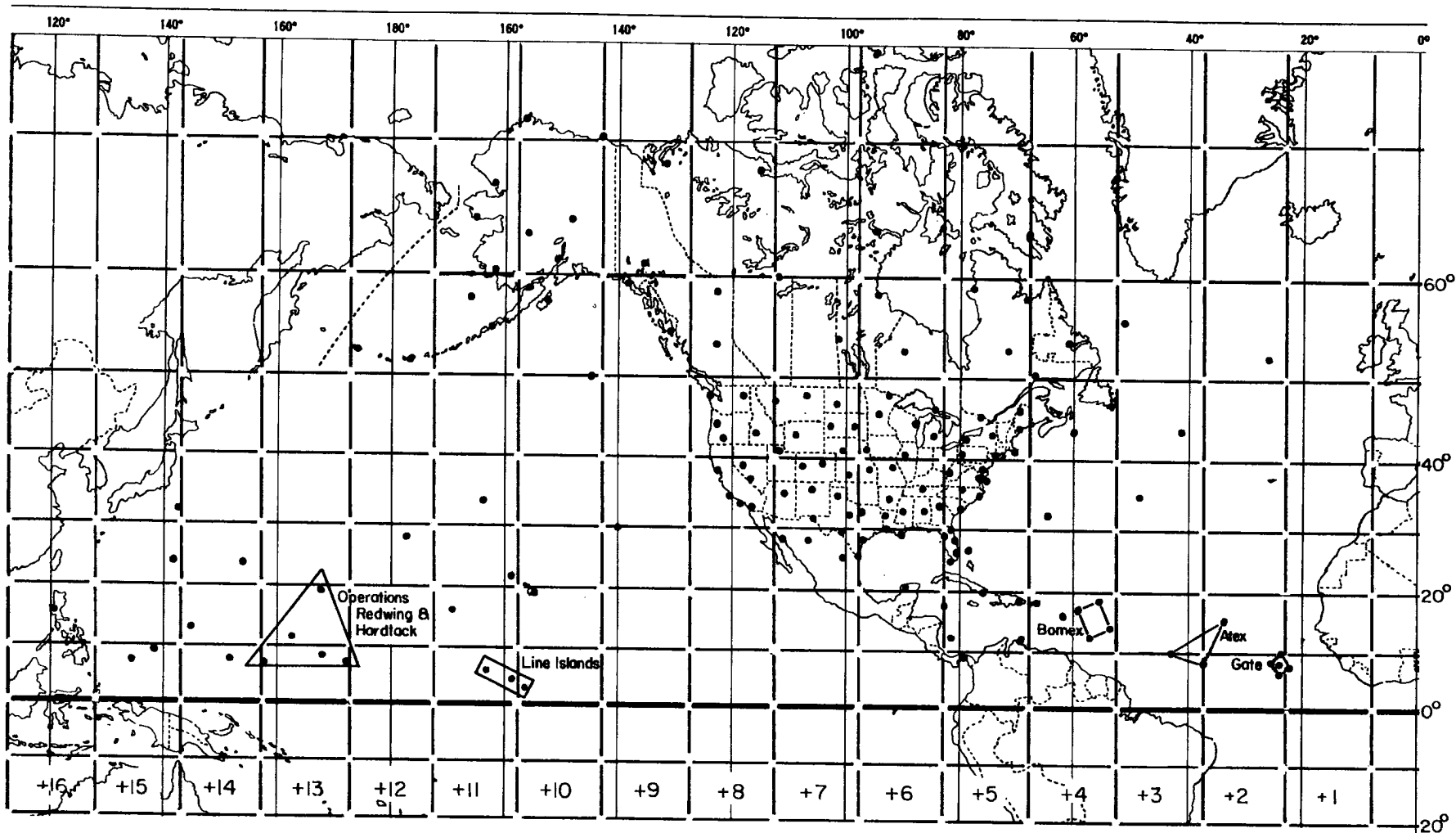


Fig. 2.2. Location of radiosonde data network and special oceanic tropical experiments. Numbers located at the bottom of map identify geographical blocks referred to in this study.

Therefore, data from different longitudes correspond to different local times. When data from several longitudinal regions are composited, increased time resolution is obtained. For example, consider four hypothetical stations located at 60°W , 90°W , 120°W , and 150°W in the $30\text{--}40^{\circ}\text{N}$ latitude belt. Mean temperatures for the 850-300 mb layer can be calculated at 00GMT and 12GMT at each station yielding mean layer temperatures at 08 and 20 LT (60°W), 06 and 18LT (90°W), 04 and 16LT (120°W), and 02 and 14LT (150°W). Thus the diurnal variability of the mean temperature in the 850-300 mb layer in a 10° latitudinal band can be determined from data collected at stations located within the band. Table 2.2 lists all stations used in this study by 10° latitudinal bands.

The 00GMT to 12GMT mean temperature difference in the 850-300 mb layer (700-300 mb over elevated locations) was determined for each station in this data set. The data used covered a 3 year period from June 1966 until January 1969. During that period virtually all the stations employed the ESSA Weather Bureau sonde (USWB-403-X or USWB-1680-X) with an outrigger type construction for the thermistor element, thus increasing the accuracy of the reported temperature considerably over the old duct-type instrument (see Appendix A for a description of the radiosonde and the pertinent instrumentation).

The data have been stratified into 2 seasons containing 2 months each. The summer season includes June and July and the winter is comprised of December and January. This particular seasonal distribution was selected as it affords the most contrast in the degree of solar energy absorption by the troposphere over middle latitude locations. In equatorial regions the solar heating effect will be similar in both seasons.

TABLE 2.2

Stations Included in the Northern Hemispheric Network

	<u>Station</u>	<u>WMO#</u>	<u>Latitude</u>	<u>Longitude</u>	<u>Elevation (meters)</u>
0-10°N	Canal Zone	78806	9.0	79.6	9
	Ponape	91348	7.0	158.2E	46
	Kwajalein	91366	8.7	167.7E	8
	Majuro	91376	7.0	171.4E	3
	Truk	91334	7.5	151.9E	2
	Koror	91408	7.3	134.5E	33
	Yap	91413	9.5	138.1E	17
10°-20°N	Raizet	78897	16.3	61.6	8
	San Juan	78526	18.4	66.0	19
	Guantanamo	78367	19.9	75.2	23
	Santa Domingo	78486	18.5	69.9	14
	Curacao	78988	12.2	69.0	17
	San Andres	80001	12.6	81.7	6
	Swan Is.	78501	17.4	83.9	11
	Hilo, Ha.	91285	19.7	155.1	11
	Johnston, Is.	91275	16.7	169.5W	5
	Wake Is.	91245	19.3	166.7E	4
	Eniwetok	91250	11.4	162.4E	6
	Guam	91217	13.6	144.8E	111
	Clark AFB	98327	15.2	120.6E	11
20°-30°N	Key West	72201	24.5	81.8	6
	Miami	72202	25.8	80.3	4
	Cape Kennedy	74794	28.2	80.6	0
	Grand Bahama	78063	26.6	78.3	7
	Tampa	72211	28.0	82.5	3
	Boothville	72232	29.0	89.4	0
	Brownsville	72250	25.9	97.4	6
	Victoria	72255	28.7	97.1	36
	Merida	76644	21.0	89.7	11
	Del Rio	72261	29.4	100.8	313
	Monterrey	76394	25.9	100.2	423
	Guaymas	76225	28.6	106.1	1428
	Chihuahua	76255	27.9	110.9	4
	Ship N	24N	30.0	140.0	0
	Lihue, Ha.	91165	22.0	159.3	45
	Midway Is.	91066	28.2	177.4	13
	Marcus	91131	24.3	154.0E	4
	Iowa Jima	91115	24.8	141.3E	5
	30°-40°N	Ship E	05E	35.0	48.0
Bermuda		78016	32.4	64.7	6
Jacksonville		72206	30.5	81.6	9
Charleston		72208	32.9	80.0	15
Cape Hatteras		72304	35.3	75.5	3
Norfolk		72308	36.9	76.2	9

TABLE 2.2 (cont'd)

	<u>Station</u>	<u>WMO#</u>	<u>Latitude</u>	<u>Longitude</u>	<u>Elevation (meters)</u>
30°-40°N	Greensboro	72317	36.1	79.9	270
	Wallops Is.	72402	35.8	75.5	15
	Washington, D.C.	72403	38.9	77.0	98
	Montgomery	72226	32.3	86.4	62
	Jackson	72235	32.3	90.2	101
	Lake Charles	72240	30.2	93.2	10
	Shreveport	72248	32.5	93.8	79
	Ft. Worth	72259	32.8	97.0	176
	Athens	72311	34.0	83.3	247
	Nashville	72327	36.1	86.7	184
	Little Rock	72340	34.7	92.2	81
	Huntington	72425	38.4	82.6	255
	Columbia	72445	39.0	92.4	274
	Topeka	72456	39.1	95.6	270
	Abilene	72266	32.4	99.7	546
	El Paso	72270	31.8	106.4	1194
	Tucson	72274	32.1	110.9	779
	Amarillo	72363	35.2	101.7	1099
	Albuquerque	72365	35.1	106.6	1620
	Winslow	72374	35.0	110.7	1488
	Dodge City	72451	37.8	100.0	790
	Denver	72469	39.8	104.9	1625
	Grand Junction	72476	39.1	108.5	1475
	San Diego	72290	32.8	117.2	9
	San Nicolas Is.	72291	33.3	119.5	174
	Yucca Flat	72385	37.0	116.0	1197
	Vandenberg	72393	34.8	120.6	121
	Ely	72486	39.3	117.8	1909
	Oakland	72493	37.8	122.2	3
	Ship V	25V	34.0	164.0E	0
Chichijima	91030	32.2	142.2E	12	
40°-50°N	Ship D	04D	44.0	41.0	0
	Sable Is.	72600	43.9	60.0	0
	Placentia	72807	47.3	54.0	0
	New York	74486	40.7	73.8	4
	Nantucket	72506	41.3	70.1	4
	Albany	72518	42.8	73.8	89
	Pittsburgh	72520	40.5	80.2	373
	Buffalo	72528	42.9	78.7	215
	Portland	72606	43.7	70.3	19
	Caribou	72712	46.9	68.0	146
	Maniwaki	72722	46.4	76.0	170
	Flint	72637	43.0	83.7	233
	Peoria	72532	40.7	89.7	202
	Omaha	72553	41.4	96.0	406
	Green Bay	72645	44.5	88.1	214
	St. Cloud	72655	45.6	94.2	312
S.S. Marie	72734	46.5	84.4	221	

TABLE 2.2 (cont'd)

	<u>Station</u>	<u>WMO#</u>	<u>Latitude</u>	<u>Longitude</u>	<u>Elevation (meters)</u>
40-50°N	Int'l Falls	72747	48.6	93.4	361
	North Platte	72562	41.1	100.7	849
	Salt Lake	72572	40.8	112.0	1287
	Lander	72576	42.8	108.8	1692
	Huron	72654	44.4	98.2	393
	Rapid City	72662	44.0	103.1	966
	Bismarck	72764	46.8	100.8	506
	Glasgow	72768	48.2	106.6	700
	Great Falls	72775	47.6	117.5	1115
	Winnemucca	72583	40.9	117.8	1312
	Medford	72597	42.4	122.9	405
	Boise	72681	43.6	116.2	871
	Salem	72694	44.9	123.0	61
	Spokane	72785	47.7	117.5	721
	Quillayute	72797	48.0	124.6	137
	Ship P	17P	46.0	145.0	0
50-60°N	Ship C	03C	52.8	35.5	0
	Ship B	02B	56.5	51.0	0
	Sept-Iles	72811	50.2	66.3	58
	Goose	72816	53.3	60.4	44
	Nitchequon	72826	53.2	70.9	537
	Moonsonee	72836	51.3	80.7	0
	Ft. Chimo	72906	58.1	68.4	36
	Inoucdjovac	72907	58.5	78.1	0
	Trout Lake	72848	53.8	89.9	219
	Churchill	72913	58.8	94.1	35
	The Pas	72867	54.0	101.1	272
	Prince George	72896	53.9	122.7	676
	Ft. Nelson	72945	58.8	122.6	375
	Yakutat	70361	59.5	131.7	9
	Annette Is.	70398	55.0	131.6	36
	King Salmon	70326	58.7	156.7	15
	Kodiak	30350	57.8	152.5	34
	St. Paul	70308	59.2	170.2	9
	Cold Bay	70316	55.2	162.7	31
Shemya	70414	52.7	174.1E	3	
Adak	70454	51.9	176.7	4	
60-70°N	Frobisher Bay	72909	63.8	68.8	21
	Coral Harbor	72915	64.2	83.4	59
	Baker Lake	72926	68.3	96.0	11
	Ft. Smith	72934	60.0	112.0	203
	Coopermine	72938	67.8	115.1	0
	Inuvik	72957	68.3	133.5	61
	Whitehorse	72964	60.7	135.1	698
	McGrath	70231	63.0	155.6	103

TABLE 2.2 (cont'd)

	<u>Station</u>	<u>WMO#</u>	<u>Latitude</u>	<u>Longitude</u>	<u>Elevation</u> (meters)
60-70°N	Fairbanks	70261	64.8	147.9	138
	Anchorage	70273	61.2	150.0	40
	Kotzebue	70133	66.9	162.6	5
	Nome	70200	64.5	165.4	7
	Kethel	70219	60.8	161.8	46
70-80°N	Eureka	72919	80.0	85.9	0
	Resolute	72924	74.7	95.0	64
	Pt. Barrow	70026	71.3	156.8	4
	Barter Is.	70086	70.1	143.6	15

2.3 Determination of Mean Temperature Difference

The radiosonde listing had been previously obtained on magnetic tape from the National Climatic Center in Asheville, N.C. Computations were performed on the Colorado State University CDC 6400 Computer. Two methods were used to measure the 00GMT minus 12GMT temperature differences. Both methods gave similar results.

1. The first method calculated the mean 00GMT minus 12GMT temperature and height differences from the following equation

$$\overline{\Delta X} = \frac{1}{n} \sum_{i=1}^n [X(00)]_i - \frac{1}{n} \sum_{i=1}^n [X(12)]_i$$

where $\overline{\Delta X}$ represents the average temperature ($\overline{\Delta T}$) or geopotential height ($\overline{\Delta H}$) difference for one season. $X(00)$ and $X(12)$ are the layer averaged values observed for a sounding at 00GMT and 12GMT, respectively, and n is the number of observations taken in any season for the 3 year data sample (typically 6 months or 180 individual soundings). Data from an individual station was utilized only if at least 75% of the total possible soundings for a season were recorded and the number of soundings at one observation time was no less than 80% of the number of soundings at the other time. These calculations were made for the 850-300 mb layer except over elevated regions when the 700-300 mb layer was used.

2. The second method was implemented only for the determination of ΔT . The computations were accomplished by applying the hypsometric relation to the seasonal mean sounding.

$$\bar{T}_v = \frac{g}{R} \frac{\Delta H}{\ln P_2/P_1}$$

where

\bar{T}_v - mean virtual temperature of the layer
 R - universal gas constant
 g - acceleration of gravity
 ΔH - thickness of the layer
 P_2 - upper bounding pressure level
 P_1 - lower bounding pressure level

$\Delta \bar{T}_v$ represents the difference in the mean virtual temperature calculated for the 850-300 mb layer (occasionally the 700-300 mb layer) at 00GMT and 12GMT. $\Delta \bar{T}_v$ is an extremely close approximation to $\Delta \bar{T}$ (determined by method 1). The variation of the observed mixing ratio has been found to be generally small in the layers under consideration.

Several studies (Ostapoff et al., 1970; Betts, 1972; Ruprecht, 1975; and others) have documented the spurious diurnal variations of specific humidity in the troposphere. In order to represent the mean temperature differences of the middle tropospheric layer by the mean virtual temperature difference, the diurnal variations of $\Delta \bar{T}_v$ must not be a result of the diurnal variation in specific humidity. By applying the virtual temperature correction relationship

$$T_v = T \left[\frac{1+1.609w}{1+w} \right]$$

where w = mixing ratio
 T = temperature
 T_v = virtual temperature

and assuming a 10% error in the daytime specific humidity observations, the daytime \bar{T}_v for 850-300 mb layer will be approximately 0.13°C less than the real \bar{T} for the layer. This value was computed for a station (Johnston Island) in the tropics where the daytime observation is taken near noon and therefore it is expected to include the maximum possible specific humidity error.

Table 2.3 compares the computed mean virtual temperature difference at all the upper-air stations between the equator and 20°N. This is where the largest moisture errors occur because of the high moisture content of the troposphere. The difference between $\overline{\Delta T_V}$ and $\overline{\Delta T}$ is quite small - generally less than .08°C in the 850-300 mb layer. The erroneous daytime moisture reduction error source acts in the opposite direction from the temperature error caused by solar radiation absorption. Therefore, the total error included in the mean temperature of the layer is reduced by using the mean virtual temperature difference of a deep tropospheric layer. Unless otherwise stated the mean temperature of the layer under consideration will henceforth be represented by the mean virtual temperature of the layer.

TABLE 2.3

Comparison of Observed 850-300 mb Mean 00GMT - 12GMT Temperature Difference (ΔT) with the Mean Virtual Temperature Difference (ΔT_V)

Stations	WMO#	Summer			Winter		
		$\overline{\Delta T_V}$	$\overline{\Delta T}$	$\overline{\Delta T_V - \Delta T}$	$\overline{\Delta T_V}$	$\overline{\Delta T}$	$\overline{\Delta T_V - \Delta T}$
<u>0-10°N</u>							
Canal Zone	78806	.33	.36	-.03	.28	.32	-.04
Ponape	91348	.40	.43	-.03	.36	.38	-.02
Kwajalein	91366	.23	.28	-.05	.41	.45	-.04
Majuro	91376	.47	.48	-.01	.50	.53	-.03
Truk	91334	.30	.38	-.08	.27	.27	.00
Koror	91408	.11	.18	-.07	.32	.35	-.03
Yap	91413	.16	.20	-.04	.36	.38	-.02
<u>10-20°N</u>							
Raizet	78897	-.01	-.09	.08	-.13	-.13	.00
San Juan	78526	.00	-.03	.03	-.10	-.11	.01
Guantanamo	78367	.25	.16	.09	.10	.06	.04
Santo Domingo	78486	-.09	-.07	-.02	-.26	-.28	.02

TABLE 2.3 (cont'd)

Stations	WMO#	Summer			Winter		
		$\overline{\Delta T_v}$	$\overline{\Delta T}$	$\overline{\Delta T_v - \Delta T}$	$\overline{\Delta T_v}$	$\overline{\Delta T}$	$\overline{\Delta T_v - \Delta T}$
10-20°N							
Curacao	78988	.10	.14	-.04	.15	.19	-.04
San Andres	80001	.32	.40	-.08	.28	.32	-.04
Swan Is.	78501	.26	.31	-.05	.13	.14	-.01
Hilo, Ha.	91285	.77	.78	-.01	.65	.63	.03
Johnston Is.	91275	.62	.67	-.05	.58	.62	-.04
Wake Is.	91245	.40	.42	-.02	.30	.32	-.02
Eniwetok	91250	---	---	---	.28	.42	.14
Guam	91217	.35	.39	-.04	.17	.17	.00
Clark AFB	98327	-.10	-.08	-.02	.00	.08	-.08

2.4 Layer of Consideration

The layer of the troposphere selected for examination is between 850 and 300 mb. This layer was chosen as it is relatively free from surface effects and contains a large portion of the layer of the atmosphere which is undergoing continuous radiational cooling. This region is below the tropopause boundary in all but the most northern latitudes in winter. Also, by choosing to study the layers below 300 mb the possible effects of solar radiationally induced instrument error are greatly reduced. The 850 mb level was selected as the lower boundary over oceanic and low altitude terrain because it is above the top of the planetary boundary layer and should be relatively free from surface induced heating sources. Observations obtained from upper air stations situated at elevated locations (above 500 m) were examined between the 700 mb level and 300 mb level so as to reduce the elevated heat source influence. Examples of mean 00GMT and 12GMT summer soundings (when solar influence is the largest) are displayed in Fig. 2.3. The surface

induced effects on the lapse rates are quite evident at lower levels and over elevated land regions.

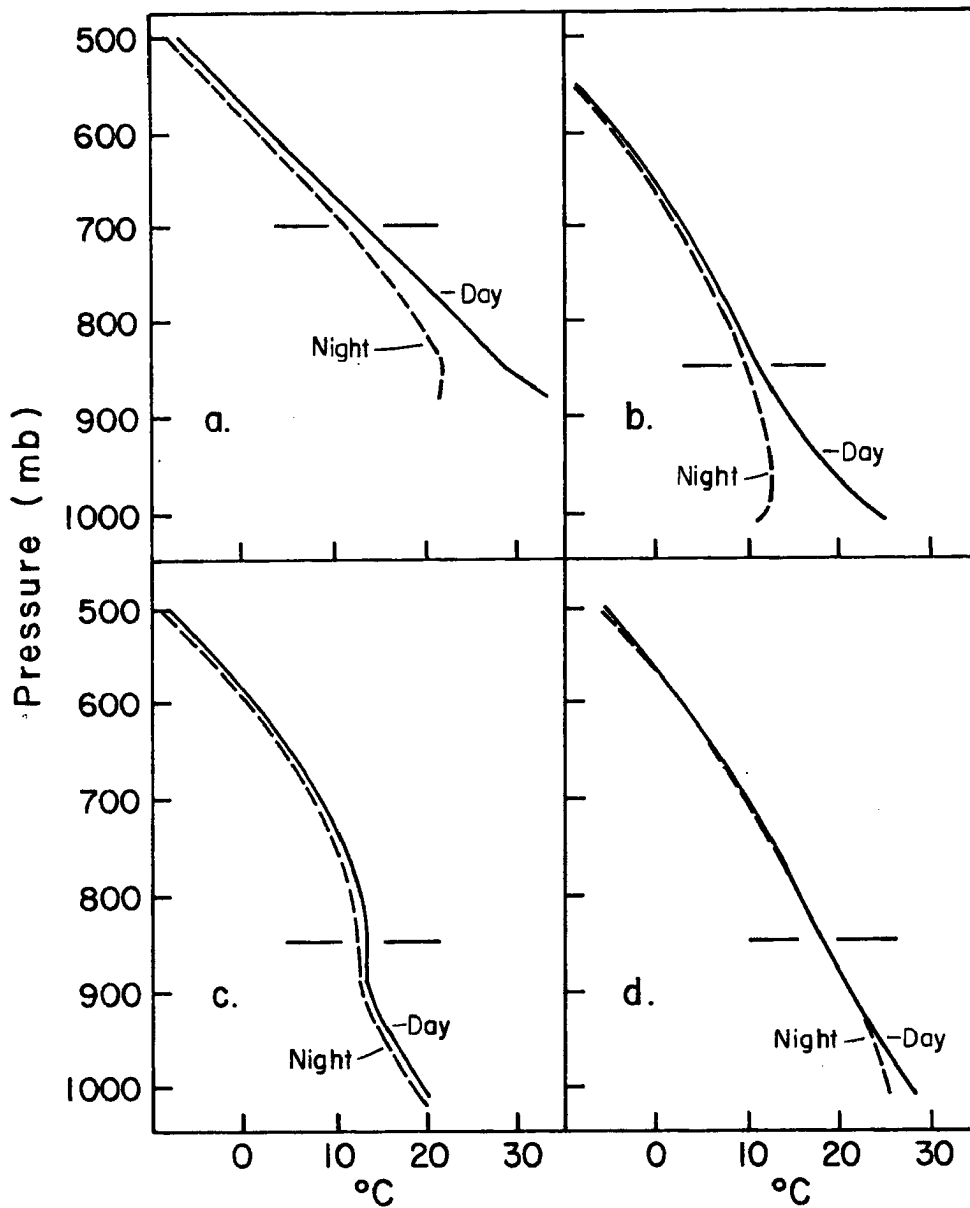


Fig. 2.3 a-d. Daytime (00Z) and nighttime (12Z) mean summer soundings at (a) mid-latitude elevated location - El Paso, Texas, (b) mid-latitude low altitude location - Salem, Oregon, (c) subtropical oceanic ship location - Ship N, (d) tropical island location - Truk.

2.5 Plotting and Analysis of the Temperature Difference Data

Other studies (Pressman, 1955; Finger and McInturff, 1968; others) have shown a latitudinal dependency of the 12-hour temperature difference. Since this data set was fairly extensive in terms of latitude, the data was divided into latitudinal bands. The 12-hour temperature difference $[\overline{T(00)} - \overline{T(12)}]$ is plotted relative to local time and longitude of the upper-air station taking the observation. Figures 2.4a to 2.4f depict the temperature differences in the summer season in 10° latitudinal belts from the equator to 60°N . Figures 2.5a to 2.5f are similar examples of the temperature differences in each latitudinal belt during the winter. Table 2.4 lists the values of the 12-hour temperature difference for each season at each station.

Area Averaging. In order to gain an understanding of the march of diurnal temperature and compare the observed 12-hour temperature differences with the calculated short wave and long wave radiation heating values, a method was devised to combine all stations within a certain geographical area into a single block average. Figure 2.2 shows these blocks and Table 2.5 contains the values of mean $\overline{\Delta T}$ for each geographical block. Each block is 10° latitude by 15° longitude centered longitudinally on the meridian representing an even hour from Greenwich Mean Time. The block is identified by the number of hours which must be added to the local time to obtain GMT. With this system the block average contains only observations taken within a half hour of the time delineating the block. The block averages are plotted in Figs. 2.4 and 2.5 along with the station values of $\overline{\Delta T}$. If there are stations located below 500 m and others above 500 m in one geographical block, 2 different averages for the block are calculated.

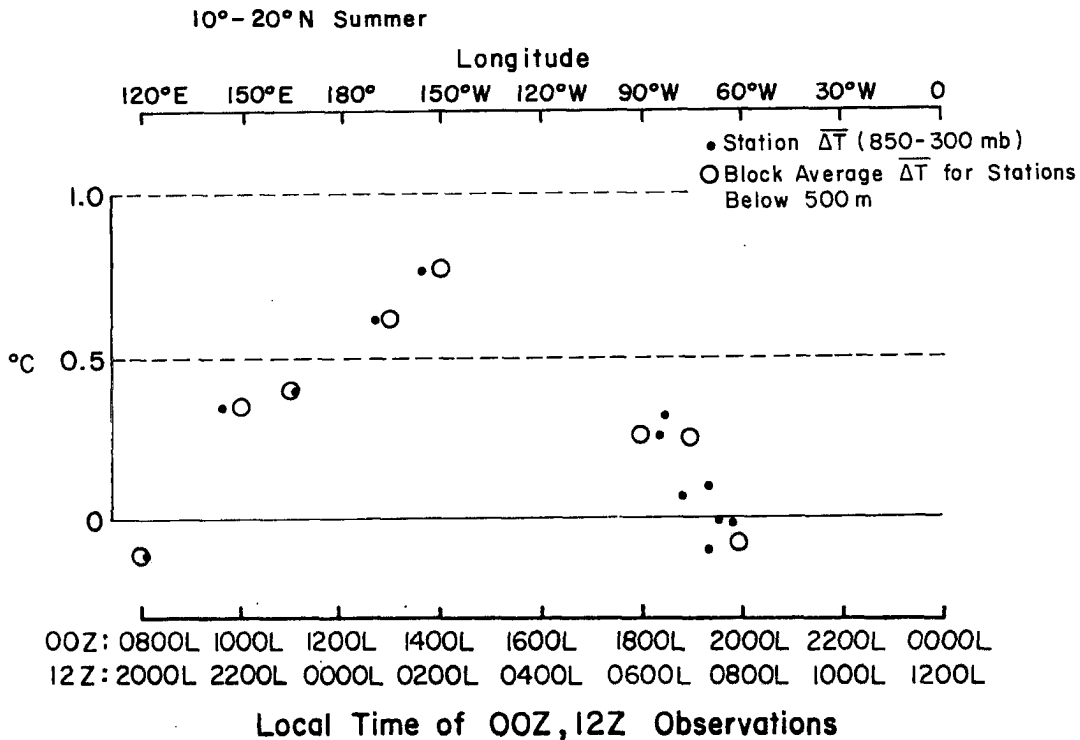
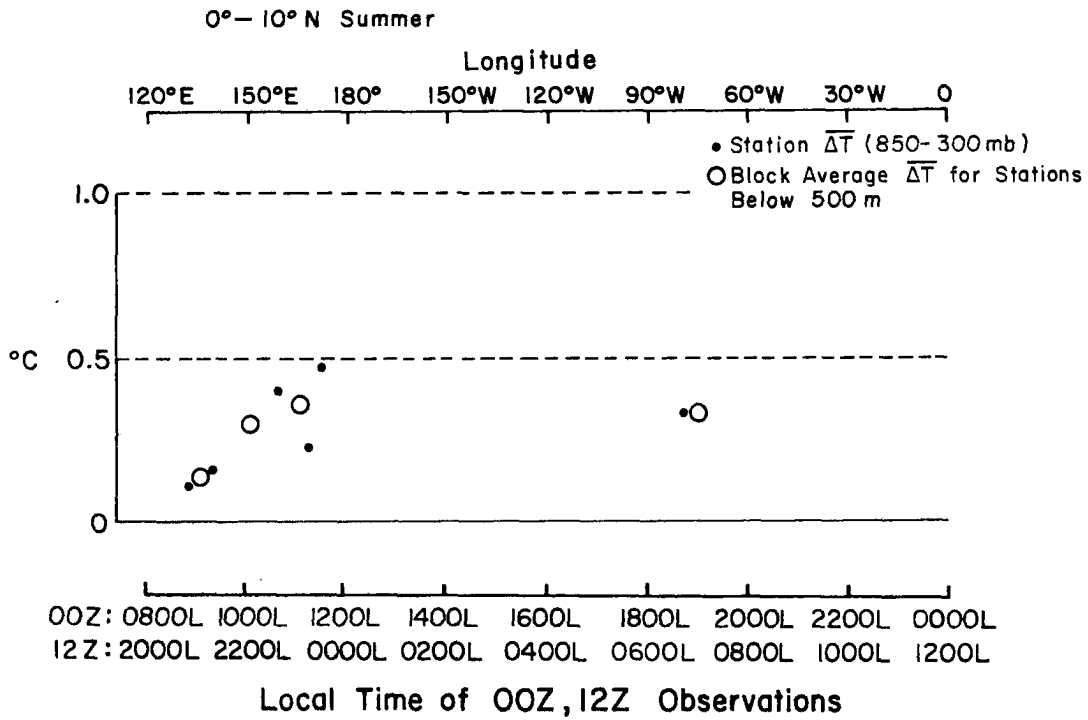


Fig. 2.4 a-b. 12-hour mean temperature difference ($\overline{T}_{00Z} - T_{12Z}$) of the middle tropospheric layer for stations and geographical blocks in 10° latitude bands from the equator to 60°N during the summer. Since the different longitudes correspond to different local times for the soundings, the diurnal temperature change of the layer can be seen.

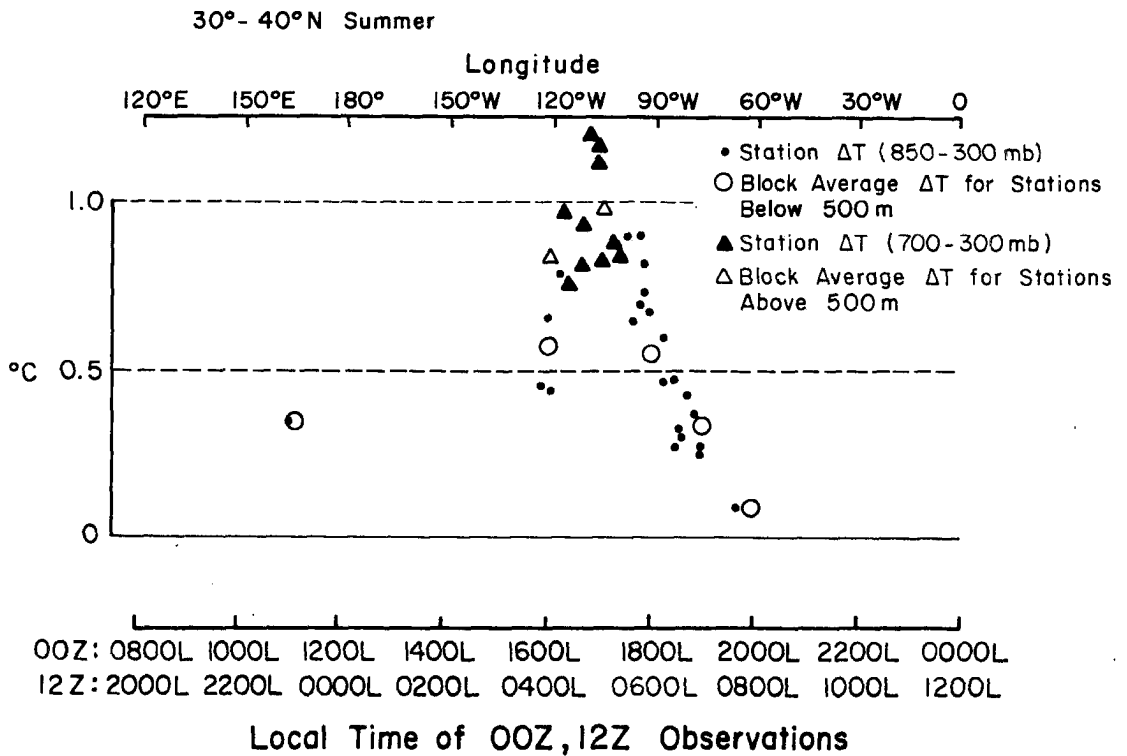
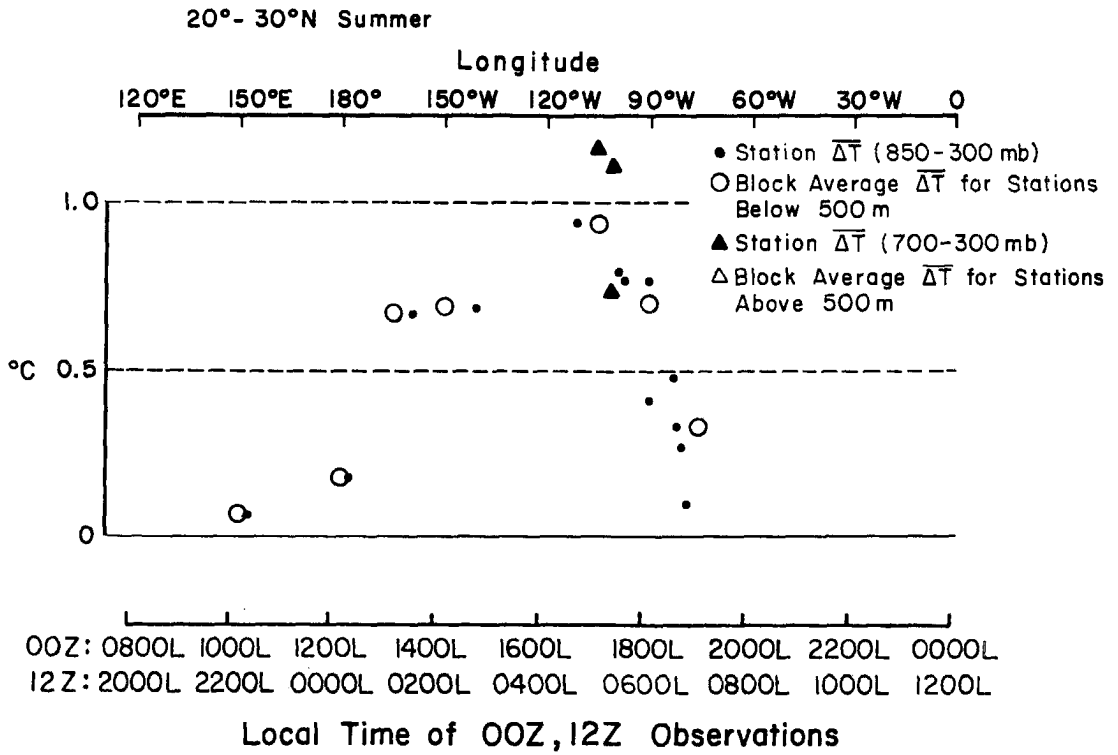


Fig. 2.4 c-d. Same as Fig. 2.4 a-b.

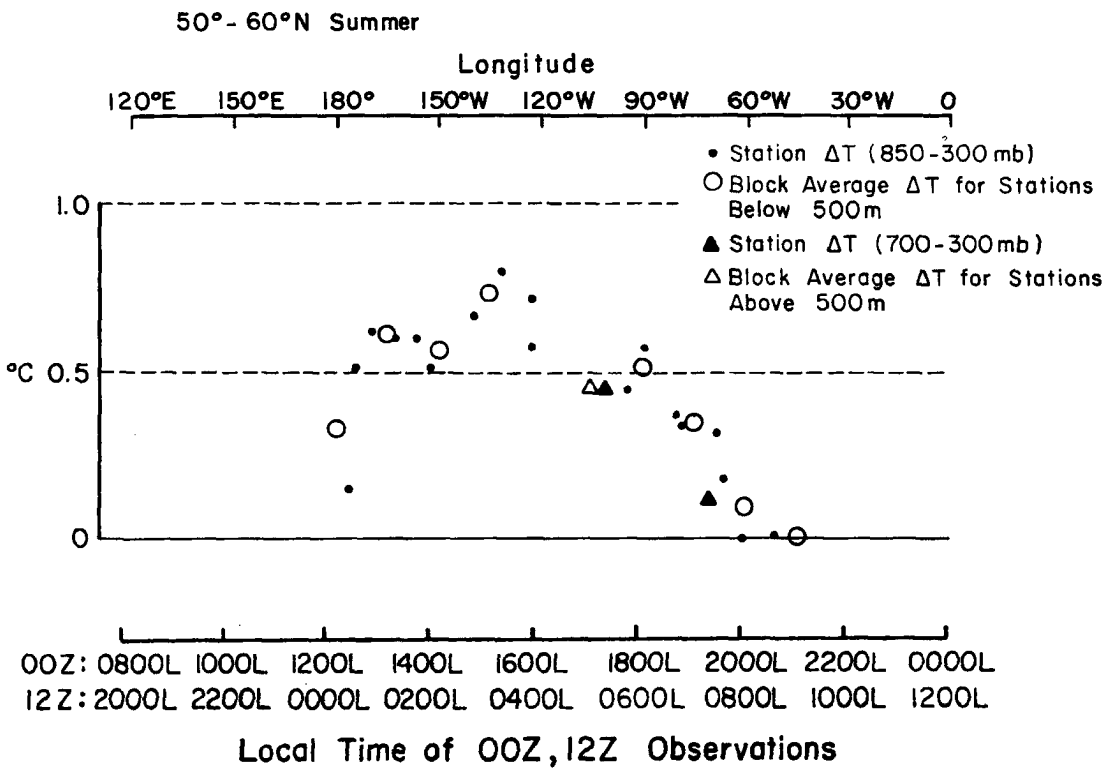
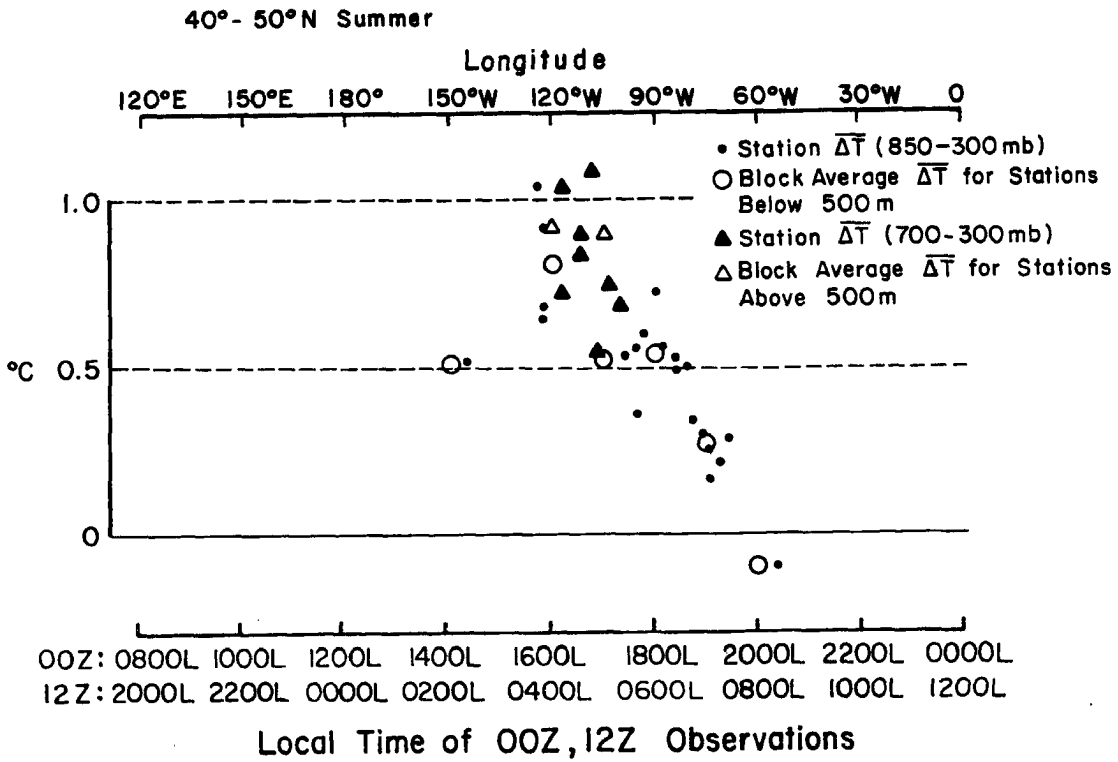


Fig. 2.4 e-f. Same as Fig. 2.4 a-b.

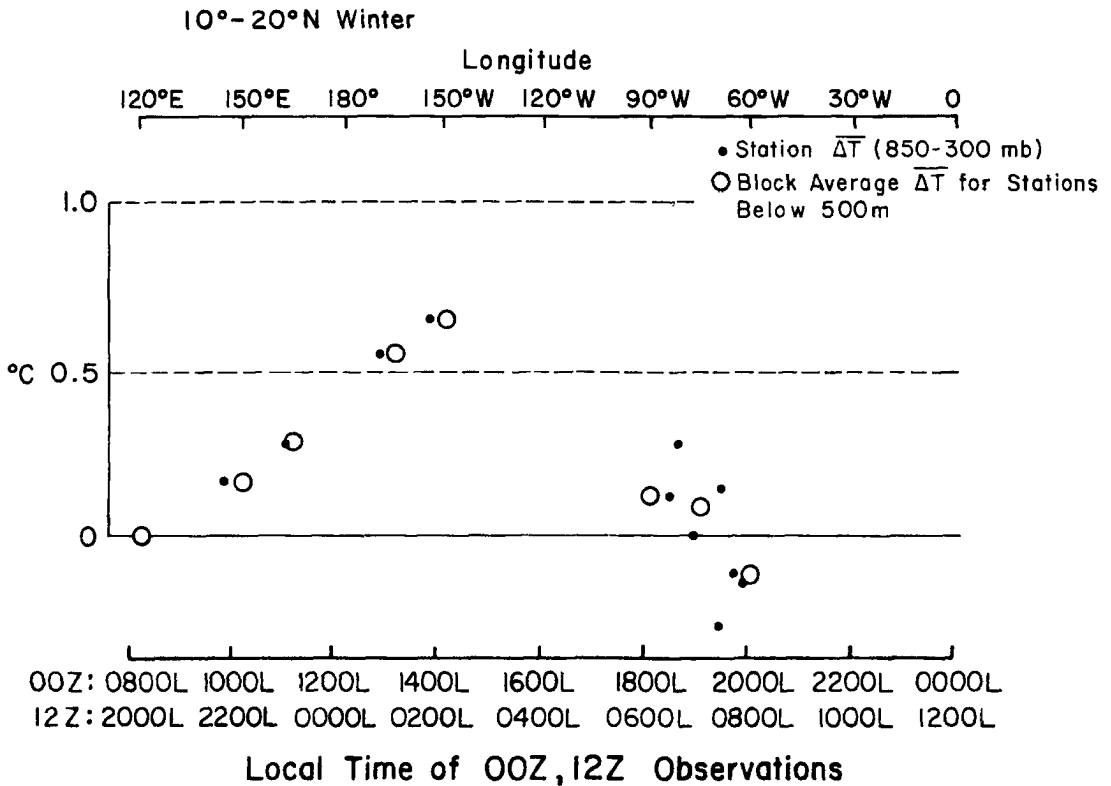
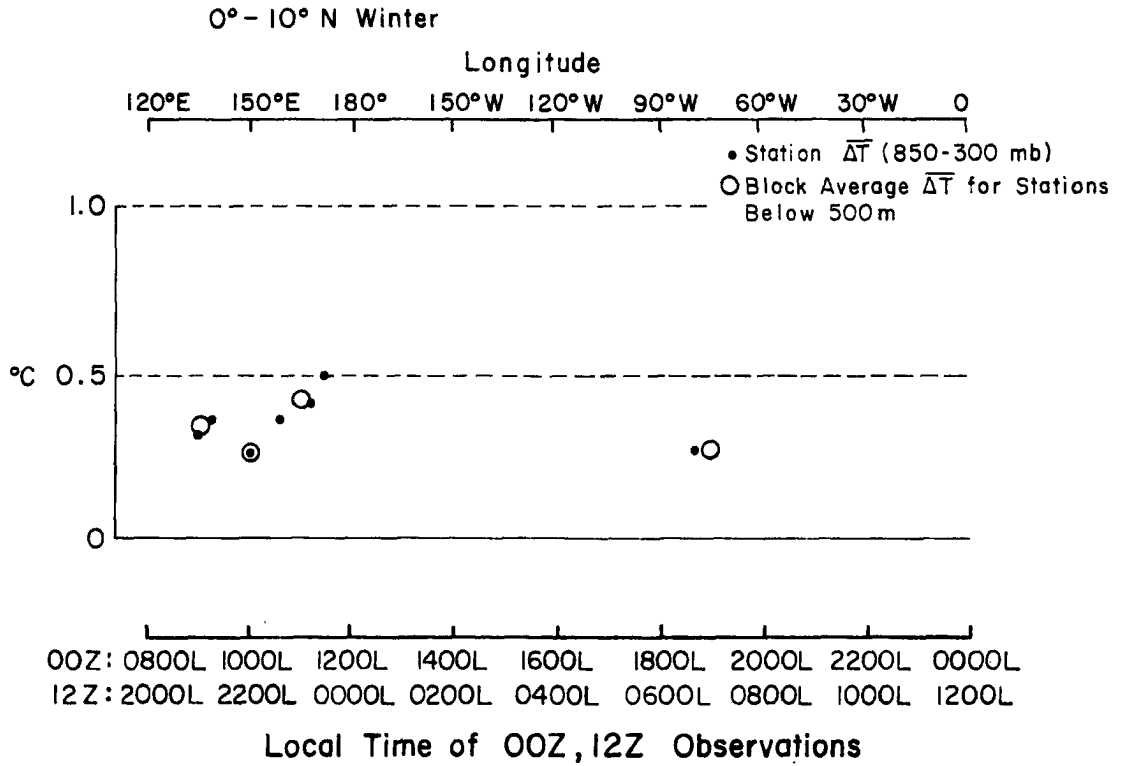


Fig. 1.5 a-b. 12-hour mean temperature difference (00Z - 12Z) of the middle tropospheric layer for stations and geographical blocks in 10° latitude bands from the equator to 60°N during the winter.

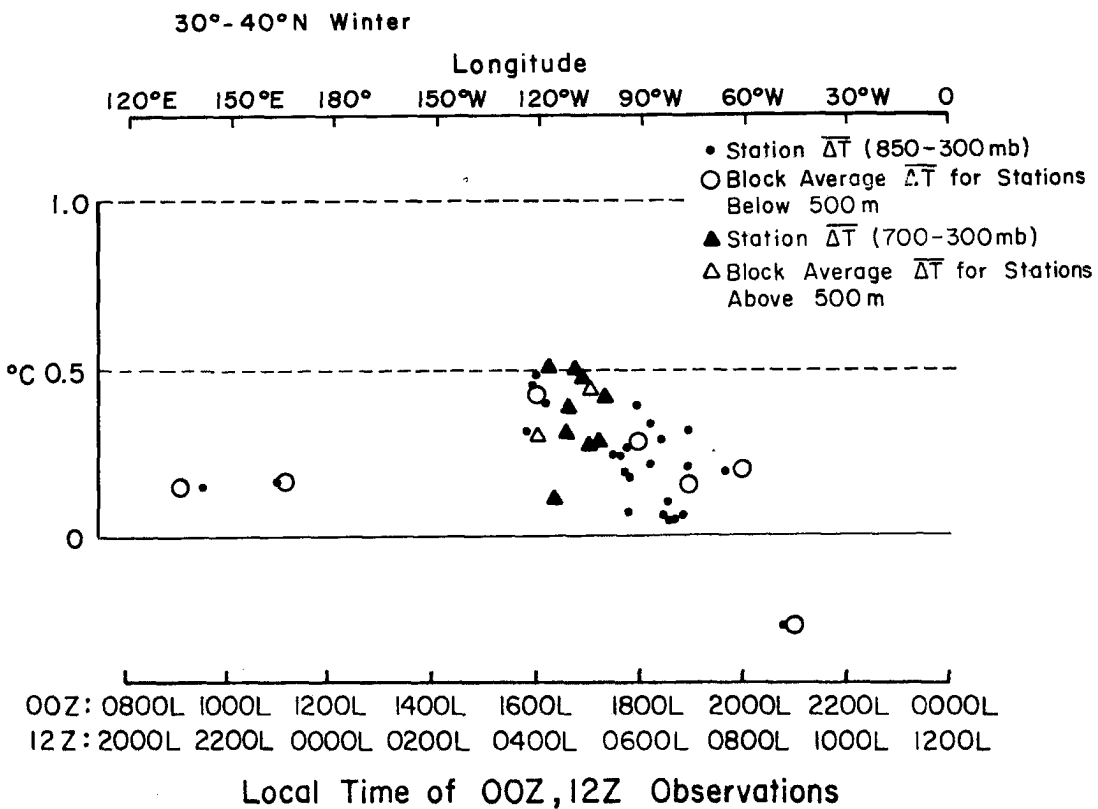
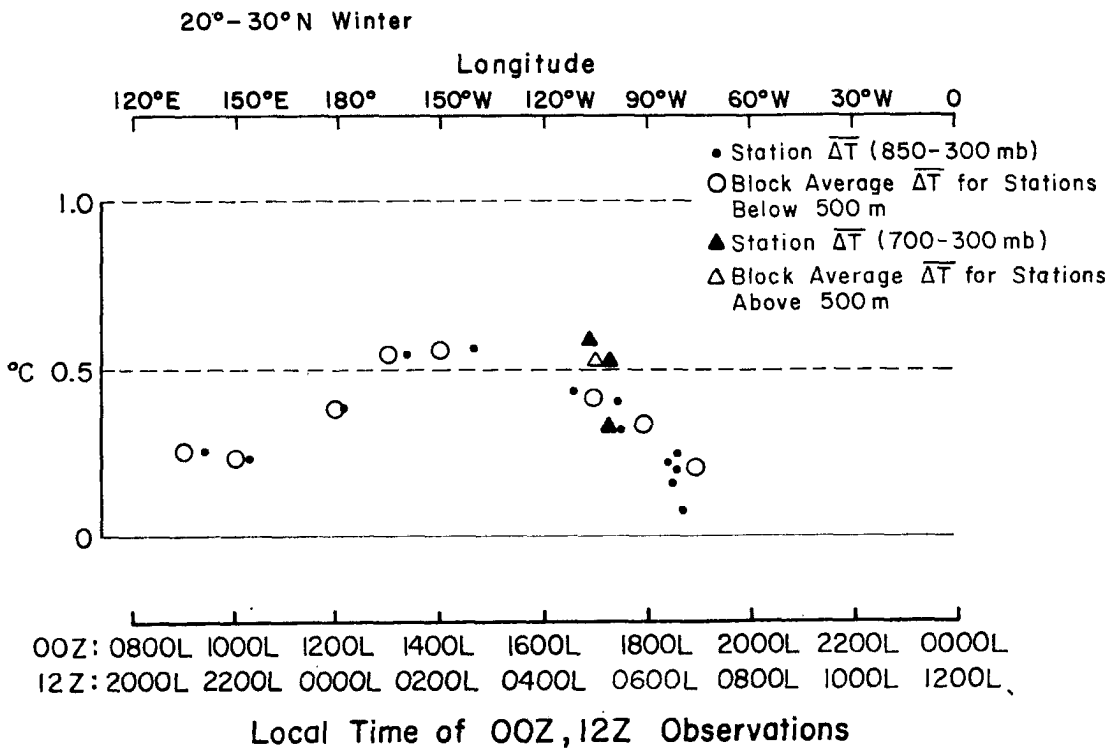


Fig. 2.5 c-d. Same as Fig. 2.5 a-b.

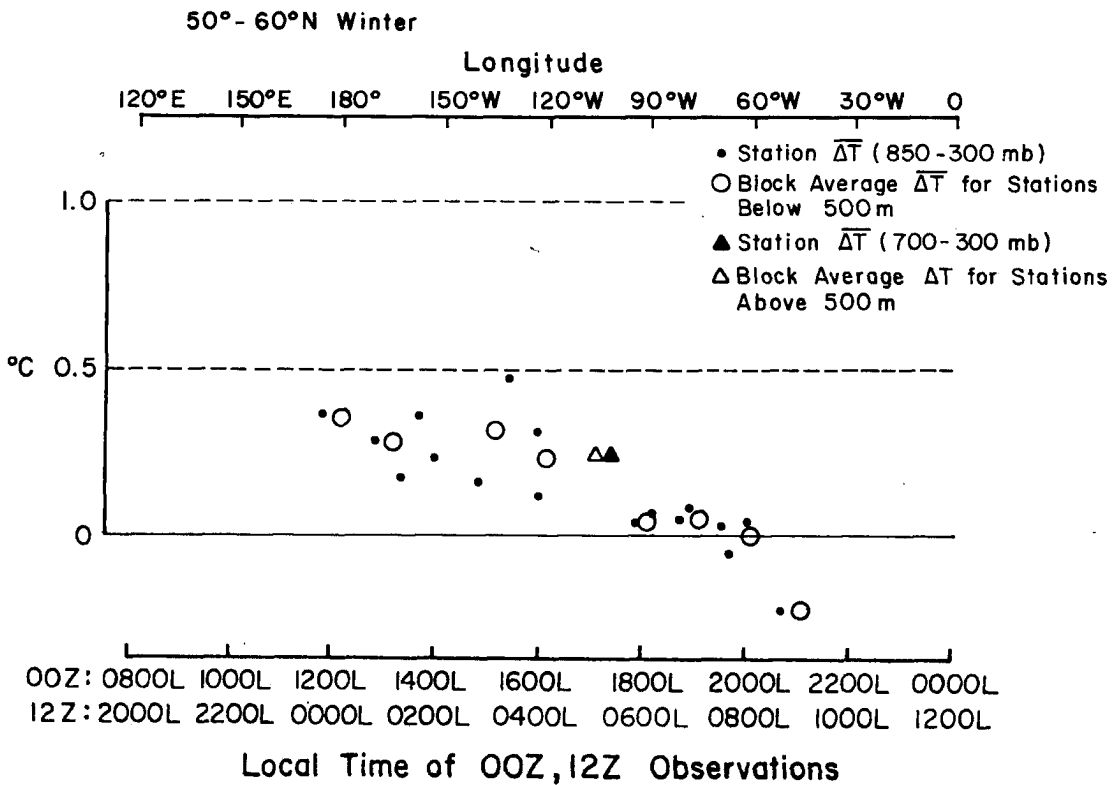
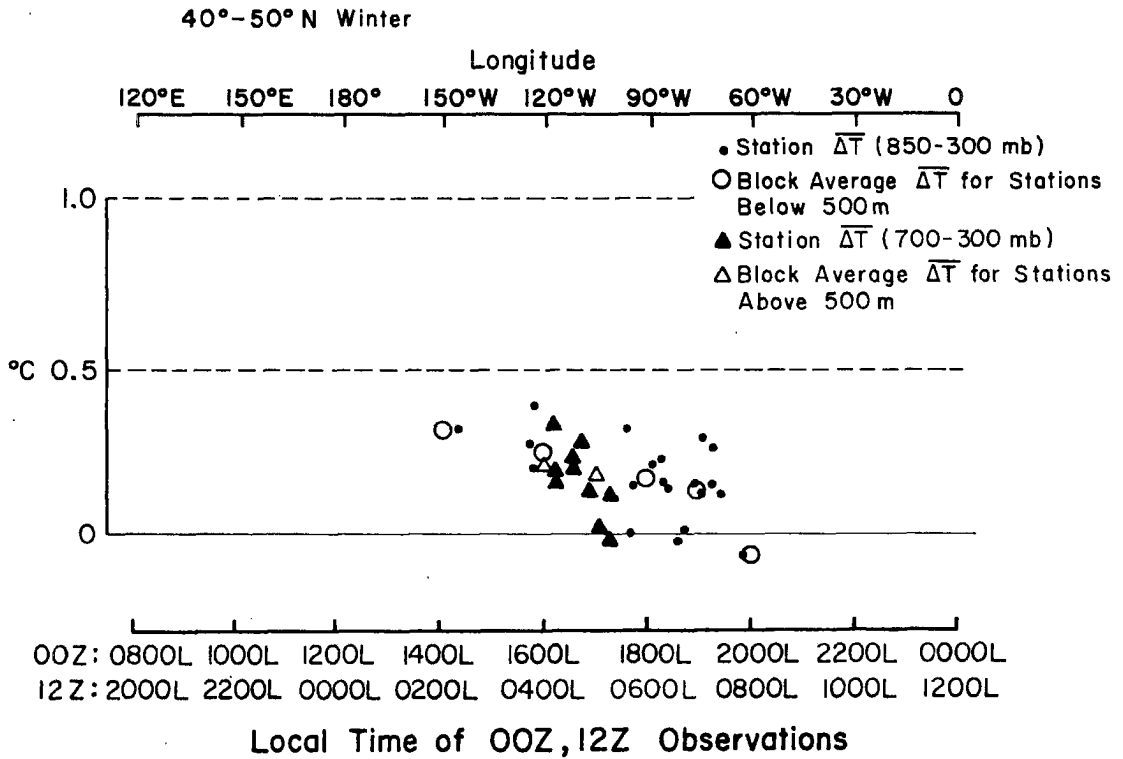


Fig. 2.5 e-f. Same as Fig. 2.5 a-b.

TABLE 2.4

(00GMT - 12 GMT) Mean Temperature Differences ($^{\circ}$ C) for the Summer and Winter Block: Geographical Block in Which Station is Located (Number Represents Number of Hours Earlier Than GMT)

Station	WMO#	$\overline{\Delta T}$ for 850-300 mb layer	$\overline{\Delta T}$ for 700-300 mb layer	Block	Summer $\overline{\Delta T}$	Winter $\overline{\Delta T}$
Latitude Belt 0-10 $^{\circ}$ N						
Canal Zone	78806	x		+5	.33	.28
Ponape	91348	x		+13	.40	.36
Kwajalein	91366	x		+13	.23	.41
Majuro	91376	x		+13	.47	.50
Truk	91334	x		+14	.30	.27
Koror	91408	x		+15	.11	.32
Yap	91413	x		+15	.16	.36
Latitude Belt 10-20 $^{\circ}$ N						
Raizet	78897	x		+4	-.01	-.13
San Juan	78526	x		+4	.00	-.10
Guantanamo	78367	x		+5	.25	.10
Santo Domingo	78486	x		+5	-.09	-.26
Curacao	78988	x		+5	.10	.15
San Andres	80001	x		+5	.32	.28
Swan Is.	78501	x		+6	.26	.13
Hilo, Ha.	91285	x		+10	.77	.65
Johnston Is.	91275	x		+11	.62	.58
Wake Is.	91245	x		+13	.40	.30
Eniwetok	91250	x		+13	---	.28
Guam	91217	x		+14	.35	.17
Clark AFB	98327	x		+16	-.10	.00
Latitude Belt 20-30 $^{\circ}$ N						
Key West	72201	x		+5	.33	.16
Miami	72202	x		+5	.27	.20
Cape Kennedy	74794	x		+5	---	.24
Grand Bahama	78063	x		+5	.10	.08
Tampa	72211	x		+6	.48	.22
Boothville	72232	x		+6	.76	.34
Brownsville	72250	x		+6	.79	.40
Victoria	72255	x		+6	.77	.41
Merida	76644	x		+6	.41	.33
Del Rio	72261		x	+7	1.11	.54
Monterrey	76394		x	+7	.74	.34
Guaymas	76255	x		+7	.94	.44
Chihuahua	76225		x	+7	1.16	.59
Ship N	24N	x		+10	.69	.56

TABLE 2.4 (cont'd)

Station	WMO#	$\overline{\Delta T}$ for	$\overline{\Delta T}$ for	Block	Summer	Winter
		850-300 mb layer	700-300 mb layer		$\overline{\Delta T}$	$\overline{\Delta T}$
Lihue, Ha	91165	x		+11	.67	.54
Midway Is.	91066	x		+12	.18	.38
Marcus Is.	91131	x		+14	.07	.23
Iowa Jima	91115	x		+15	---	.25
Latitude Belt 30-40°N						
Ship E	05E	x		+3	-.28	-.26
Bermuda	78016	x		+4	.10	.20
Jacksonville	72206	x		+5	.33	.11
Charleston	72208	x		+5	.32	.06
Cape Hatteras	72304	x		+5	.26	.21
Norfolk	72308	x		+5	---	---
Greensboro	72317	x		+5	.43	-.06
Wallops Is.	72402	x		+5	.27	.32
Washington	72403	x		+5	.37	.07
Montgomery	72226	x		+6	.47	.34
Jackson	72235	x		+6	.68	.39
Lake Charles	72240	x		+6	.70	.20
Shreveport	72248	x		+6	.90	.27
Ft. Worth	72259	x		+6	.90	.25
Athens	72311	x		+6	.48	.29
Nashville	72327	x		+6	.60	.22
Little Rock	72340	x		+6	.82	.18
Huntington	72425	x		+6	.38	.07
Columbia	72445	x		+6	.73	.31
Topeka	72456	x		+6	.65	.25
El Paso	72270		x	+7	1.17	.27
Tucson	72274		x	+7	.81	.32
Amarillo	72363		x	+7	.87	.29
Albuquerque	72365		x	+7	1.12	.48
Winslow	72374		x	+7	.93	.39
Dodge City	72451		x	+7	.85	.42
Denver	72469		x	+7	.83	.28
Grand Junction	72476		x	+7	1.20	.51
San Diego	72290	x		+8	.79	.40
San Nicolas	72291	x		+8	.44	.48
Yucca Flat	72385		x	+8	.96	.51
Vandenberg	72393	x		+8	.66	.45
Ely	72486		x	+8	.76	.12
Oakland	72493	x		+8	.46	.32
Ship V	25V	x		+13	.35	.17
Chichijima	91030	x		+15	---	.16
Latitude Belt 40-50°N						
Ship D	04D	x		+3	-.32	---
Sable Is.	72600	x		+4	-.10	-.05

TABLE 2.4 (cont'd)

Station	WMO#	$\overline{\Delta T}$ for	$\overline{\Delta T}$ for	Block	Summer	Winter
		850-300 mb layer	700-300 mb layer		$\overline{\Delta T}$	$\overline{\Delta T}$
Placentia	72807	x		+4	-.09	---
New York	74486	x		+5	.17	.30
Nantucket	72506	x		+5	.10	.16
Albany	72518	x		+5	.25	.12
Pittsburgh	72520	x		+5	.50	-.02
Buffalo	72528	x		+5	.34	.02
Portland	72606	x		+5	.22	.27
Caribou	72712	x		+5	.29	.13
Maniwaki	72722	x		+5	.30	.16
Flint	72637	x		+6	.49	.14
Peoria	72532	x		+6	.72	.24
Omaha	72553	x		+6	.55	.32
Green Bay	72645	x		+6	.56	.22
St. Cloud	72655	x		+6	.36	.00
S.S. Marie	72734	x		+6	.53	.16
Int'l Falls	72747	x		+6	.60	.16
North Platte	72562		x	+7	.68	.13
Salt Lake	72572		x	+7	.83	.24
Lander	72576		x	+7	1.08	.29
Huron	72654	x		+7	.54	---
Rapid City	72662		x	+7	.74	.03
Bismarck	72764		x	+7	.39	.00
Glasgow	72768		x	+7	.54	.15
Great Falls	72775		x	+7	.89	.20
Winnemucca	72583		x	+8	1.03	.34
Medford	72597	x		+8	.68	.39
Boise	72681		x	+8	1.00	.16
Salem	72694	x		+8	.64	.21
Spokane	72785		x	+8	.73	.21
Quillayute	72797	x		+8	1.04	.28
Ship P	17P	x		+10	.18	.32
Latitude Belt 50-60°N						
Ship C	03C	x		+2	-.39	---
Ship D	02B	x		+3	.01	---
Sept. Iles	72811	x		+4	.18	-.04
Goose	72816	x		+4	.01	.05
Nitcheguom	72826		x	+5	.13	-.10
Moonsonee	72836	x		+5	.37	.06
Ft. Chimo	72906	x		+5	.32	.04
Inouckjouac	72907	x		+5	.34	.09
Trout Lake	72848	x		+6	.57	.07
Churchill	72913	x		+6	.45	.05
The Pas	72867		x	+7	.45	.25
Prince George	72896	x		+8	.72	.13
Ft. Nelson	72945	x		+8	.58	.32

TABLE 2.4 (cont'd)

Station	WMO#	$\overline{\Delta T}$ for	$\overline{\Delta T}$ for	Block	Summer	Winter
		850-300 mb layer	700-300 mb layer		$\overline{\Delta T}$	$\overline{\Delta T}$
Yakutat	70361	x		+9	.67	.17
Annette Is.	70398	x		+9	.80	.47
King Salmon	70326	x		+10	.60	.36
Kodiak	70350	x		+10	.51	.24
St. Paul	70308	x		+11	.62	.29
Cold Bay	70316	x		+11	.60	.18
Shemya	70414	x		+12	.51	.37
Adak	70454	x		+12	.15	.78
Latitude Belt 60-70°N						
Frobisher Bay	72909	x		+5	.28	.14
Coral Harbor	72915	x		+6	.31	.13
Baker Lake	72926	x		+6	.42	.17
Ft. Smith	72934	x		+7	.53	.10
Coppermine	72938	x		+8	.23	.06
Inuvik	72957	x		+9	.34	.12
Whitehorse	72964		x	+9	.87	.25
McGrath	70231	x		+10	.51	.40
Fairbanks	70261	x		+10	.76	.02
Anchorage	70273	x		+10	.78	.25
Kotzebue	70133	x		+11	.60	.26
Nome	70200	x		+11	.53	.68
Bethel	70219	x		+11	.64	.32
Latitude Belt 70-80°N						
Eureka	72917	x		+6	-.08	.04
Resolute	72924	x		+6	.13	.11
Pt. Barrow	70026	x		+10	.60	.22
Barter Is.	70086	x		+10	.47	.05

TABLE 2.5

00GMT-12GMT Mean Temperature Differences ($^{\circ}\text{C}$) for
Each Geographic Block in the Summer and Winter

Latitude Belt	Block Identification	Longitude West	Boundaries East	$\Delta\bar{T}$ for 850-300 mb	$\Delta\bar{T}$ for 700-300 mb	Local Time of Difference	Summer $\Delta\bar{T}$	Winter $\Delta\bar{T}$
0-10 $^{\circ}$ N	+5	67.5 $^{\circ}$ W	82.5 $^{\circ}$ W	X		1900-0700	.33	.28
	+13	172.5 $^{\circ}$ E	157.5 $^{\circ}$ E	X		1100-2300	.36	.42
	+14	157.5 $^{\circ}$ E	142.5 $^{\circ}$ E	X		1000-2200	.30	.27
	+15	142.5 $^{\circ}$ E	127.5 $^{\circ}$ E	X		0900-2100	.13	.34
10-20 $^{\circ}$ N	+4	52.5 $^{\circ}$ W	67.5 $^{\circ}$ W	X		2000-0800	-.07	-.11
	+5	67.5 $^{\circ}$ W	82.5 $^{\circ}$ W	X		1900-0700	.25	.09
	+6	82.5 $^{\circ}$ W	97.5 $^{\circ}$ W	X		1800-0600	.26	.13
	+10	142.5 $^{\circ}$ W	157.5 $^{\circ}$ W	X		1400-0200	.77	.64
	+11	157.5 $^{\circ}$ W	172.5 $^{\circ}$ W	X		1300-0100	.62	.55
	+13	172.5 $^{\circ}$ E	157.5 $^{\circ}$ E	X		1100-2300	.40	.29
	+14	157.5 $^{\circ}$ E	142.5 $^{\circ}$ E	X		1000-2200	.35	.17
	+16	127.5 $^{\circ}$ E	112.5 $^{\circ}$ E	X		0800-2000	-.10	.00
20-30 $^{\circ}$ N	+5	67.5 $^{\circ}$ W	82.5 $^{\circ}$ W	X		1900-0700	.33	.21
	+6	82.5 $^{\circ}$ W	97.5 $^{\circ}$ W	X		1800-0600	.70	.34
	+7	97.5 $^{\circ}$ W	112.5 $^{\circ}$ W	X		1700-0500	.94	.52
	+10	142.5 $^{\circ}$ W	157.5 $^{\circ}$ W	X		1400-0200	.69	.56
	+11	157.5 $^{\circ}$ W	172.5 $^{\circ}$ W	X		1300-0100	.67	.54
	+12	172.5 $^{\circ}$ W	172.5 $^{\circ}$ E	X		1200-0000	.18	.38
	+14	157.5 $^{\circ}$ E	142.5 $^{\circ}$ E	X		1000-2200	.07	.23
	+15	142.5 $^{\circ}$ E	127.5 $^{\circ}$ E	X		0900-2100	-	.25
30-40 $^{\circ}$ N	+3	37.5 $^{\circ}$ W	52.5 $^{\circ}$ W	X		2100-0900	-.28	-.26
	+4	52.5 $^{\circ}$ W	67.5 $^{\circ}$ W	X		2000-0800	.10	.20
	+5	67.5 $^{\circ}$ W	82.5 $^{\circ}$ W	X		1900-0700	.34	.14
	+6	82.5 $^{\circ}$ W	97.5 $^{\circ}$ W	X		1800-0600	.65	.29
	+7	97.5 $^{\circ}$ W	112.5 $^{\circ}$ W		X	1700-0500	.98	.44

TABLE 2.5 (cont'd)

Latitude Belt	Block Identification	Longitude West	Longitude East	Boundaries East	ΔT for 850-300 mb	ΔT for 700-300 mb	Local Time of Difference	Summer ΔT	Winter ΔT
30-40°N	+8A	112.5°W	127.5°W		X		1600-0400	.58	.43
	+8B	112.5°W	127.5°W			X	1600-0400	.79	.30
	+13	172.5°E	157.5°E		X		1100-2300	.35	.17
	+15	142.5°E	127.5°E		X		0900-2100	-	.16
40-50°N	+3	37.5°W	52.5°W		X		2100-0900	-.32	-
	+4	52.5°W	67.5°W		X		2000-0800	-.05	-.14
	+5	67.5°W	82.5°W		X		1900-0700	.28	.14
	+6	82.5°W	97.5°W		X		1800-0600	.54	.18
	+7A	97.5°W	112.5°W			X*	1700-0500	.53	.10
	+7B	97.5°W	112.5°W			X*	1700-0500	.89	.19
	+8A	112.5°W	127.5°W		X		1600-0400	.81	.25
	+8B	112.5°W	127.5°W			X	1600-0400	.92	.23
	+10	142.5°W	157.5°W		X		1400-0200	.51	.32
	50-60°N	+2	22.5°W	37.5°W		X		2200-1000	-.39
+3		37.5°W	52.5°W		X		2100-0900	.01	-.21
+4		52.5°W	67.5°W		X		2000-0800	.10	.01
+5		67.5°W	82.5°W		X		1900-0700	.35	.06
+6		82.5°W	97.5°W		X		1800-0600	.51	.06
+7		97.5°W	112.5°W		X		1700-0500	.45	.11
+8		112.5°W	127.5°W			X	1600-0400	.63	.24
+9		127.5°W	142.5°W		X		1500-0300	.73	.47
+10		142.5°W	157.5°W		X		1400-0200	.56	.24
+11		157.5°W	172.5°W		X		1300-0100	.61	.29
+12		172.5°W	172.5°E		X		1200-0000	.33	.36

*While all stations in block (40-50°N, +7) are considered to be at elevated locations, some were above 1000m while others were near 500m, thus the separate calculation.

Discussion. An examination of the data shows that the temperature differences for stations located in close proximity to each other are relatively similar. Although in some cases the data within a latitudinal band is somewhat limited in the longitudinal direction, there is a definite 00-12 GMT diurnal temperature trend evident throughout the hemisphere. The amplitude of this variation is reduced in the winter season (Figs. 2.5a - 2.5f) when compared to the summer (Figs. 2.4a - 2.4f), and the amplitude diminishes as the observations are taken farther to the north. In the summer the greatest mean temperature difference is more than a degree, and it diminishes to about a half a degree in the winter. This difference is primarily a reflection of increased incident short wave radiation, but it also includes some effects of surface sensible heat transport to upper layers. As the lower latitudinal bands are examined (Figs. 2.4a,b and 2.5a,b), it is apparent that the seasonal change is minimal. This is expected as the winter and summer seasons in the tropics are climatically similar. In the middle latitudes, where the data is more dense, the summer and winter maximum temperature difference occurs in the afternoon between 15 and 17 LT. This result may be influenced by the location ascents over the large North America land mass.

Instrument Error Induced by Solar Radiation. The magnitude of instrument error caused by solar radiation absorption, which is implicit in the observed value of the daily variation of temperature below 300 mb, is believed to be generally less than 0.2°C . The rationale for this conclusion is discussed in Appendix B which shows the small magnitude of this solar induced error source.

In an effort to obtain the real tropospheric 12-hour temperature difference without significant contamination from solar radiational

error, the method used by Finger and McInturff (1968) was applied. This procedure identified that region containing upper-air stations whose successive 00GMT and 12GMT radiosonde ascents are made completely in darkness during the winter season. The data collected at these stations during the winter is considered to be free of solar radiation error. Finger and McInturff also determined that the solar radiation error is a function of the sun's elevation angle. Utilizing this information, the mean solar elevation angle for the summer season at both 00GMT and 12GMT for the central North American upper-air stations was calculated. If the solar elevation angle at a single station is approximately the same at both 00GMT and 12GMT, the mean temperature difference for that station can also be considered free from solar radiation error.

This procedure allowed the examination of 00Z vs. 12Z temperature differences which were relatively free from solar radiation error. It gave increased confidence to the values observed at the other locations throughout the hemisphere since there were no discontinuities between sunlight and darkness observations, such as those which occur in the middle and upper stratosphere. It also indicated that the mean temperature of the 850-300 mb layer varies diurnally both in the summer and in the winter, with the variation being greater at lower latitudes and in the summer. A more detailed presentation of the results of this solar error elimination scheme can be found in Appendix C. Based on instrument error information obtained from several sources (see Appendix B and C), it is concluded that the error contained in the temperature observation is much less than the magnitude of the real diurnal change of temperature. The solar radiation error is greatest at local noon when the sun is at its highest elevation angle.

These results indicate a definite diurnal variation of the mean temperature of the layer under consideration. It is concluded that although solar radiationally induced error is inherent in the daytime temperature observations, the magnitude of that error is much smaller than the actual temperature variation. Therefore, the observed values of $\overline{\Delta T}$ will be used in subsequent calculations.

3. EXPECTED TROPOSPHERIC ENERGY GAIN/LOSS FROM RADIATION

To determine the warming required to compensate for the continual net radiative cooling of the troposphere, it was necessary to compute the heating of the middle tropospheric layer by short wave absorption and the cooling by long wave radiation. This was accomplished by employing two numerical radiative transfer models. The heating rates and total heating due to the absorption of broadband solar irradiance were computed by following the technique described by Manabe and Strickler (1964). The broadband infrared irradiances at specified levels were calculated using a model described by Cox (1974). The irradiances were then used to determine the cooling rates through the net flux divergence. Appendix D presents a more detailed explanation of the short wave heating and long wave cooling models. Observational studies conducted in the tropics and mid-latitudes will also be examined in an effort to verify the radiation computations.

3.1 Cloud-Free Radiational Model Results for Short Wave Radiation (SW)

The short wave radiation model calculates the temperature change for an increment of time by determining the amount of incident solar radiation absorbed by the atmospheric constituents (H_2O , CO_2 and O_3) in a cloud-free atmosphere. Figure 3.1 shows two examples of the results from the short wave model.

The mean total amount of daily heating from solar energy for the middle tropospheric layer was obtained by computing an average for all 50 mb layers contained in the 850-300 mb region. Table 3.1 portrays summer and winter theoretically derived cloud-free solar radiation induced temperature changes for each geographical block from which

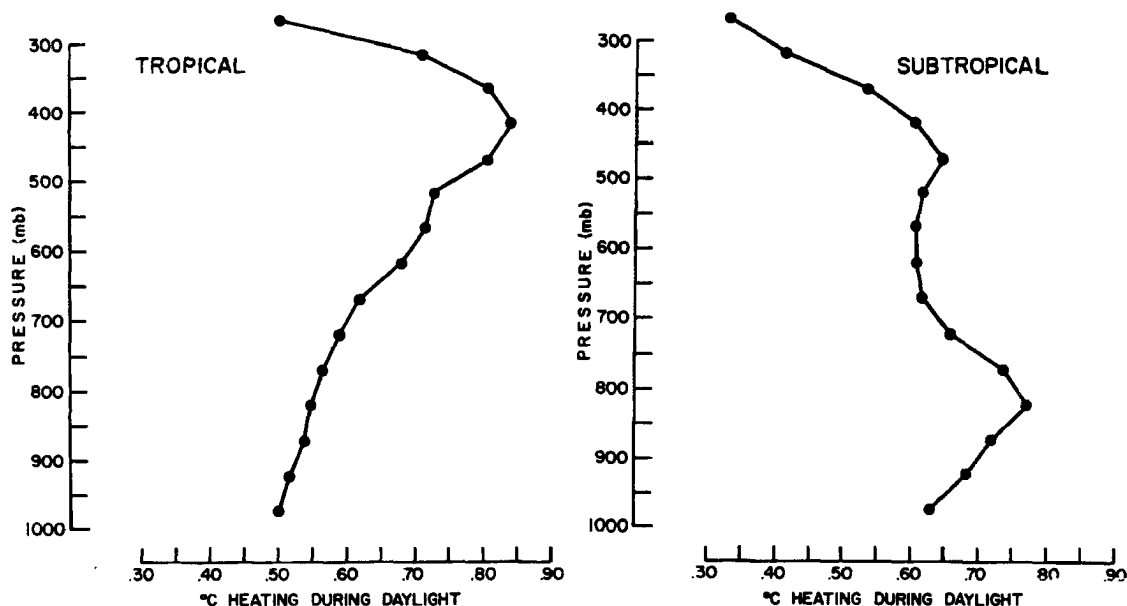


Fig. 3.1. Vertical profiles of calculated total daytime heating from short wave absorption in 50 mb layers at tropical (left) and subtropical (right) locations.

radiosonde data was available. The calculations were performed for each block in order to delineate continental-ocean, latitudinal, seasonal, and other radiation differences.

These results indicate that the daytime temperature change due to insolation is greater in the summer than in the winter at all latitudes as would be expected. Also the higher latitudes show an appreciable amount of warming in the summer. This indicates that although the optical path is long because of a relatively high zenith angle, the sun is above the horizon for an extremely long period of time. In the winter at high latitudes, the absence of sunlight is indicated by the low heating values. At low latitudes ($0-10^{\circ}\text{N}$) there is little seasonal difference in short wave warming as the sun is at the extreme declination angle in summer and winter relative to the equator.

TABLE 3.1

Magnitude of Cloud-Free Short Wave (SW) Daytime Warming
For Each Geographical Block ($^{\circ}\text{C}$)

Latitude Belt	Longitude ⁺ Block	Summer	Winter	Latitude Belt	Longitude ⁺ Block	Summer	Winter													
0 $^{\circ}$ -10 $^{\circ}$ N	+5	.74	.66	40 $^{\circ}$ -50 $^{\circ}$ N	+3	.71	--													
	+13	.72	.66		+4	.71	.19													
	+14	.71	.64		+5	.74	.18													
	+15	.65	.61		+6	.77	.18													
10 $^{\circ}$ -20 $^{\circ}$ N	+4 +5 +6 +10 +11 +13 +14 +16	.69 .70 .71 .64 .67 .72 .74 .72	.52 .49 .53 .49 .49 .53 .54 .55		+7A*	.74	.19													
					+7B	.74	.20													
					+8A	.73	.19													
					+8B*	.67	.20													
					+10	.66	.18													
					50-60 $^{\circ}$ N	+2 +3 +4 +5 +6 +7*	.67 .70 .75 .69 .71 .74	-- .07 .09 .09 .09 .10	+2 +3 +4 +5 +6 +7*	.67 .70 .75 .69 .71 .74	-- .07 .09 .09 .09 .10									
				20 $^{\circ}$ -30 $^{\circ}$ N								+5 +6 +7 +10 +11 +12 +14 +15	.76 .76 .75 .73 .67 .72 .73 --	.48 .40 .36 .36 .46 .38 .45 .43	+7*	.74 .76 .69 .69 .64 .64	.10 .06 -- .07 .07 .10			
30 $^{\circ}$ -40 $^{\circ}$ N	+3 +4 +5 +6 +7* +8A +8B* +13 +15	.71 .79 .75 .76 .80 .70 .77 .74 --	.31 .36 .29 .27 .29 .30 .30 .32 .36															+10 +11 +12	.69 .64 .64	.07 .07 .10

+See Table 2.7 for dimensions of longitude blocks.

*For 700-300 mb layer.

Observational studies (Hanson, Vonder Haar, and Suomi, 1967; Cox, Vonder Haar, Hanson, and Suomi, 1973; Reynolds, Vonder Haar, and Cox, 1975) conducted in both the middle latitudes and in the tropics have attempted to determine the amount of short wave absorption in the troposphere. Although these studies examine various tropospheric layers, their results are essentially consistent with the cloud-free computations performed for the 850-300 mb layer in this study. The variations between the observational data and theoretical calculations mainly occur in the lower layers (below 850 mb) and when clouds and aerosols are present in the troposphere.

3.2 Cloud-Free Radiational Model Results For Long Wave Radiation (LW)

The finite difference form of the radiative transfer equation, neglecting scattering processes, is the basis for this calculation, (Cox, 1974). The net radiative flux divergence for each 50 mb layer is computed in order to determine the cooling rate. Figure 3.2 shows two example vertical profiles of long wave cooling. The mean long wave cooling rate for the 850-300 mb layer is calculated by averaging the cooling rate values for each 50 mb layer between the 850 mb level and 300 mb level. Table 3.2 exhibits these values for each geographical block examined in this study.

An examination of the results of the long wave cooling calculation shows that again there is little seasonal change in the cooling rates at lower latitudes. At higher latitudes the summer season cooling rates are somewhat greater than in the winter. These cooling rates are essentially a function of the temperature and humidity content of the troposphere. Cox (1969a) observationally determined the infrared cooling rate in the tropics during the Line Islands experiment. The

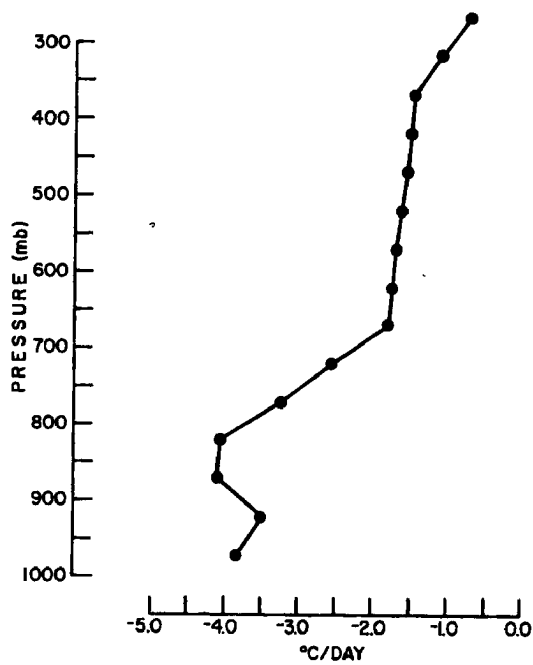
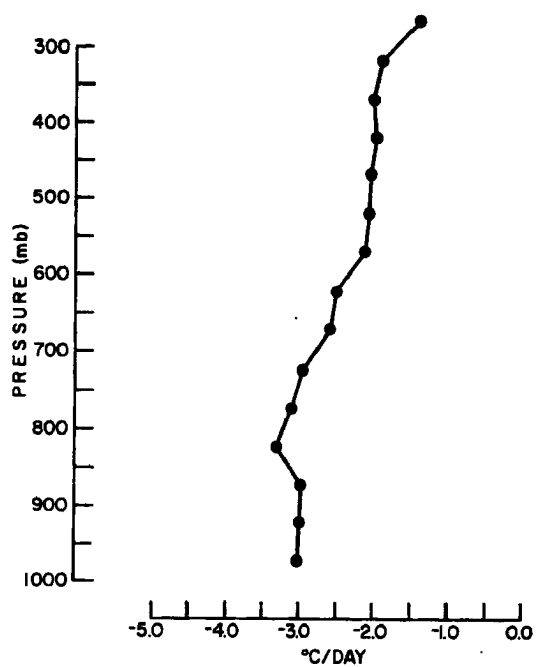


Fig. 3.2. Vertical profiles of calculated cooling rates from long wave irradiance in 50 mb layers at tropical (top) and subtropical (bottom) locations.

TABLE 3.2

Magnitude of Cloud-Free Long Wave (LW) Cooling
In Each Geographical Block ($^{\circ}\text{C}/\text{Day}$)

Latitude Belt	Longitude Block	Summer	Winter	Latitude Belt	Longitude Block	Summer	Winter
0 $^{\circ}$ -10 $^{\circ}$ N	+5	-2.44	-2.26	50 $^{\circ}$ -60 $^{\circ}$ N	+2	-1.42	--
	+13	-2.42	-2.34		+3	-1.30	-.76
	+14	-2.38	-2.26		+4	-1.34	-.84
	+15	-2.36	-2.22		+5	-1.24	-.76
					+6	-1.28	-.82
					+7	-1.32	-.94
10 $^{\circ}$ -20 $^{\circ}$ N	+4	-1.94	-1.86	+8	-1.18	-.54	
	+5	-1.96	-1.74	+9	-1.22	--	
	+6	-2.04	-1.96	+10	-1.20	-.78	
	+10	-1.88	-1.82	+11	-1.20	-.80	
	+11	-2.02	-1.80	+12	-1.28	-.74	
	+13	-2.10	-2.02				
	+14	-2.34	-2.08				
	+16	-2.16	-2.00				
20 $^{\circ}$ -30 $^{\circ}$ N	+5	-2.04	-1.64				
	+6	-1.98	-1.46				
	+7	-2.00	-1.36				
	+10	-1.64	-1.40				
	+11	-1.82	-1.68				
	+12	-1.80	-1.44				
	+14	-2.06	-1.78				
	+15	--	-1.76				
30 $^{\circ}$ -40 $^{\circ}$ N	+3	-1.62	-1.48				
	+4	-1.80	-1.50				
	+5	-1.84	-1.24				
	+6	-1.96	-1.28				
	+7	-1.70	-1.16				
	+8A	-1.68	-1.28				
	+8B	-1.54	-1.16				
	+13	-1.88	-1.20				
	+15	--	-1.48				
40 $^{\circ}$ -50 $^{\circ}$ N	+3	-1.60	--				
	+4	-1.54	-1.04				
	+5	-1.64	-.98				
	+6	-1.68	-1.00				
	+7A	-1.48	-.98				
	+7B	-1.48	-1.00				
	+8A	-1.38	-.94				
	+8B	-1.37	-.96				
	+10	-1.36	-.88				

theoretical results determined in this study are in basic agreement with his measured values for a clear atmosphere. Cox (1969b) also obtained long wave radiation measurements for various mid-latitude synoptic weather systems and computed cooling rates for 100 mb layers. While there was a variation in vertical cooling rate profiles in different sectors of each weather system type, the cloud-free cooling rates for the mid-latitudes calculated in this paper are consistent with Cox's observations.

3.3 Summary

Cloud-free short wave heating (\overline{SW}) and long wave cooling (\overline{LW}) values were calculated for the middle tropospheric layer utilizing two radiative transfer models. Table 3.3 gives \overline{SW} and \overline{LW} warming rates for each latitudinal band for mean cloud and cloud-free conditions. The cloud case values are taken from Dopplick (1970) who refined previous estimates of short wave heating and long wave cooling rates by incorporating a mean cloud distribution. Dopplick obtained his cloud distribution from satellite observations, where possible, and from London's (1957) cloud cover estimates.

In the summer and winter the short wave daily warming (\overline{SW}) is greater for the mean cloudiness conditions indicating that more solar energy is absorbed when clouds are present than when skies are clear. The long wave cooling rate in the 0-10⁰N latitude band is greater for the cloud-free situation in both the summer and winter. However, the mean cloudiness condition causes more cooling than a clear atmosphere for most of the other latitudinal bands, particularly in the high latitudes during the winter. This indicates that irradiance off the tops of low level clouds is causing increased cooling in the 850-300 mb layer.

TABLE 3.3

Latitudinal Distribution of Average Cloud-Free \overline{SW} and \overline{LW} Radiational Warming With Similar Values of Dopplick (1970) For Estimated Mean Cloud Conditions in the 850-300 mb Layer ($^{\circ}\text{C}/\text{Day}$)

Latitude Belt	<u>Summer</u>		<u>LW</u>		Net Radiative Warming	
	\overline{SW} Cloud Free	Mean Cloudiness	Cloud Free	Mean Cloudiness	Cloud Free	Mean Cloudiness
0 $^{\circ}$ -10 $^{\circ}$ N	.71	.94	-2.40	-2.07	-1.69	-1.13
10 $^{\circ}$ -20 $^{\circ}$ N	.70	1.00	-2.06	-2.05	-1.36	-1.05
20 $^{\circ}$ -30 $^{\circ}$ N	.73	1.02	-1.91	-1.98	-1.13	-.96
30 $^{\circ}$ -40 $^{\circ}$ N	.76	1.03	-1.75	-1.78	-.99	-.75
40 $^{\circ}$ -50 $^{\circ}$ N	.72	1.07	-1.50	-1.59	-.78	-.52
50 $^{\circ}$ -60 $^{\circ}$ N	.67	1.12	-1.27	-1.46	-.60	-.34
<u>Winter</u>						
0 $^{\circ}$ -10 $^{\circ}$ N	.65	.87	-2.26	-2.02	-1.61	-1.15
10 $^{\circ}$ -20 $^{\circ}$ N	.52	.71	-1.88	-1.98	-1.36	-1.27
20 $^{\circ}$ -30 $^{\circ}$ N	.40	.57	-1.55	-1.70	-1.15	-1.13
30 $^{\circ}$ -40 $^{\circ}$ N	.31	.44	-1.27	-1.31	-.96	-.87
40 $^{\circ}$ -50 $^{\circ}$ N	.19	.30	-.96	-1.09	-.77	-.79
50 $^{\circ}$ -60 $^{\circ}$ N	.09	.15	-.74	-1.03	-.65	-.88

The theoretically derived values for \overline{SW} and \overline{LW} are consistent with observational data. Therefore, they will now be utilized in the calculation of the tropospheric required warming, \overline{RW} . Also, both cloud-free and mean cloudiness radiation estimates will be used in separate computations of \overline{RW} so that a more complete understanding of the diurnal variation of tropospheric energy processes is obtained.

4. DIURNAL VARIATION OF TROPOSPHERIC REQUIRED WARMING

The determination of the mean observed 12-hour temperature difference ($\overline{\Delta T}$) and the net radiative cooling rate ($\overline{SW} + \overline{LW}$) allows the calculation of the required layer warming (\overline{RW}). Thus, the diurnal nature of the required warming term can be ascertained.

4.1 Computational Procedures

Equation 1.7 from Chapter 1, describes the relationship between the local temperature change, the net radiative cooling rate, and the tropospheric required warming:

$$\overline{\Delta T} = \overline{SW} + \overline{LW} + \overline{RW}$$

The above equation was solved for \overline{RW} in each geographical block. $\overline{\Delta T}$ and \overline{LW} are applied directly from Tables 2.5 and 3.2, respectively. However, an additional computation must be performed with the \overline{SW} term. From Table 3.1 the total heating due to solar radiation absorption throughout the daylight hours is obtained, and the distribution of this heating between sunrise and sunset is then determined from the short wave radiational model. The model calculates the heating rate in each of 23 time increments between sunrise and noon and assumes an identical distribution from noon to sunset. By applying the results of this procedure to the total heating value, a time distribution of each particular increment's contribution to the total heating from sunlight hours can be obtained. By knowing the heating results from short wave absorption in time increments, the amount of heating in any daylight period can be computed. Figure 4.1 depicts the percentage of warming by solar radiation absorption for each of the 46-time steps in a tropospheric layer situated between 850 mb and 300 mb.

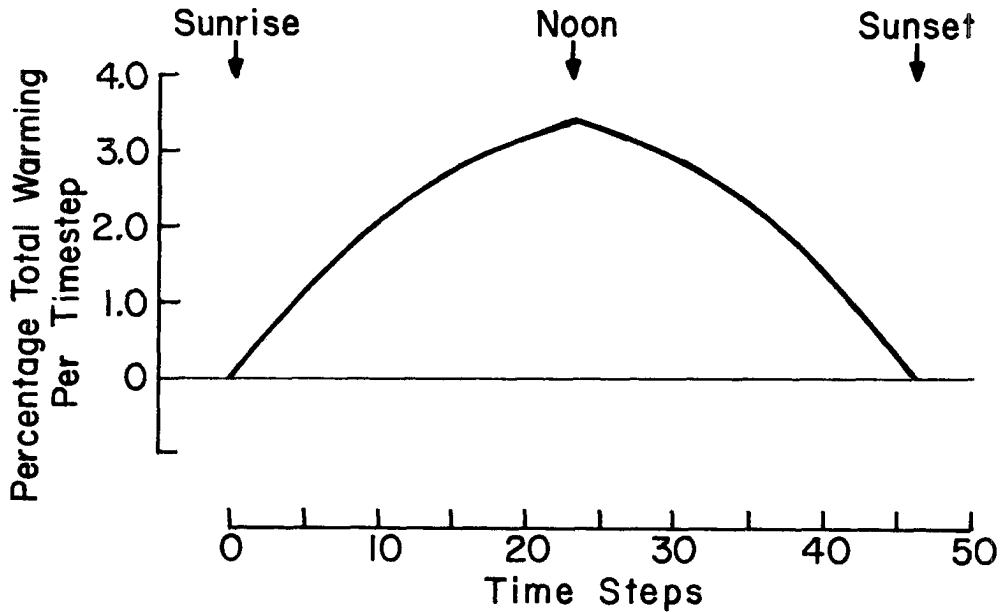


Figure 4.1. Percentage of total warming for each time step in short wave model (Summer, 0-10°N).

Since $\overline{\Delta T}$, \overline{SW} , and \overline{LW} are known quantities, \overline{RW} can be solved for as a residual from Eq. 1.7. A value of \overline{RW} for each 12-hour time interval in each geographical block is calculated, and the diurnal variation of the mean required warming through a deep tropospheric layer is determined. Table 4.1 exhibits the values of $\overline{\Delta T}$, \overline{SW} , \overline{LW} , and \overline{RW} for the 12-hour periods from 00GMT to 12GMT and 12GMT to 00GMT during the summer, and Table 4.2 includes the same information for winter. The required warming (\overline{RW}) can then be examined relative to the local times of the standard observations, and a depiction of the diurnal cycle in required tropospheric warming is obtained. Figures 4.2 and 4.3 show the diurnal variability of \overline{RW} which must occur in order to explain the observed temperature difference and the continual net radiative cooling of the troposphere. Figures 4.2a through 4.2f contain information for the summer season in 10° latitudinal bands and Figures 4.3a through 4.3f are the winter values of \overline{RW} .

TABLE 4.1

Summer Observed and calculated 12-hour differences in temperature ($\overline{\Delta T}$), solar heating (\overline{SW}), infrared cooling (\overline{LW}), and required warming (\overline{RW}) for each geographical block. Units: °C/12 hrs.

Latitude Belt	Longitude Block	00Z to 12Z				12Z to 00Z			
		$\overline{\Delta T}$	\overline{SW}	\overline{LW}	\overline{RW}	$\overline{\Delta T}$	\overline{SW}	\overline{LW}	\overline{RW}
0°-10°N	+5	-.33	.04	-1.22	.85	.33	.70	-1.22	.85
	+13	-.36	.50	-1.21	.35	.36	.22	-1.21	1.35
	+14	-.30	.53	-1.19	.36	.30	.18	-1.19	1.31
	+15	-.13	.54	-1.18	.51	.13	.11	-1.18	1.20
10°-20°N	+4	.07	.05	-.97	.99	-.07	.64	-.97	.26
	+5	-.25	.03	-.98	.70	.25	.67	-.98	.56
	+6	-.26	.01	-1.02	.75	.26	.70	-1.02	.58
	+10	-.77	.20	-.94	-.03	.77	.44	-.94	1.27
	+11	-.62	.28	-1.01	.11	.62	.39	-1.01	1.24
	+13	-.40	.43	-1.05	.22	.40	.29	-1.05	1.16
	+14	-.35	.57	-1.17	.25	.35	.17	-1.17	1.35
+16	-.10	.67	-1.08	.31	.10	.10	-1.08	1.13	
20°-30°N	+5	-.33	.05	-1.02	.64	.33	.71	-1.02	.64
	+6	-.70	.01	-.99	.28	.70	.75	-.99	.94
	+10	-.69	.17	-.82	-.04	.69	.56	-.82	.95
	+11	-.67	.24	-.91	.02	.67	.45	-.91	1.13
	+12	-.18	.36	-.90	.36	.18	.36	-.90	.72
+14	-.07	.49	-1.03	.47	.07	.24	-1.03	.86	
30°-40°N	+3	.28	.14	-.81	.95	-.28	.57	-.81	-.04
	+4	-.10	.12	-.90	.68	.10	.67	-.90	.33
	+5	-.34	.06	-.92	.52	.34	.69	-.92	.57
	+6	-.65	.06	-.98	.27	.65	.70	-.98	.93
	+7*	-.98	.06	-.85	-.19	.98	.74	-.85	1.09
	+8A	-.58	.11	-.77	.15	.58	.65	-.77	.91
	+8B*	-.79	.12	-.84	-.14	.79	.59	-.84	.83
	+13	-.35	.44	-.94	.15	.35	.30	-.94	.99
40°-50°N	+3	.32	.14	-.80	.98	-.32	.57	-.80	-.09
	+4	-.05	.11	-.77	.71	.05	.60	-.77	.12
	+5	-.28	.11	-.82	.43	.28	.63	-.82	.47
	+6	-.54	.10	-.84	.20	.54	.67	-.84	.71
	+7A*	-.53	.04	-.74	.17	.53	.70	-.74	.57
	+7B*	-.89	.04	-.74	-.19	.89	.71	-.74	.92
	+8A	-.81	.05	-.69	-.17	.81	.60	-.69	.90
	+8B*	-.91	.07	-.69	-.30	.92	.66	-.69	.95
	+10	-.51	.20	-.68	-.03	.51	.46	-.68	.73
50°-60°N	+2	.39	.21	-.71	.89	-.39	.46	-.71	-.14
	+3	-.01	.16	-.65	.48	.01	.54	-.65	.12
	+4	-.10	.12	-.67	.45	.10	.63	-.67	.14

TABLE 4.1 (cont'd)

Latitude Belt	Longitude Block	00Z to 12Z				12Z to 00Z			
		$\overline{\Delta T}$	\overline{SW}	\overline{LW}	\overline{RW}	$\overline{\Delta T}$	\overline{SW}	\overline{LW}	\overline{RW}
50°-60°N	+5	-.35	.10	-.62	.17	.35	.59	-.62	.38
	+6	-.51	.06	-.64	.07	.51	.65	-.64	.50
	+7*	-.45	.07	-.66	.14	.45	.67	-.66	.44
	+8	-.63	.17	-.59	-.21	.63	.59	-.59	.63
	+9	-.73	.19	-.61	-.31	.73	.50	-.61	.84
	+10	-.56	.21	-.60	-.17	.56	.48	-.60	.68
	+11	-.61	.27	-.60	-.28	.61	.37	-.60	.84
	+12	-.33	.32	-.64	-.01	.33	.32	-.64	.65

*For 700-300 mb layer.

TABLE 4.2

Winter Observed and calculated 12-hour differences in temperature ($\overline{\Delta T}$), solar heating (\overline{SW}), infrared cooling (\overline{LW}), and required warming (\overline{RW}) for each geographical block. Units: $^{\circ}\text{C}/12$ hrs.

Latitude Belt	Longitude Block	00Z to 12Z				12Z to 00Z			
		$\overline{\Delta T}$	\overline{SW}	\overline{LW}	\overline{RW}	$\overline{\Delta T}$	\overline{SW}	\overline{LW}	\overline{RW}
0 $^{\circ}$ -10 $^{\circ}$ N	+5	-.28	--	-1.13	.85	.28	.66	-1.13	.75
	+13	-.42	.38	-1.17	.37	.42	.28	-1.17	1.31
	+14	-.27	.49	-1.13	.37	.27	.15	-1.13	1.25
	+15	-.34	.51	-1.11	.26	.34	.10	-1.11	1.35
10 $^{\circ}$ -20 $^{\circ}$ N	+4	.11	.04	-.93	1.00	-.11	.48	-.93	.34
	+5	-.09	--	-.87	.78	.09	.49	-.87	.47
	+6	-.15	--	-.98	.83	.15	.53	-.98	.60
	+10	-.64	.12	-.91	.15	.64	.37	-.91	1.18
	+11	-.58	.20	-.90	.12	.58	.29	-.90	1.19
	+13	-.29	.33	-1.01	.39	.29	.20	-1.01	1.10
	+14	-.17	.41	-1.04	.46	.17	.13	-1.04	1.08
+16	.00	.52	-1.00	.48	.00	.03	-1.00	.97	
20 $^{\circ}$ -30 $^{\circ}$ N	+5	-.21	--	-.82	.61	.21	.48	-.82	.55
	+6	-.34	--	-.73	.39	.34	.40	-.73	.67
	+7	-.52	.01	-.68	.15	.52	.35	-.68	.85
	+10	-.56	.09	-.70	.05	.56	.27	-.70	.99
	+11	-.54	.15	-.84	.15	.54	.31	-.84	1.07
	+12	-.38	.19	-.72	.15	.38	.19	-.72	.91
	+14	-.23	.34	-.89	.32	.23	.11	-.89	1.01
+15	-.25	.39	-.88	.24	.25	.04	-.88	1.09	
30 $^{\circ}$ -40 $^{\circ}$ N	+3	.26	.05	-.74	.95	-.26	.26	-.74	.22
	+4	-.20	.02	-.75	.53	.20	.34	-.75	.61
	+5	-.14	--	-.62	.48	.14	.29	-.62	.47
	+6	-.29	--	-.64	.35	.29	.27	-.64	.66
	+7*	-.44	--	-.58	.14	.44	.29	-.58	.73
	+8A	-.30	.04	-.58	.24	.30	.26	-.58	.62
	+8B*	-.43	.04	-.64	.17	.43	.26	-.64	.81
	+13	-.17	.19	-.60	.24	.17	.13	-.60	.64
+15	-.16	.33	-.74	.25	.16	.03	-.74	.87	
40 $^{\circ}$ -50 $^{\circ}$ N	+4	+.14	--	-.52	.66	-.14	.19	-.52	.19
	+5	-.14	--	-.49	.35	.14	.18	-.49	.45
	+6	-.18	--	-.50	.32	.18	.18	-.50	.50
	+7*	-.19	--	-.50	.31	.19	.20	-.50	.49
	+8A	-.25	--	-.47	.21	.25	.13	-.47	.56
	+8B*	-.23	.01	-.48	.24	.23	.19	-.48	.52
	+10	-.32	.04	-.44	.08	.32	.14	-.44	.62
50 $^{\circ}$ -60 $^{\circ}$ N	+3	.21	--	-.38	.59	-.21	.07	-.38	.10

TABLE 4.2 (cont'd)

Latitude Belt	Longitude Block	00Z to 12Z				12Z to 00Z			
		$\overline{\Delta T}$	\overline{SW}	\overline{LW}	\overline{RW}	$\overline{\Delta T}$	\overline{SW}	\overline{LW}	\overline{RW}
50°-60°N	+4	-.01	--	-.42	.41	.01	.09	-.42	.34
	+5	-.06	--	-.38	.32	.06	.09	-.38	.35
	+6	-.06	--	-.41	.35	.06	.09	-.41	.38
	+7*	-.11	--	-.47	.36	.11	.10	-.47	.49
	+8	-.24	--	-.27	.03	.24	.06	-.27	.45
	+10	-.24	.02	-.39	.13	.24	.05	-.39	.58
	+11	-.29	.02	-.40	.09	.29	.05	-.40	.64
	+12	-.36	.05	-.37	-.04	.36	.05	-.37	.68

*For 700-300 mb layer.

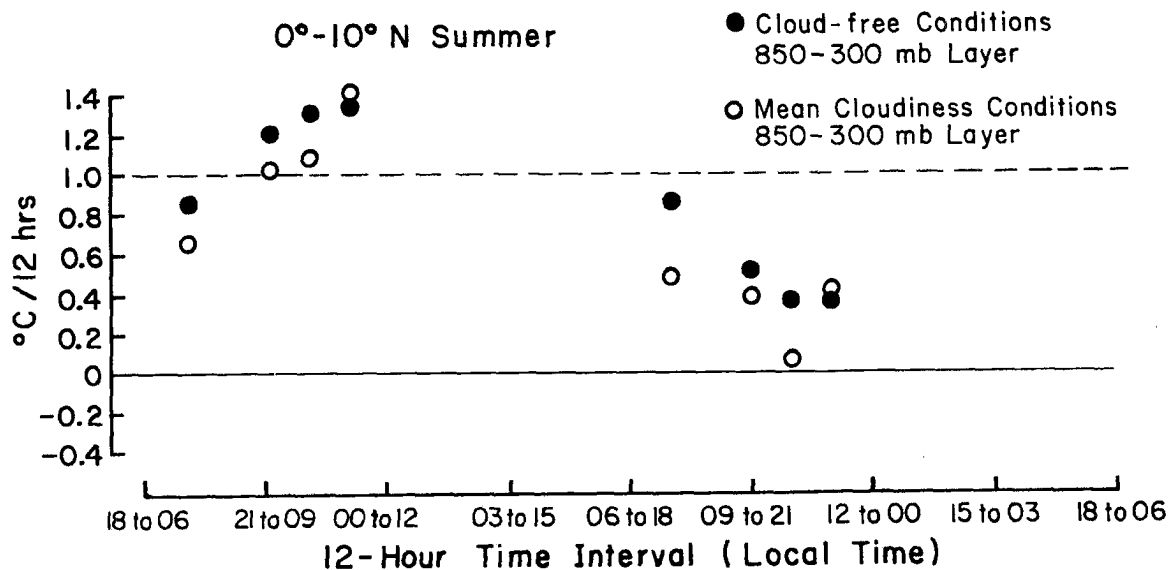


Fig. 4.2a. Diurnal variation of required warming (\overline{RW}) from 0-10°N latitude in the summer (850-300 mb layer-surface elevation <500 m; 700-300 mb layer-surface elevation 7500 m.). 18 to 06 means 1800 LT to 0600 LT.

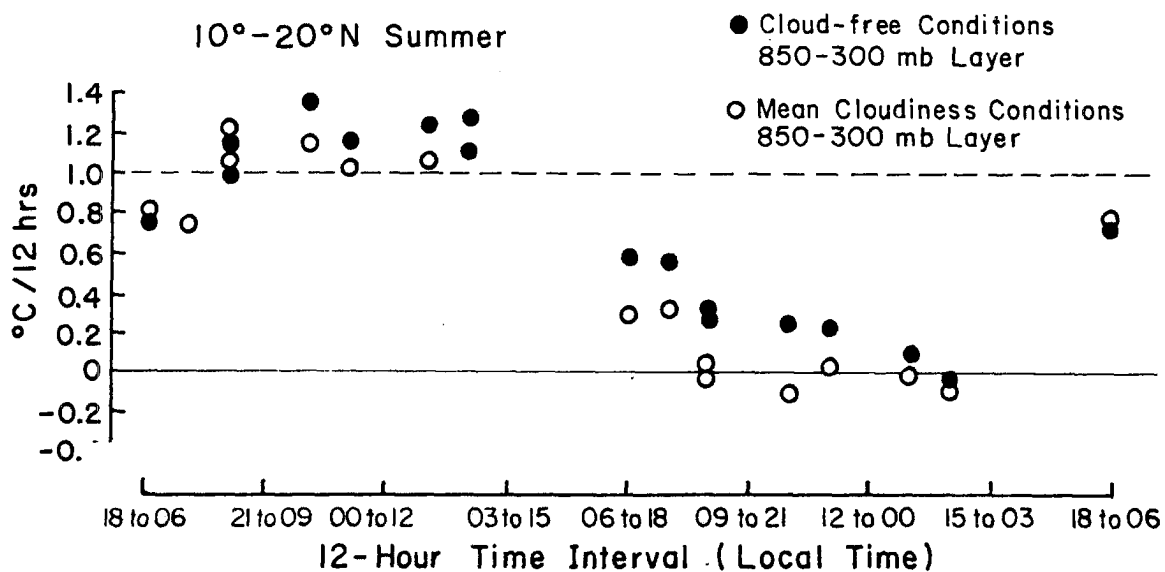


Fig. 4.2b. Same as Fig. 4.2a for 10-20°N.

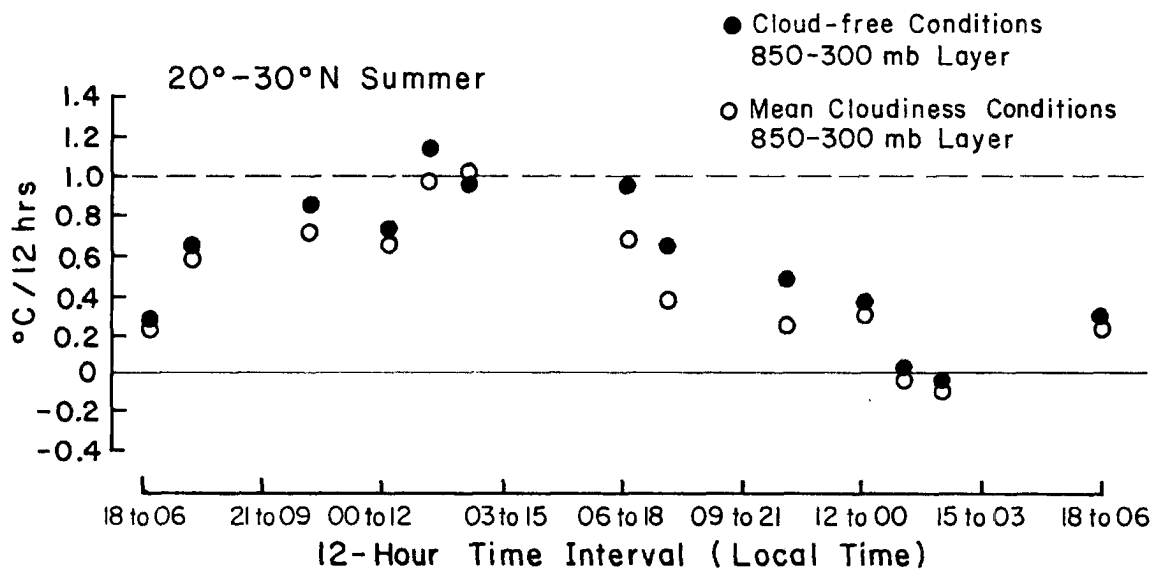


Fig. 4.2c. Same as Fig. 4.2a for 20-30°N.

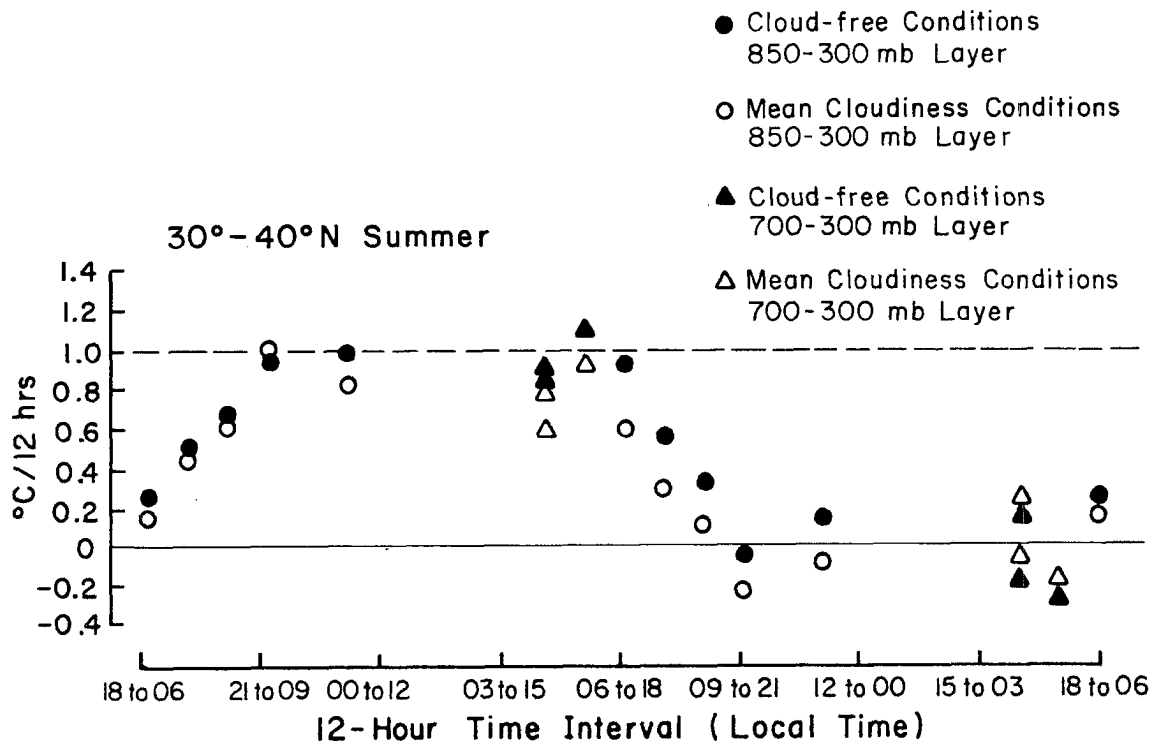


Fig. 4.2d. Same as Fig. 4.2a for 30-40°N.

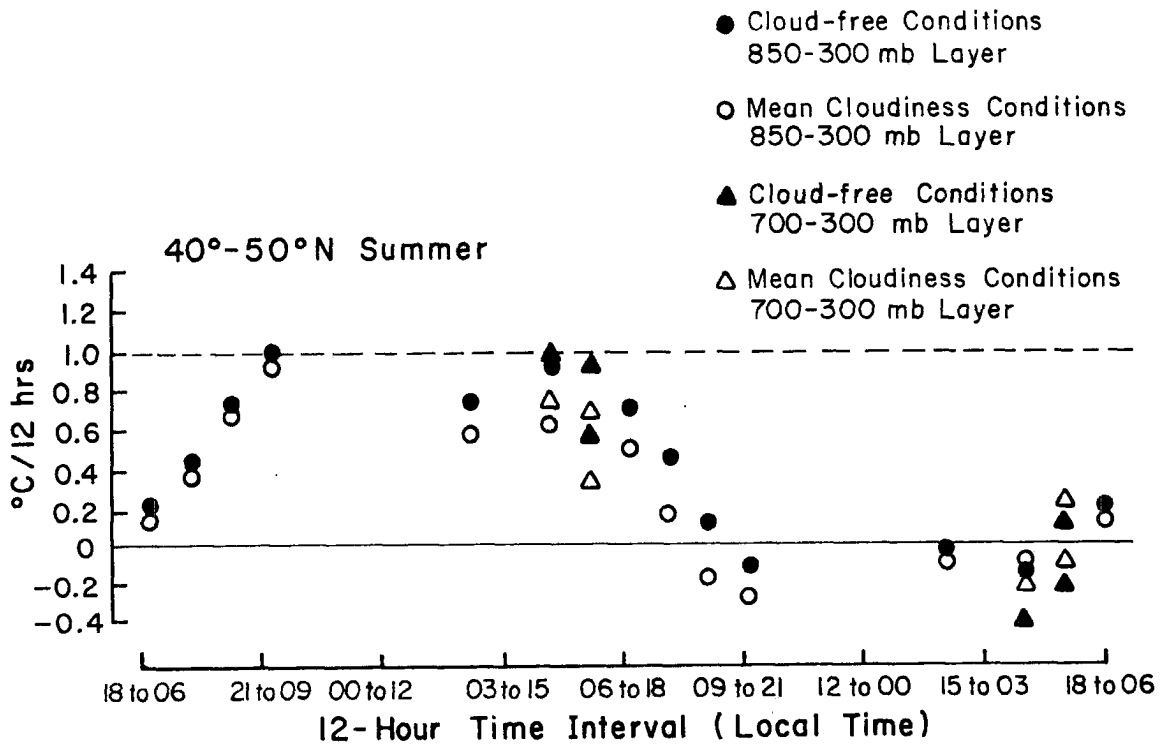


Fig. 4.2e. Same as Fig. 4.2a for 40-50°N

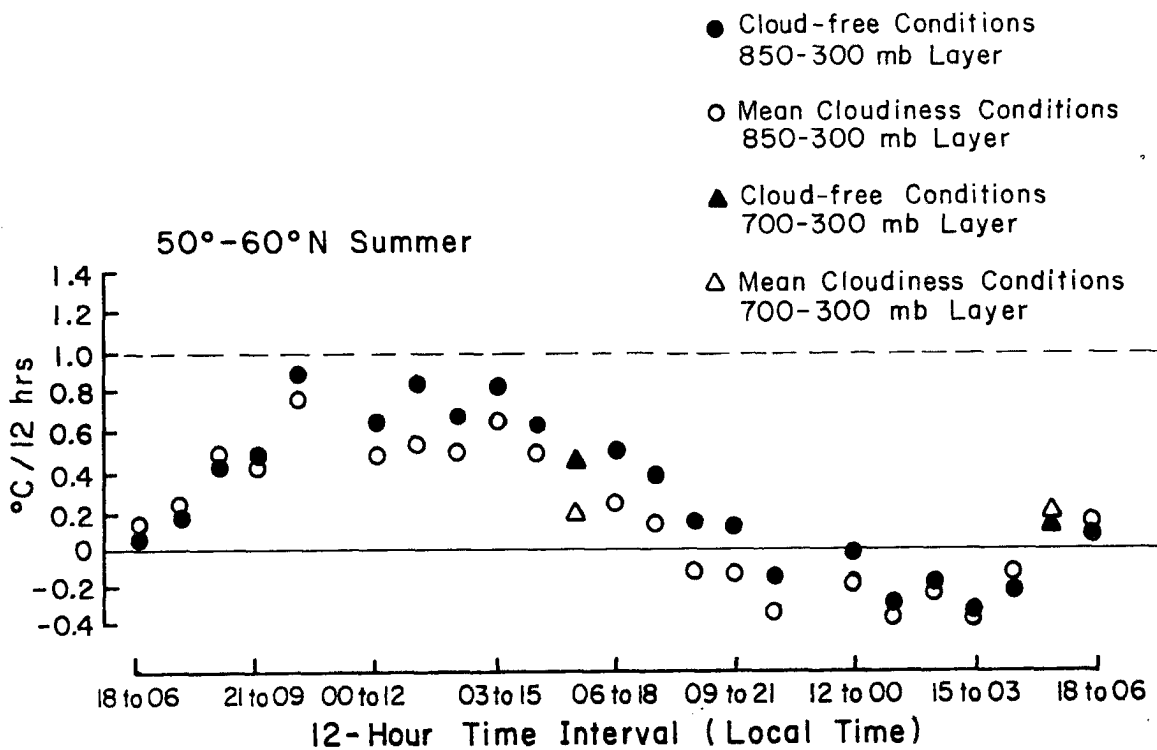


Fig. 4.2f. Same as Fig. 4.2a for 50-60°N.

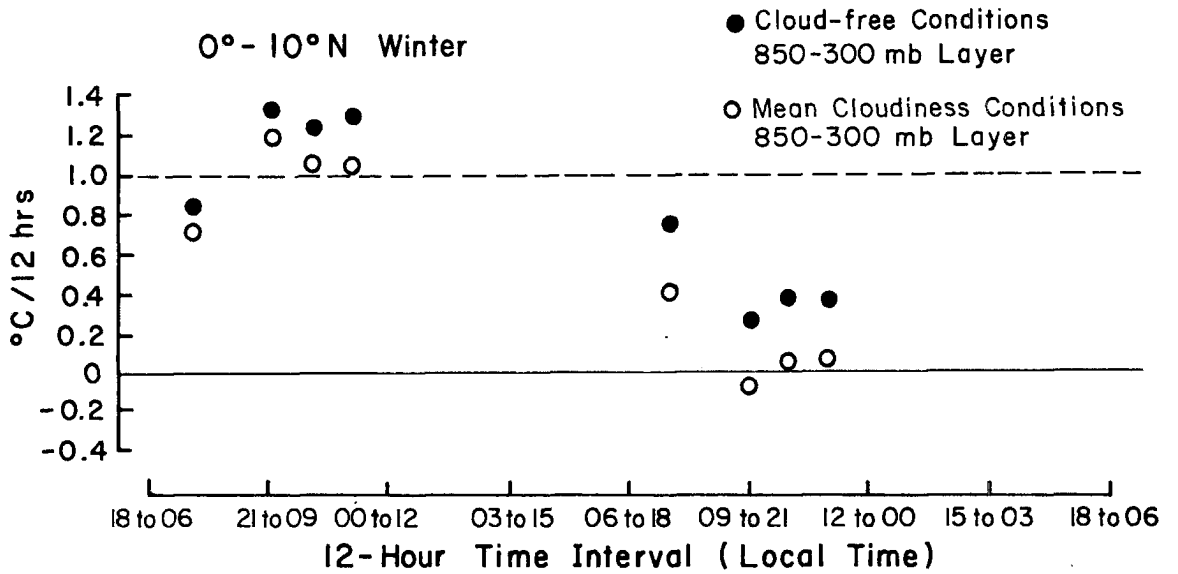


Fig. 4.3a. Diurnal variation of required warming (\overline{RW}) from 0-10°N latitude in the winter (850-300 mb layer - surface elevation <500 m; 700-300 mb layer-surface elevation >500 m.). 18 to 06 means 1800LT to 0600 LT.

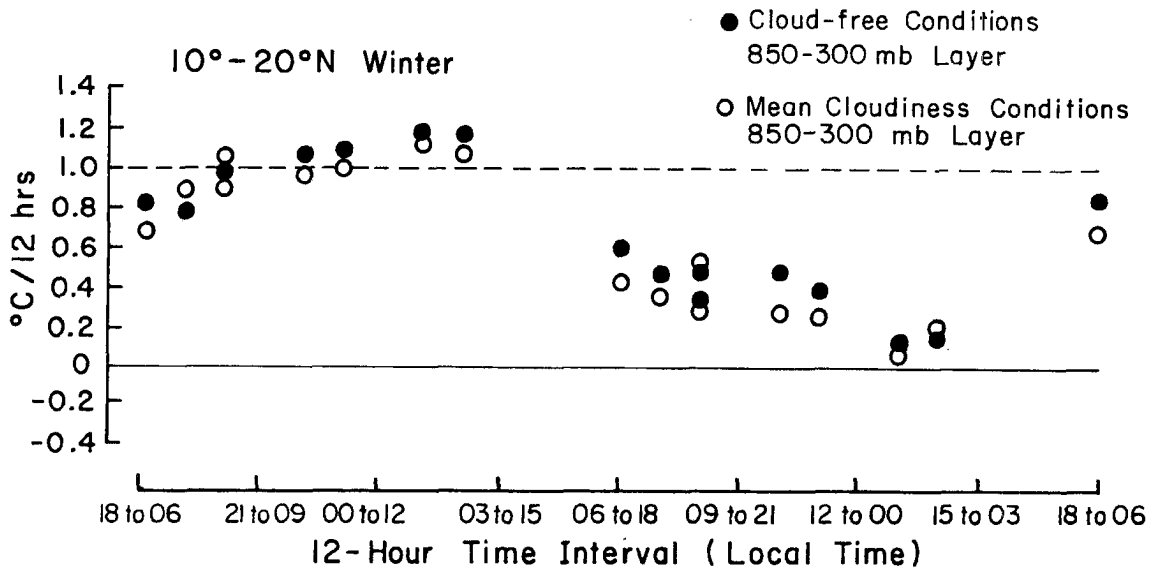


Fig. 4.3b. Same as Fig. 4.3a for 10-20°N.

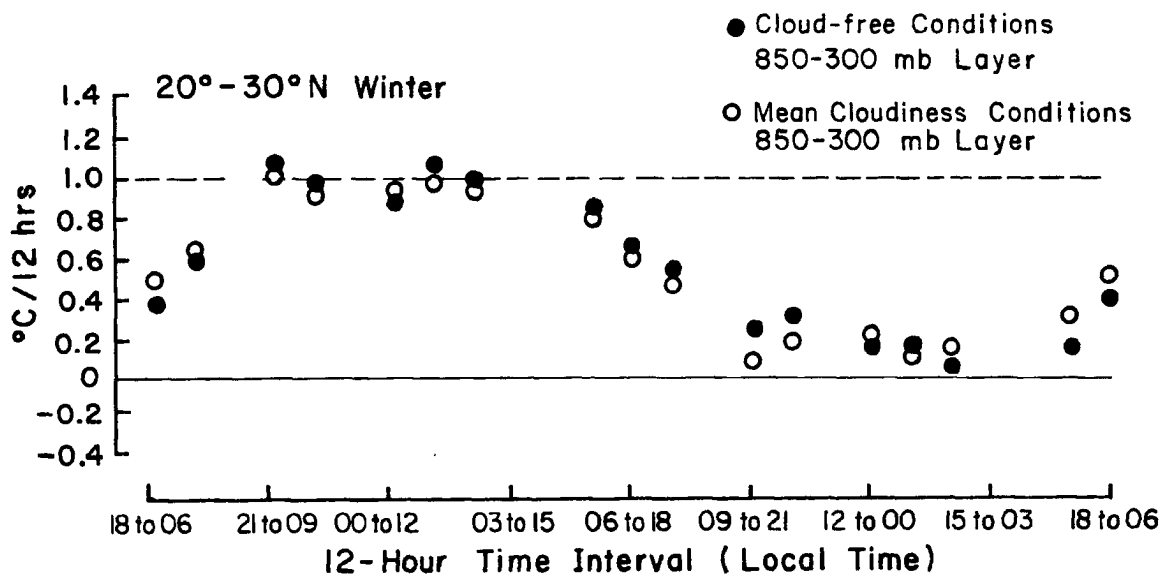


Fig. 4.3c. Same as Fig. 4.3a for 20-30°N.

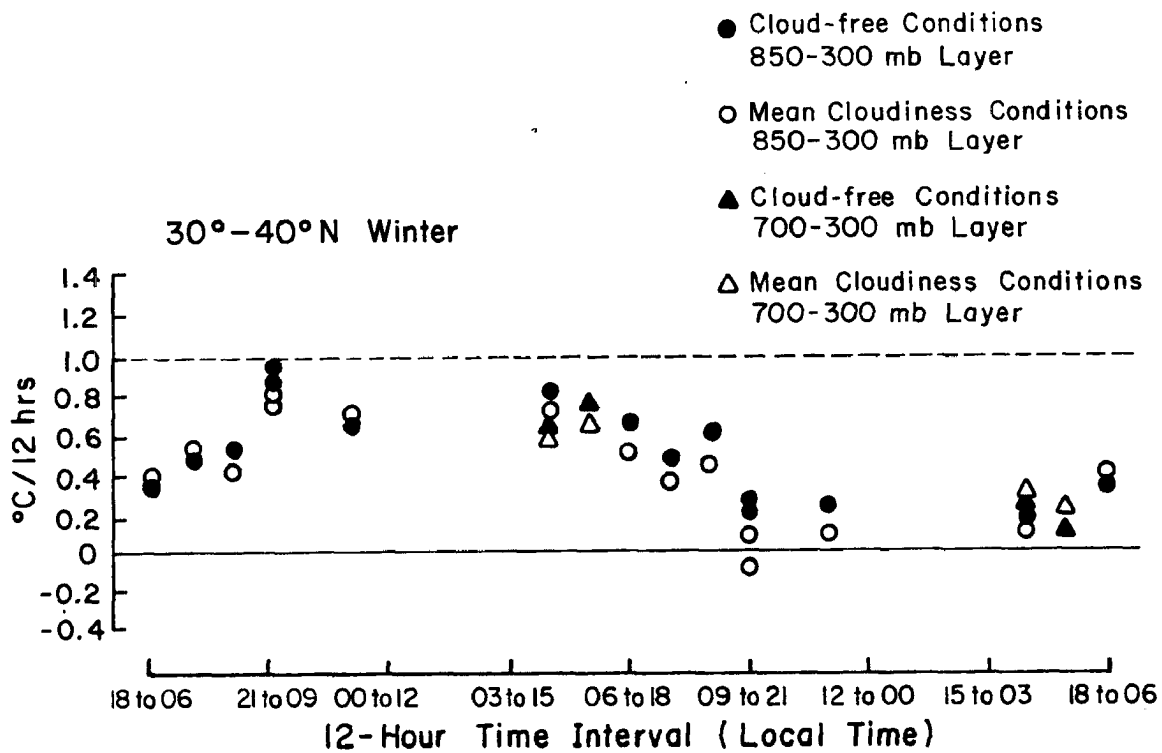


Fig. 4.3d. Same as Fig. 4.3a for 30-40°N.

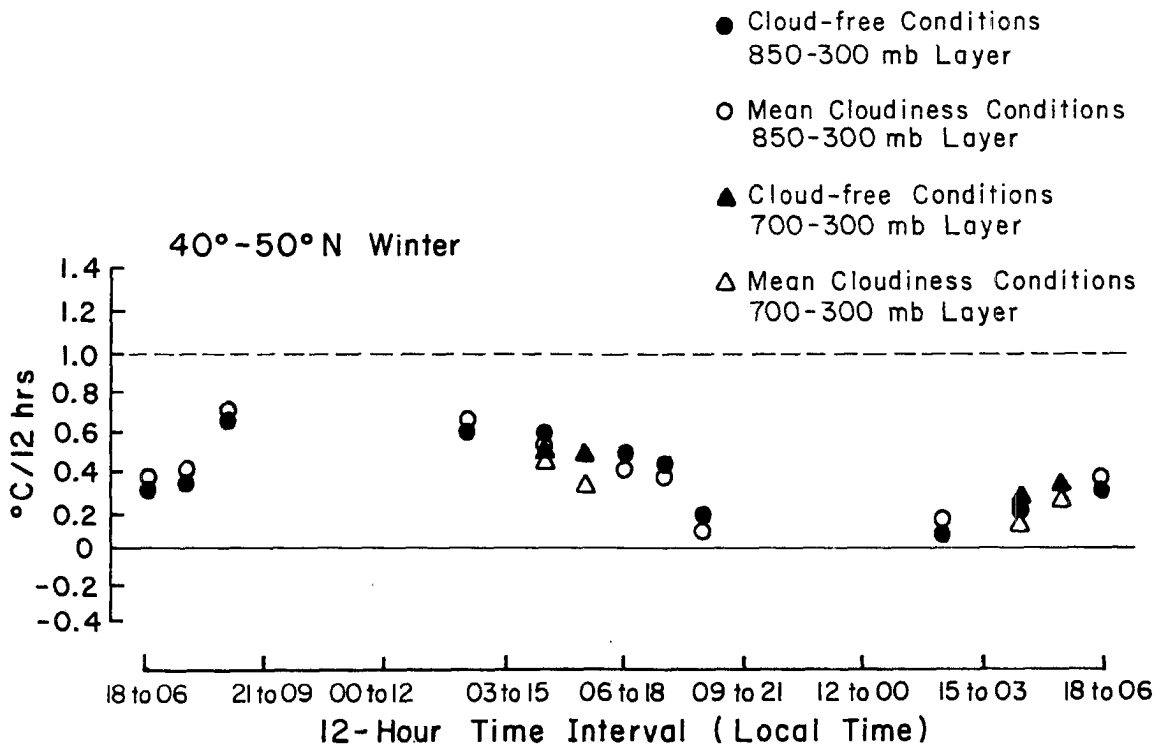


Fig. 4.3e. Same as Fig. 4.3a for 40-50°N.

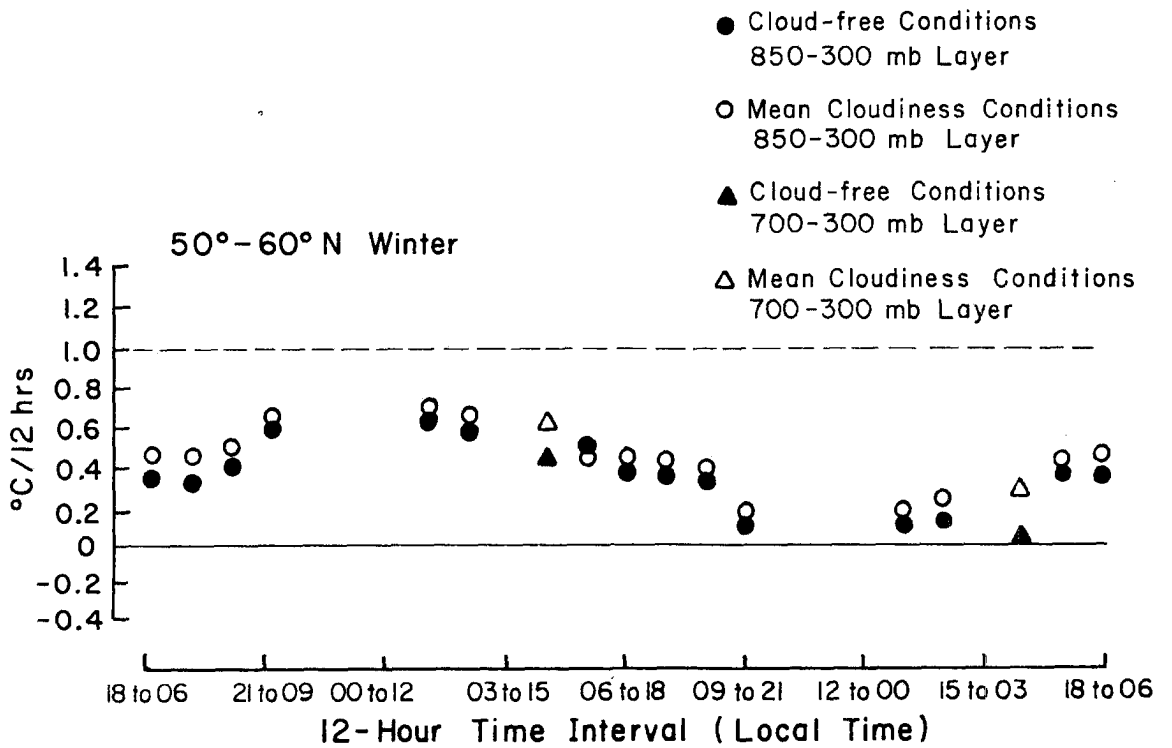


Fig. 4.3f. Same as Fig. 4.3a for 50-60°N.

4.2 Results

An extremely consistent pattern is apparent in each latitudinal band for each season. The maximum required tropospheric warming invariably occurs in the 12-hour time period centered on the early morning hours. During the summer season the range of the \overline{RW} oscillation is maintained throughout all latitudes with a maximum morning magnitude of about 1.0°C for the 12-hour periods. In the winter tropical latitudes maintain approximately a 1.0°C diurnal range while at higher latitudes the variation is reduced to about 0.5°C . This dampening is expected as the solar radiation incident upon the 850-300 mb layer at higher latitudes is reduced during the winter and the observed layer temperature variation is not as great.

The tropical latitudes display very similar patterns in both seasons. This is consistent with the fact that seasonal changes in the tropics are small. Finally, it must be noted that during the afternoon in the summer, small negative values or required cooling conditions are found primarily over the mid-latitudes.¹

Summary. It is apparent that these 12-hour data sets require a pronounced diurnal variation of tropospheric warming with a strong maximum in the morning.

¹These required cooling values should be reduced somewhat due to instrument error (see Appendix C) inherent in the 12-hour temperature change.

5. DAILY REQUIRED WARMING IN THE TROPICS AS DETERMINED FROM SPECIAL TROPICAL EXPERIMENTS

Tropospheric temperature information from special tropical experiments has also been examined to ascertain the relationship of their diurnal variations to those found in the Northern Hemispheric portion of the study.

5.1 GATE Experiment

Recently, upper air data from five United States ships during Phase 3 (29 August - 19 September 1974) of GATE (GARP² Atlantic Tropical Experiment) have been analyzed for diurnal temperature variations. As the GATE data has a much higher time resolution than the standard 12-hour observational period, it has been carefully scrutinized for more refined verifying information, i.e., does this data also exhibit a large diurnally varying compensating warming cycle?

During the 20 day Phase 3 observation period, soundings were taken at 3 hour intervals beginning at 00GMT. The data for this analysis were obtained from five United States research ships - RESEARCHER, GILLIS, DALLAS, OCEANOGRAPHER, and VANGUARD (see Fig. 5.1). Although an effort was made by each ship to launch 8 radiosondes each day, this was not always accomplished due to equipment and other problems. The data collected on all the ships except the VANGUARD have been lag corrected to the reported pressure level. The VANGUARD data could not be corrected by the same process as it utilized a different recording procedure. Nevertheless, this amounts to less than a 2 mb error at

²Global Atmospheric Research Program.

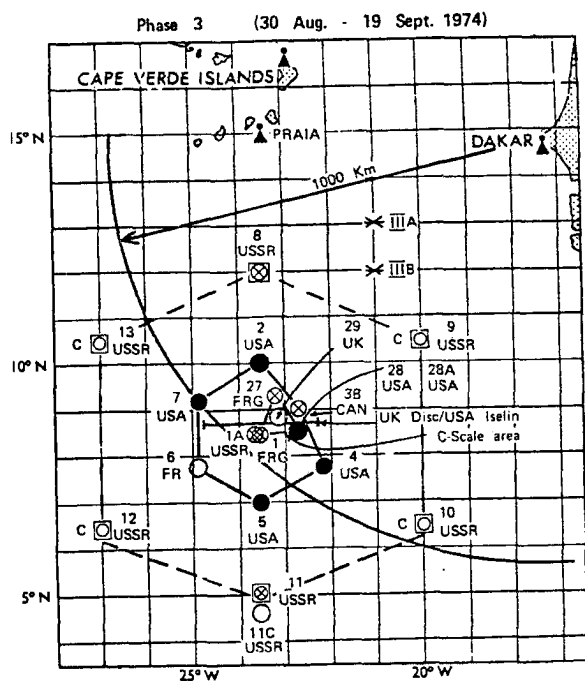


Fig. 5.1. Locations of United States ships RESEARCHER, GILLIS, DALLAS, OCEANOGRAPHER, and VANGUARD during Phase 3 of GATE.

850 mb and 300 mb and can be considered negligible when determining the mean temperature of the 850-300 mb layer. Table 5.1 delineates the number of sonde ascents recorded for each ship at each standard observation time.

TABLE 5.1

Number of Recorded Radiosonde Ascents for Each Ship at Standard Observation Times - Phase 3

(Local Time)	<u>22</u>	<u>01</u>	<u>04</u>	<u>07</u>	<u>10</u>	<u>13</u>	<u>16</u>	<u>19</u>
RESEARCHER	20	7	18	6	19	5	19	5
GILLIS	18	13	19	14	17	9	20	10
DALLAS	14	17	17	16	14	16	15	15
OCEANOGRAPHER	19	20	17	22	21	20	19	18
VANGUARD	19	15	20	15	17	18	17	17
TOTAL	90	72	91	73	86	68	90	65

Mean soundings at each standard observation time for each ship and for the 5 ship experiment mean were calculated, and the mean temperature of the 850-300 mb layer was consequently determined. Table 5.2 shows the observed mean 3-hourly temperature changes for each ship. Table 5.3 exhibits these same temperature changes after a simple overlapping data smoothing technique has been employed. The experiment mean 3-hour temperature change is also included. Figure 5.2 graphically depicts both the smoothed and observed data.

The solar radiation model and the infrared radiation model discussed in Appendix D were utilized to ascertain mean values of heating from short wave absorption and cooling due to long wave irradiance in the 850 to 300 mb layer. The 1300 LT mean 5 ship sounding supplied the radiative parameters used in the solar heating calculations, and the 0400 LT mean sounding was used in the infrared cooling model. The choice of these times is discussed in Appendix D. Humidity measurements taken in the daylight hours are considered quite accurate. The humidity sensing element on the standard NOAA radiosonde has recently been modified, and GATE was the first special tropical experiment to utilize this improved instrument. Table 5.4 indicates the cloud-free values obtained from the radiational models. Also included are the calculated mean cloudiness heating values from Doplick (1970) in the 0-10°N latitude belt for summer.

This profile exhibits a distinct maximum of required warming during the early morning hours and a minimum in mid afternoon which is consistent with the results of the 12-hour data set.

TABLE 5.2

Observed Mean 3-hourly Temperature Changes in the 850-300 mb Layer
During Phase 3 of GATE ($^{\circ}\text{C}$)

	<u>22-01</u>	<u>01-04</u>	<u>04-07</u>	<u>07-10</u>	<u>10-13</u>	<u>13-16</u>	<u>16-19</u>	<u>19-22</u>
RESEARCHER	+0.10	-.40	+0.33	+0.32	+0.09	-.50	+0.28	-.22
GILLIS	-.08	-.05	+0.09	+0.05	+0.60	-.46	+0.05	-.20
DALLAS	-.11	-.14	+0.06	+0.09	-.03	+0.18	-.29	+0.24
OCEANOGRAPHER	-.16	+0.07	+0.11	+0.08	+0.15	-.04	-.12	-.09
VANGUARD	-.14	-.21	+0.33	-.13	+0.34	-.24	+0.19	-.14

TABLE 5.3

Smoothed Mean 3-hourly Temperature Changes in the 850-300 mb Layer
During Phase 3 of GATE ($^{\circ}\text{C}$)

$$[\overline{\Delta T}_s = .25 (\overline{\Delta T}_{\text{Before}}) + .5 (\overline{\Delta T}) + .25 (\overline{\Delta T}_{\text{After}})]$$

	<u>22-01</u>	<u>01-04</u>	<u>04-07</u>	<u>07-10</u>	<u>10-13</u>	<u>13-16</u>	<u>16-19</u>	<u>19-22</u>
RESEARCHER	-.11	-.09	+0.15	+0.27	.00	-.16	-.04	-.02
GILLIS	-.11	-.02	+0.05	+0.20	+0.20	-.07	-.14	-.11
DALLAS	-.03	-.08	+0.02	+0.05	+0.05	+0.01	-.04	+0.02
OCEANOGRAPHER	-.09	+0.02	+0.09	+0.11	+0.09	-.01	-.09	-.12
VANGUARD	-.16	-.06	+0.08	+0.10	+0.08	+0.01	.00	-.06
EXPERIMENT AVERAGE	-.10	-.05	+0.08	+0.15	+0.08	-.04	-.06	-.06

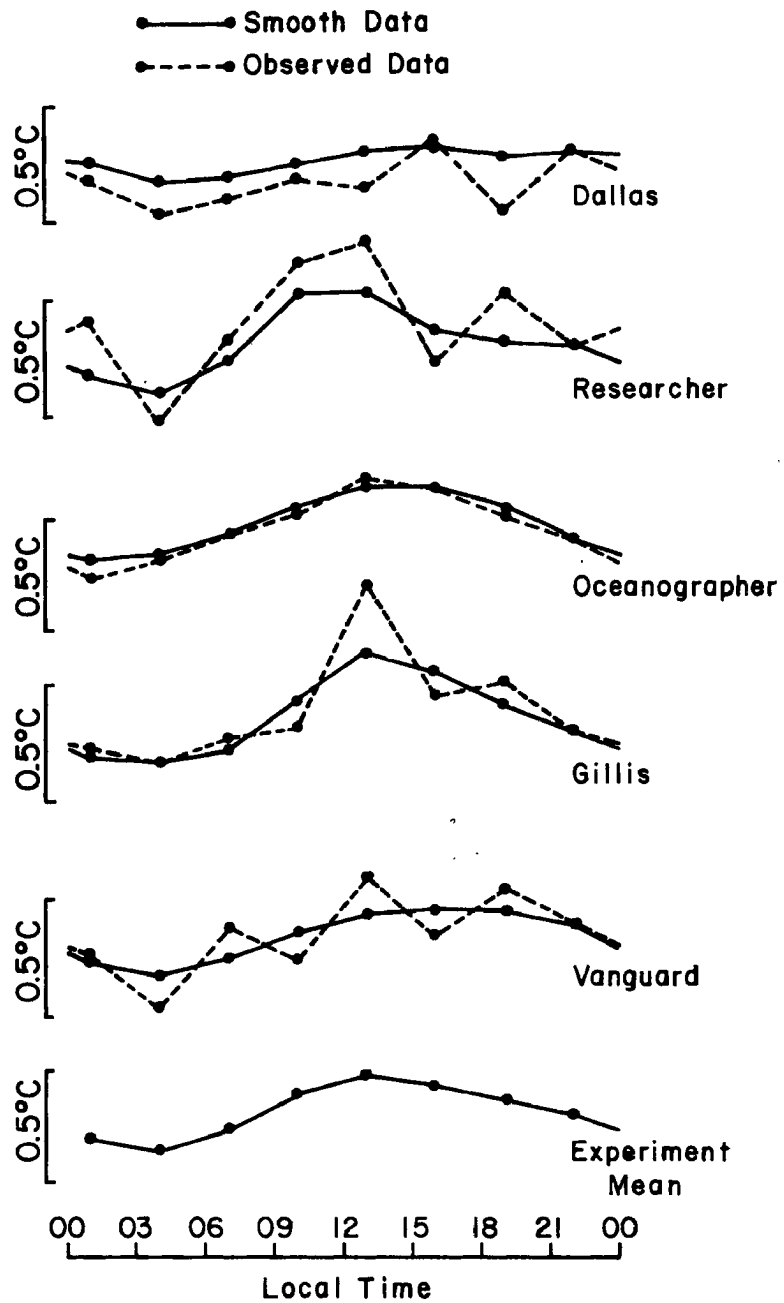


Fig. 5.2. Diurnal variation of the mean temperature for the 850-300 mb layer for Phase 3 of GATE.

TABLE 5.4

Radiative Heating and Cooling in GATE Region

	Heating from SW (°C/daylight hrs)	Cooling from IR (°C/day)	Net Cooling (°C/day)
Cloud-Free	.72	-2.32	-1.60
Mean Cloudiness	.94	-2.06	-1.12

(Dopplick, 1970)

The required warming to balance the observed temperature change and the net radiational cooling can also be resolved in 3-hour time segments. Table 5.5 portrays these values for the experiment mean and Fig. 5.3 is the graphical depiction. Required warming is maximum in the late evening and early morning hours.

TABLE 5.5

Experiment Mean Values of Temperature Change, Solar Heating, Infrared Cooling, and Required Warming for Each 3-hour Interval Between Standard Observation Times

(Local Time)		22-01	01-04	04-07	07-10	10-13	13-16	16-19	19-22
	$\overline{\Delta T}$	-.10	-.05	+.08	+.15	+.08	-.04	-.06	-.06
Cloud-free	\overline{SW}	----	----	+.03	+.17	+.27	+.19	+.05	----
	\overline{IR}	-.29	-.29	-.29	-.29	-.29	-.29	-.29	-.29
	\overline{RW}	+.19	+.24	+.34	+.27	+.10	+.06	+.18	+.23
Mean Cloudiness	ΔT	-.10	-.05	+.08	+.15	+.08	-.04	-.06	-.06
	\overline{SW}	----	----	+.04	+.22	+.35	+.25	+.06	----
	\overline{IR}	-.26	-.26	-.26	-.26	-.26	-.26	-.26	-.26
	\overline{RW}	+.16	+.21	+.30	+.13	-.01	-.03	+.14	+.20

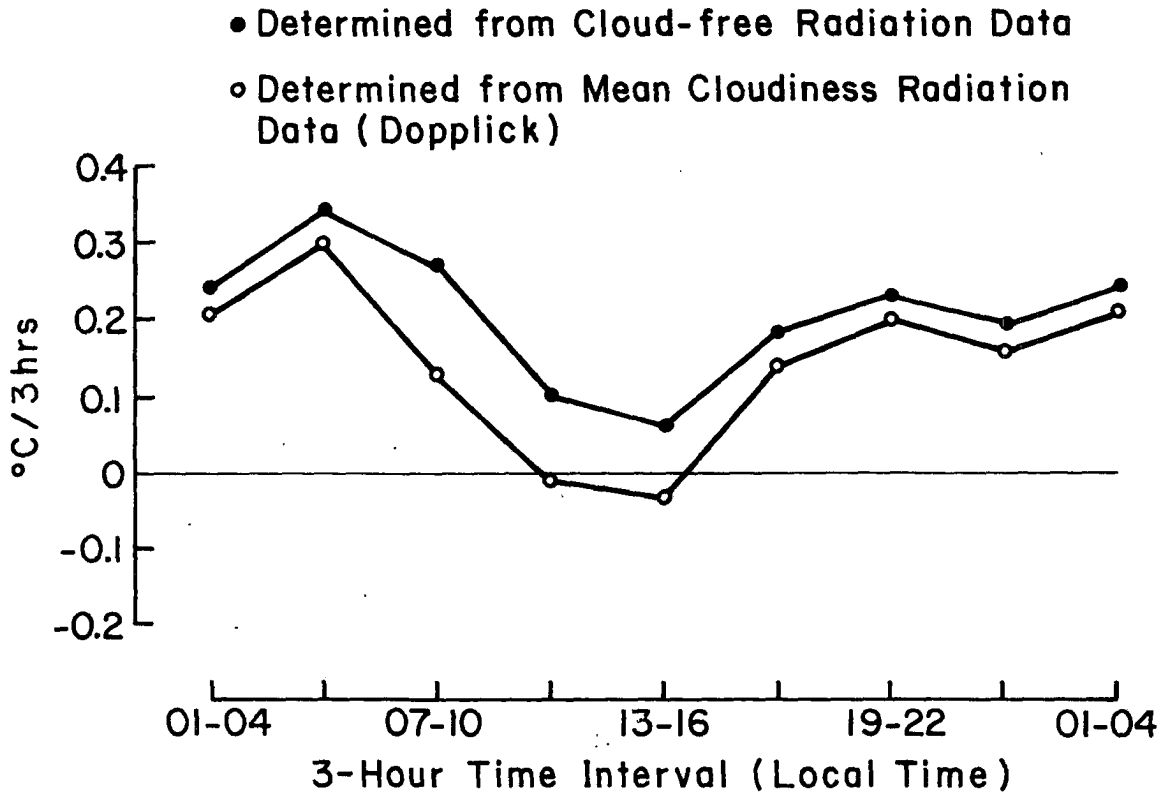


Fig. 5.3. Diurnal variation of required warming (RW) during Phase 3 of GATE.

5.2 Atlantic Trade-Wind Experiment (ATEX)

In February 1969 the Federal Republic of Germany and the U.S. conducted a meteorological air-sea exchange experiment in the North Atlantic trade-wind region. Three ships were situated to form a triangle with sides about 700 to 750 km, and a fourth ship was included within the triangular area. Figure 5.4 illustrates the positions and directions of movement for the four ships.

The DISCOVERER utilized the USWB-403-x radiosonde throughout the observation period which extended from 4 February until 23 February

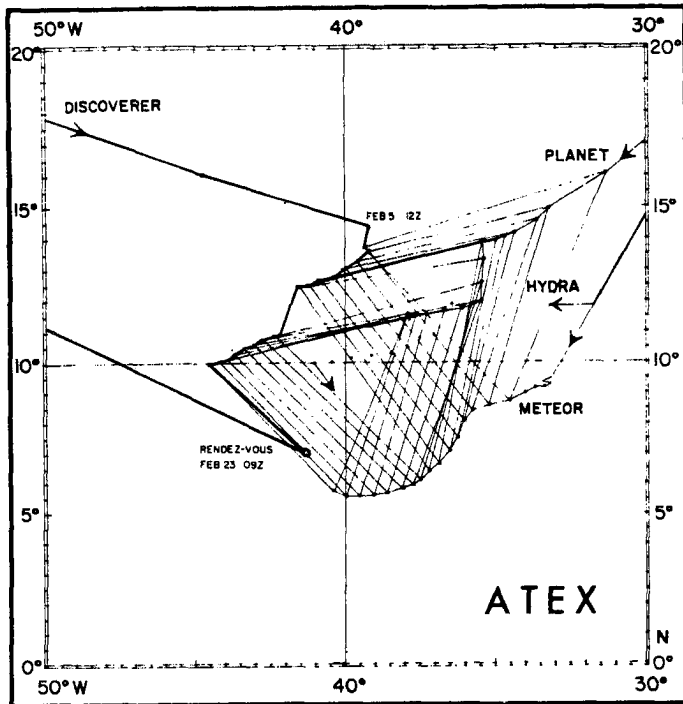


Fig. 5.4. Drift positions of the four ships--DISCOVERER, METEOR, PLANET, and HYDRA--participating in ATEX, February 5-23, 1969. From Brünner, *et al.* (1973).

1969. Observations were scheduled for every three hours. Not all soundings were successfully taken on this schedule, however (Table 5.6). The PLANET and METEOR released upper air radiosondes (USWB-403-x) at only 0900 and 2100 GMT, and the HYDRA confined its observations to the lower 5000 m. Data from ATEX was compiled by Brünner, Ostapoff and Schmidt (1973).

The mean 3-hourly temperature change in the 850-300 mb layer from data collected by the DISCOVERER is displayed in Table 5.7 and illustrated in Fig. 5.5. This diurnal variation of the temperature in the middle troposphere is consistent with the observations from the GATE.

Utilizing the winter cloud-free and mean cloudiness radiational heating and cooling values for 10° latitude, and applying previously discussed computational procedures for determining the required warming in the troposphere, the diurnal profile in Fig. 5.6 was constructed.

TABLE 5.6

Number of Soundings Obtained by Each Ship at Standard Observation Times
During ATEX

(Local Time)	21	00	03	06	09	12	15	18
Discoverer	16	14	16	17	14	17	15	13
Planet			18					15
Meteor (began sounding program 6 days earlier than other ships)			24					22

TABLE 5.7

Mean Temperature Change in 850-300 mb Layer ($\overline{\Delta T}$) Between Observation
Times

(Local Time)	21-00	00-03	03-06	06-09	09-12	12-15	15-18	18-21
$\overline{\Delta T}$ ($^{\circ}\text{C}/3\text{hrs}$)	-.09	-.01	+.10	+.40	+.09	-.10	-.10	-.29

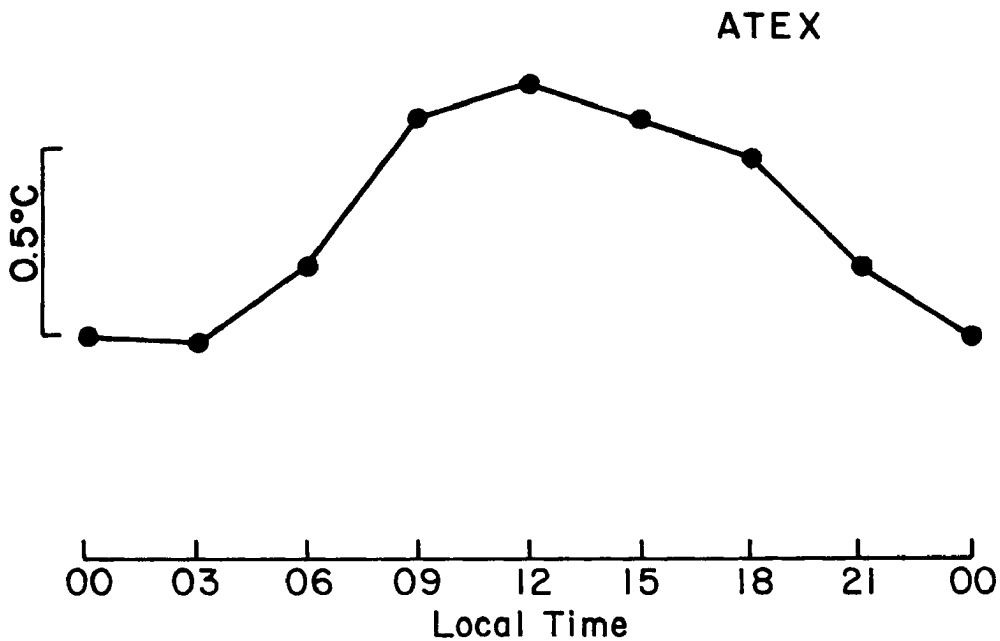


Fig. 5.5. Diurnal temperature variation of the 850-300 mb layer during ATEX .

- Determined from Cloud-free Radiation Data
- Determined from Mean Cloudiness Radiation Data (Dopplick)

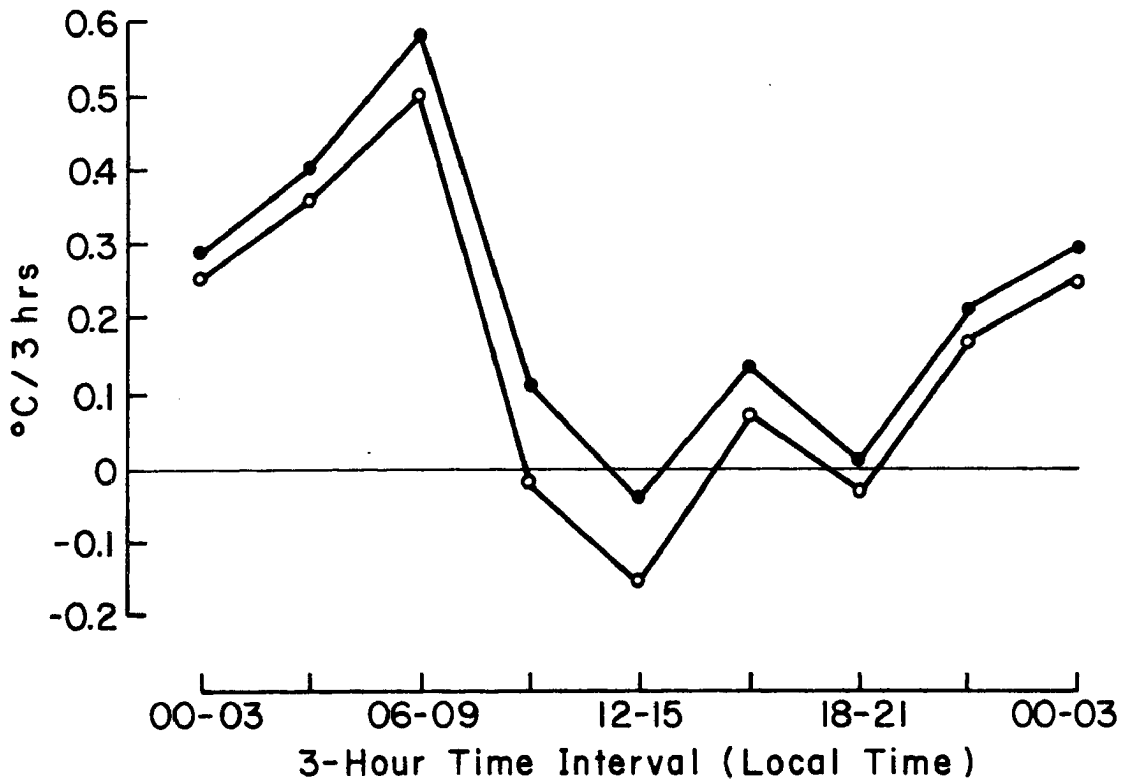


Fig. 5.6. Diurnal variation of required warming during ATEX.

The required warming component to the tropospheric energy balance shows a pronounced maximum in the morning hours near 08 LT and a minimum in the afternoon and early evening. These results agree with the other required warming calculations from the Northern Hemisphere data set and the GATE observations.

5.3 Line Islands Experiment

The data collected during the Line Islands Experiment (3 March - 21 April 1967) represents a comprehensive short term record of upper air parameters observed near the equator. Soundings were taken at 3-hour intervals from three islands situated in close proximity to each other (Fig. 5.7). Since the 0300, 0900, 1500 and 2100 GMT periods had relatively few soundings, and since these ascent times are somewhat weighted toward periods of disturbed weather, only the 0000, 0600, 1200 and 1800 GMT observations are examined. Table 5.8 gives the number of observations taken at each of these 6 hour time periods.

From data presented in the NCAR report by Madden et al., (1971) mean soundings at each standard observation period were determined, and the diurnal temperature changes at each island and for the three island average were computed. Those tabulations are shown in Table 5.9, and the experiment mean is displayed in Fig. 5.8.

The experiment mean temperature change between standard observation times is in agreement with information collected from the other special tropical experiments. While the mean temperature change profiles (850-300 mb) at Christmas Island and Fanning Island are consistent with the experiment mean, the 02-08 LT and 20-02 LT temperature change at Palmyra Island are not. It would appear that either vastly

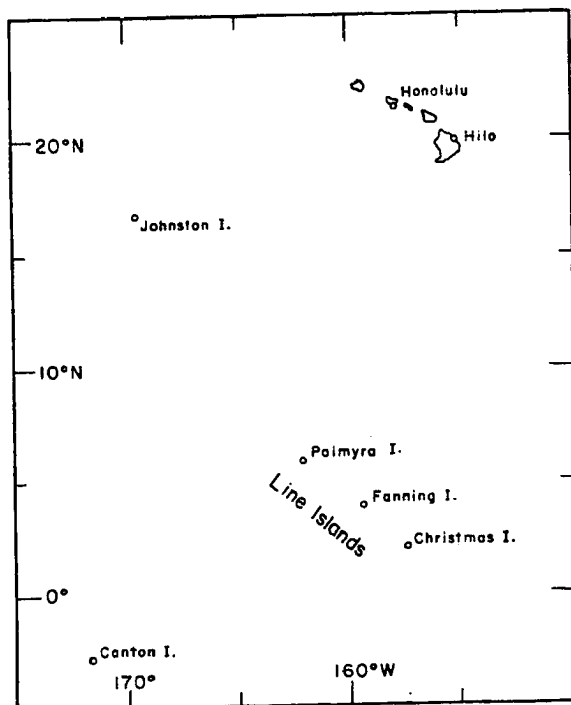


Fig. 5.7. Line Islands Experiment Region. From Madden, *et al.* (1971).

TABLE 5.8

Number of Radiosonde Ascents at Standard Observation Times During LIE

	<u>1400 LT</u>	<u>2000 LT</u>	<u>0200 LT</u>	<u>0800 LT</u>
Christmas Is.	44	44	45	43
Fanning Is.	48	49	47	47
Palmyra Is.	<u>47</u>	<u>45</u>	<u>48</u>	<u>47</u>
Total	139	138	140	137

TABLE 5.9

Diurnal Temperature Deviation From the Mean in the 850-300 mb Layer During the LIE

(Local Time)	02-08	08-14	14-20	20-02
Christmas Is.	+ .51	+ .94	- .43	-1.02
Fanning Is.	+ .23	+ .61	- .47	- .37
Palmyra Is.	- .21	+ .62	- .41	.00
Experiment Mean	+ .17	+ .72	- .44	- .46

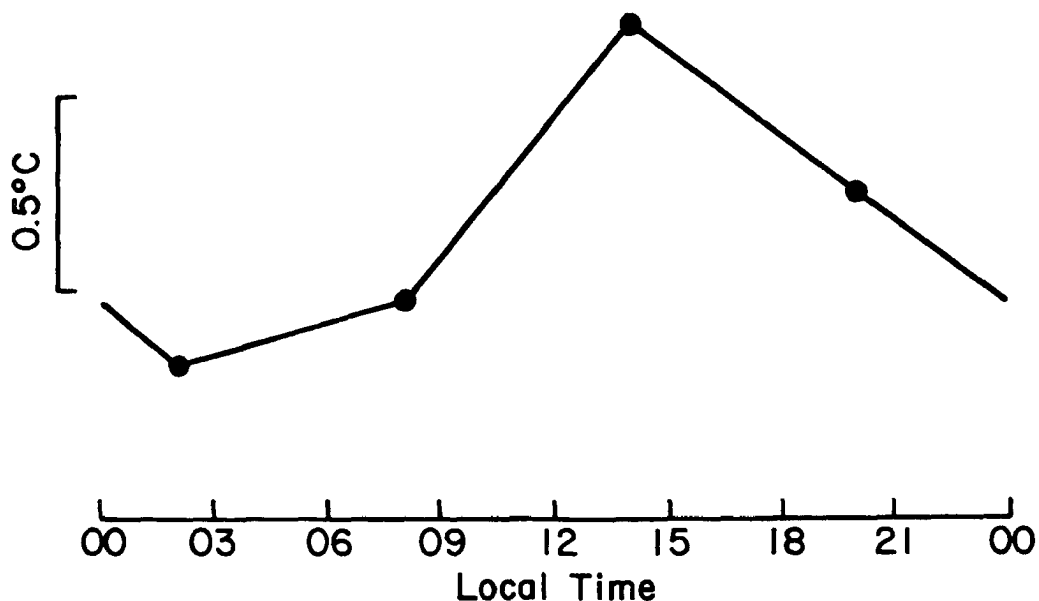


Fig. 5.8. Diurnal variation in the temperature in the 850-300 mb layer during L.I.E.

different conditions exist at these different locations or that the data from Palmyra Island may have some discrepancies.

The diurnal variations indicate that the 00 GMT (1400 LT) temperature observations show the maximum deviation from the mean. Madden *et al.*, has stated that:

"the temperature bias is most obvious at the surface and it is believed that the thermistor is sufficiently well shielded that the apparent diurnal temperature variations in the free atmosphere are at least partly real".

This view is consistent with the arguments presented in Appendix C.

Following previous procedures, the required warming for each 6-hour interval has been computed and is displayed in Fig. 5.9. The maximum required warming occurs in the morning and the minimum in the afternoon as has been determined for the other data sets. Also, the effect of a mean cloudiness distribution does not alter the profile in any appreciable manner.

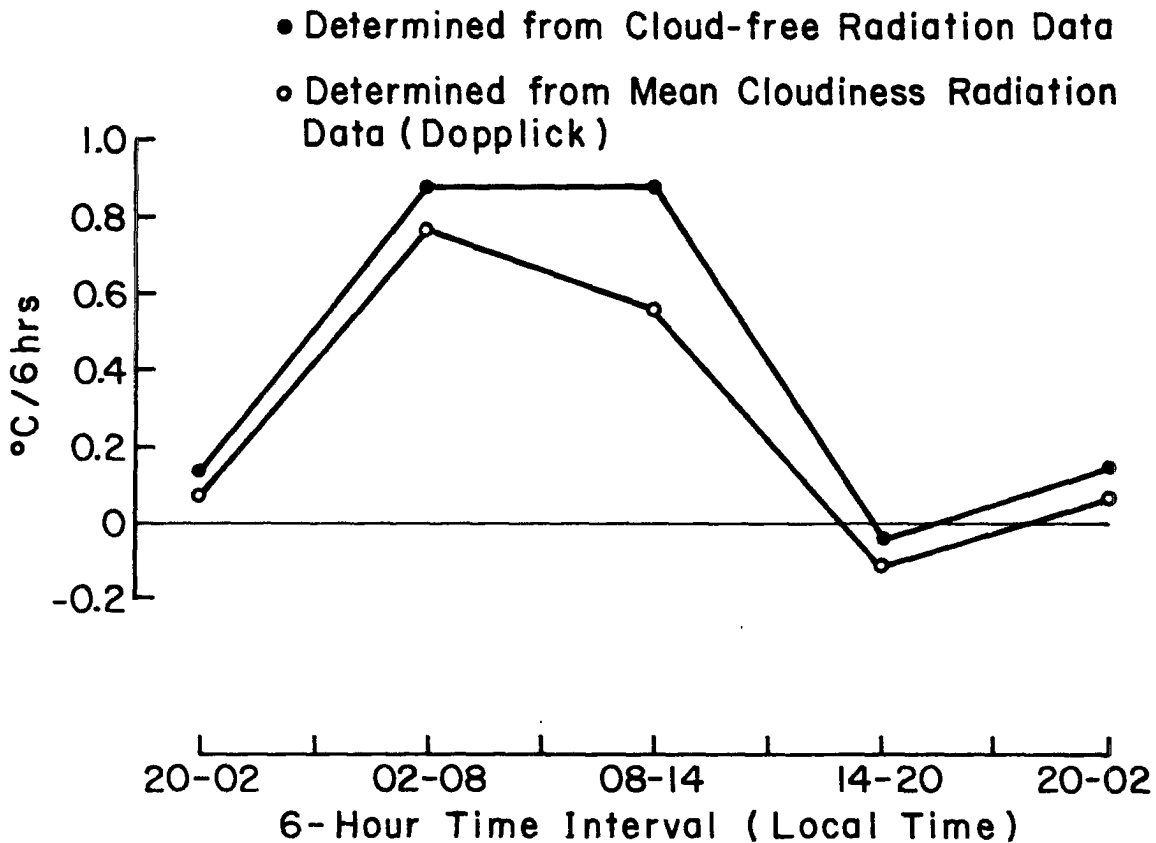


Fig. 5.9. Diurnal variation of required warming during L.I.E.

5.4 Operations Redwing and Hardtack

A very intense upper air sounding program was performed in conjunction with the nuclear testing projects Operation Redwing and Operation Hardtack during the summers of 1956 and 1958. From April until July 1956 standard observations times were 0300, 0900, 1500 and 2100 GMT, while from April to July 1958 the observations were taken at 0000, 0600, 1200 and 1800 GMT. By combining these two series of soundings in a manner described by Harris (1959) the diurnal cycle, resolved to 3 hours, can be obtained. Figure 5.10 shows the eight stations chosen for analysis.

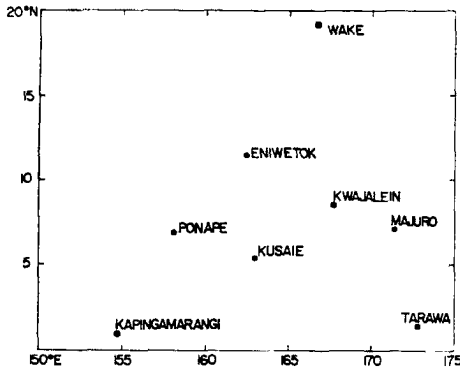


Fig. 5.10. Orientation map for 8 West Tropical Pacific Stations.

The data have been combined into an eight station mean based on the local time of observation. Hastenrath's (1972) examination of the harmonic components of the daily temperature variation provided the basis for determining the 3-hour temperature changes in the 850-300 mb layer. The daily temperature changes were constructed by combining the first and second harmonics presented in Hastenrath's paper. Although other order harmonics are present in the daily changes of temperature, their contributions are extremely small and are neglected in this analysis. The AN/AMT-4A radiosonde with an externally mounted thermistor was used primarily during the two projects. At Wake and Ponape duct-type thermistors were used, but only for nighttime soundings when solar radiationally induced instrument error is not a problem. It was also used at Majuro in the daytime.

The diurnal temperature change was computed to a 3-hour resolution as shown in Table 5.10. It is displayed in graphical form in Fig. 5.11.

TABLE 5.10

3-Hourly Temperature Changes ($\overline{\Delta T}$) at 8 West Pacific Stations, April-July, 1956 and 1958 - 850-300 mb Layer

(Local Time)	00-03	03-06	06-09	09-12	12-15	15-18	18-21	21-00
$\overline{\Delta T}$ ($^{\circ}\text{C}/3\text{hrs}$)	-.08	.04	.22	.22	.06	-.18	-.21	-.13

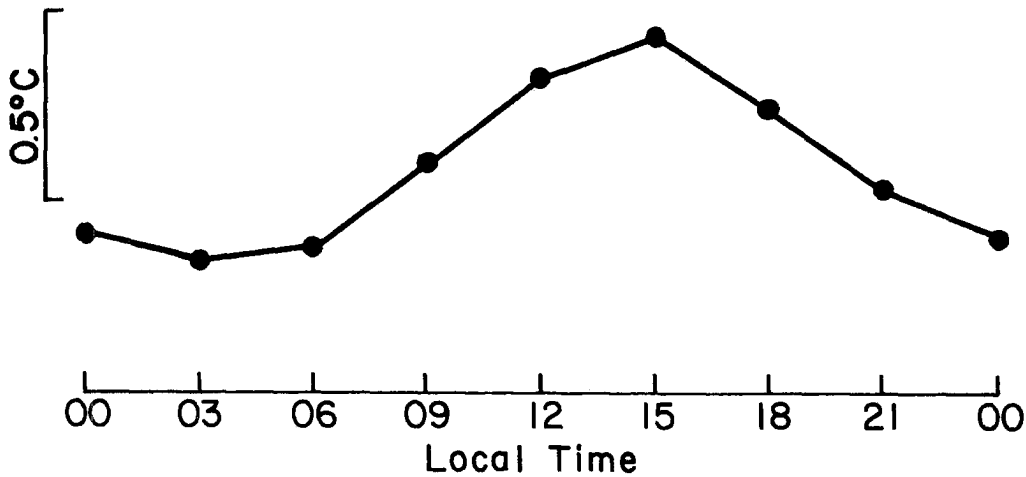


Fig. 5.11. The daily variation of the 850-300 mb layer temperature about the mean at 8 stations in the West Pacific during Operation Redwing and Hardtack (1956 and 1958).

Utilizing the $\overline{\Delta T}$ data from Table 5.10 and radiational data for the 0-10°N latitudinal belt shown in Table 3.3, the warming required from tropospheric processes for each 3 hour period was computed. Figure 5.12 displays the results.

The time when the maximum required warming occurs is again in the morning near 08 LT and the minimum occurs in the afternoon near 16 LT. This is in good agreement with the required warming calculations from other data sets in this study.

5.5 The Barbados Oceanographic and Meteorological Experiment (BOMEX)

Analysis of all rawinsonde data for Phase I, II, and III of the BOMEX Project was also accomplished. As soundings did not reach the upper troposphere, temperature-height values were information taken only between 850-450 mb levels. Again, results were similar to those obtained in the other special tropical experiments. Figure 5.13 portrays the diurnal variation of mean temperature between 850-450 mb as determined

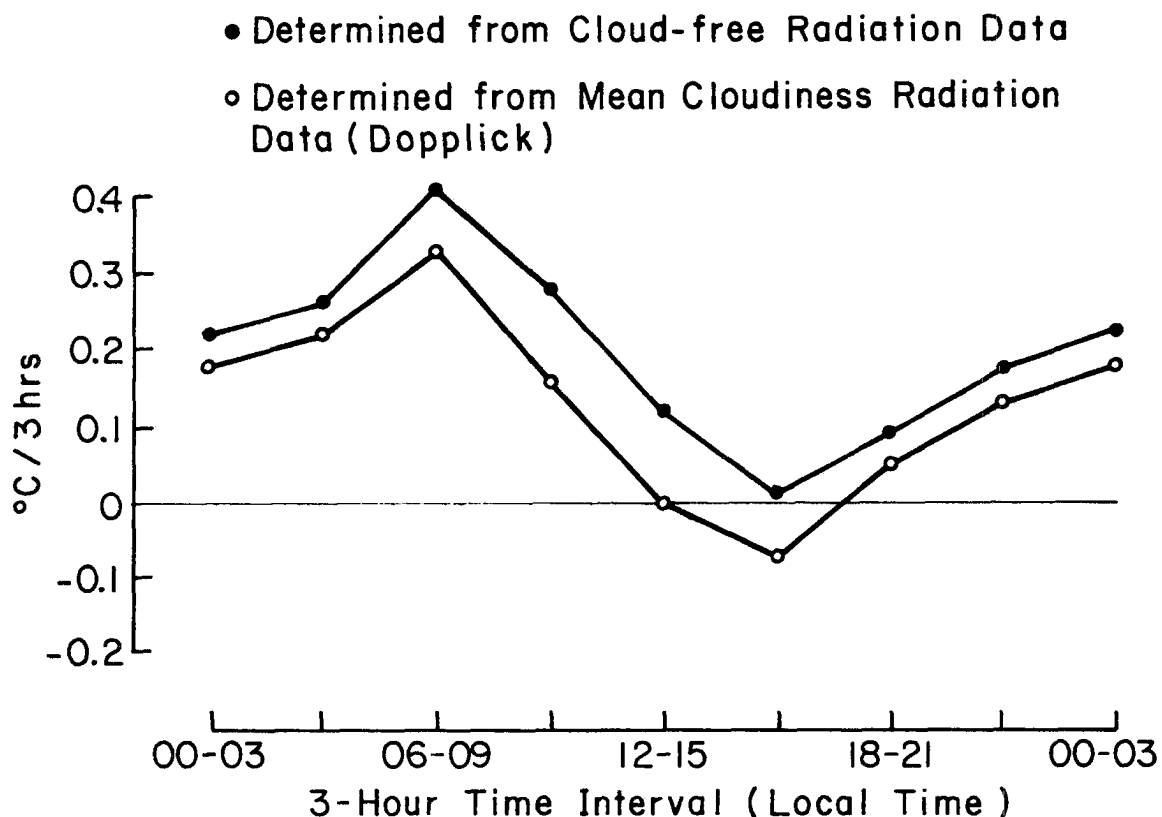


Fig. 5.12. Required warming in the 850-300 mb layer during the West Pacific Operations Redwing and Hardtack.

by 3-hourly observed pressure-thickness differences from the average of the four ships (DISCOVERER, MT. MITCHELL, OCEANOGRAPHER, and RANIER). Figure 5.14 shows the diurnal variation of mean required warming (RW) for cloud free and mean cloudiness radiation conditions. Note again that there is a pronounced maximum in required warming in the forenoon. Little warming is required in the afternoon and evening.

5.6 Summary

There is a distinct similarity between the observed temperature change ($\overline{\Delta T}$) and the required warming (RW) profiles for all five special tropical experiments. While the number of observations during any one

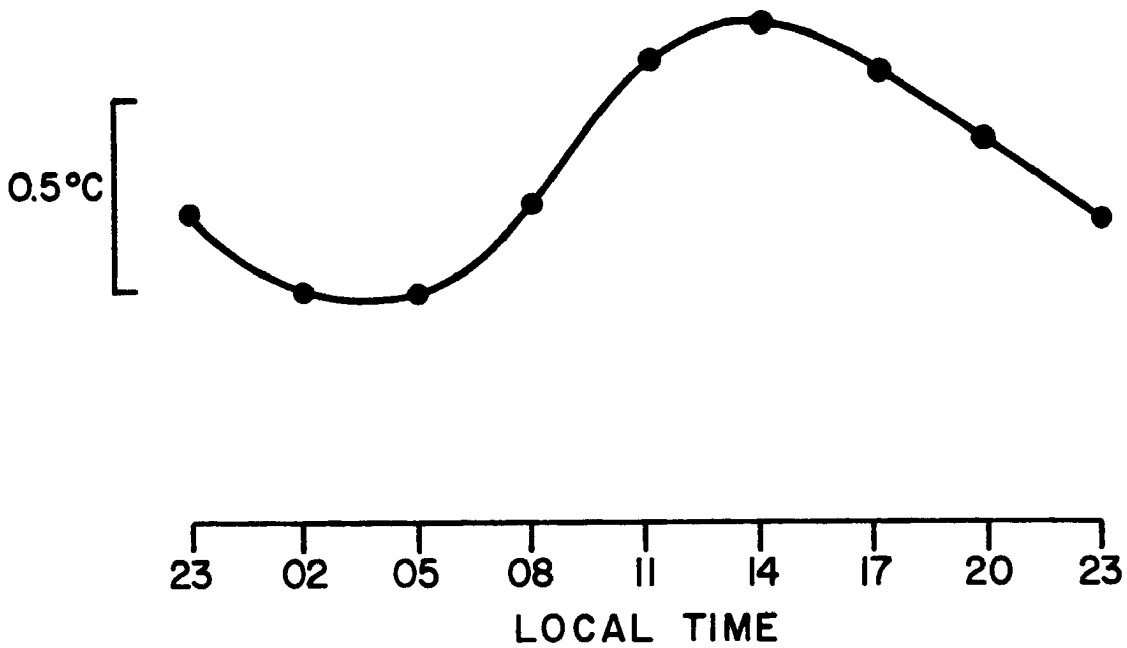


Fig. 5.13. Diurnal temperature variation in the 850-450 mb layer during Phases I, II and III of the BOMEX experiment.

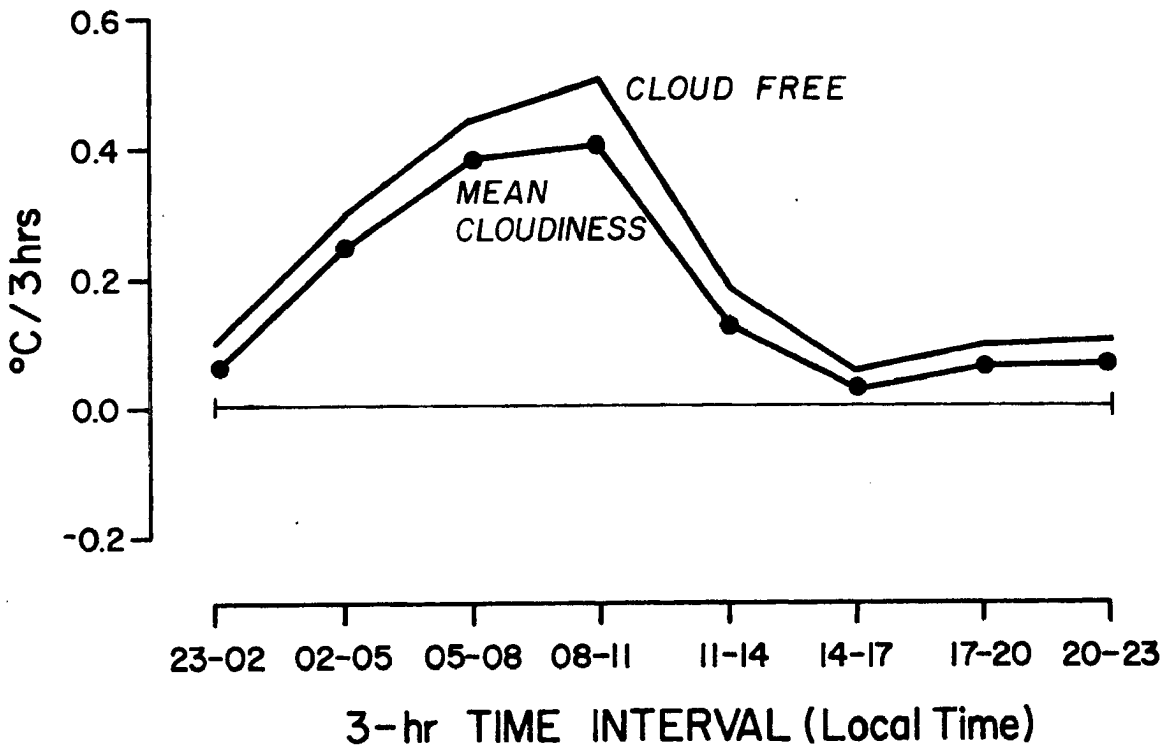


Fig. 5.14. Diurnal variation of required mean warming between 850-450 mb during the first three Phases of the BOMEX Project for cloud free and mean cloudiness conditions.

time period for each experiment may be statistically small, the fact that the resulting temperature change and required warming profiles for each experiment are consistent gives confidence to the mean curves and consequent conclusions. Figure 5.15 is a composite $\overline{\Delta T}$ curve for all five experiments. It was constructed by determining the mean hourly temperature change for all experiments. Utilizing these hourly temperature changes and determining the hourly net radiative required warming (\overline{RW}) was ascertained. The five experiment mean required warming profile is shown in Fig. 5.16. The pronounced morning maximum-afternoon minimum of tropospheric required warming is again evident.

A final graphical depiction of the required warming calculation is shown in Fig. 5.17. This shows the four components of the tropospheric energy balance (Eq. 1.7) for all the special tropical experiments. Again, the early morning maximum of RW is apparent. It develops from a rapid increase in temperature in the early morning hours.

The results of the tropospheric energy balance analysis for the five special tropical experiments verify the findings from the 12-hour Northern Hemispheric Data Set. There apparently is a quite large diurnal variability of tropospheric warming.

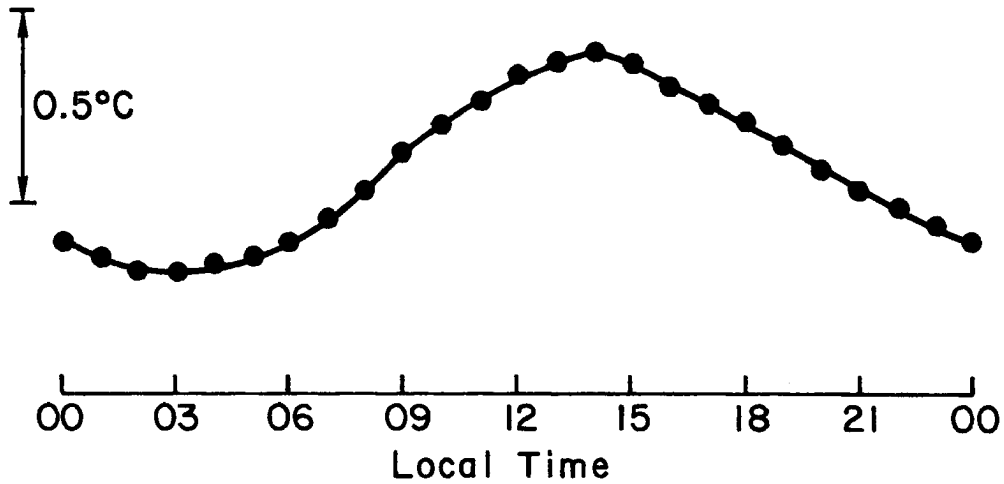


Fig. 5.15. Mean hourly temperature change in the 850-450 mb layer for the five tropical experiments (GATE, ATEX, LIE, Operations Redwing and Hardtack, and BOMEX).

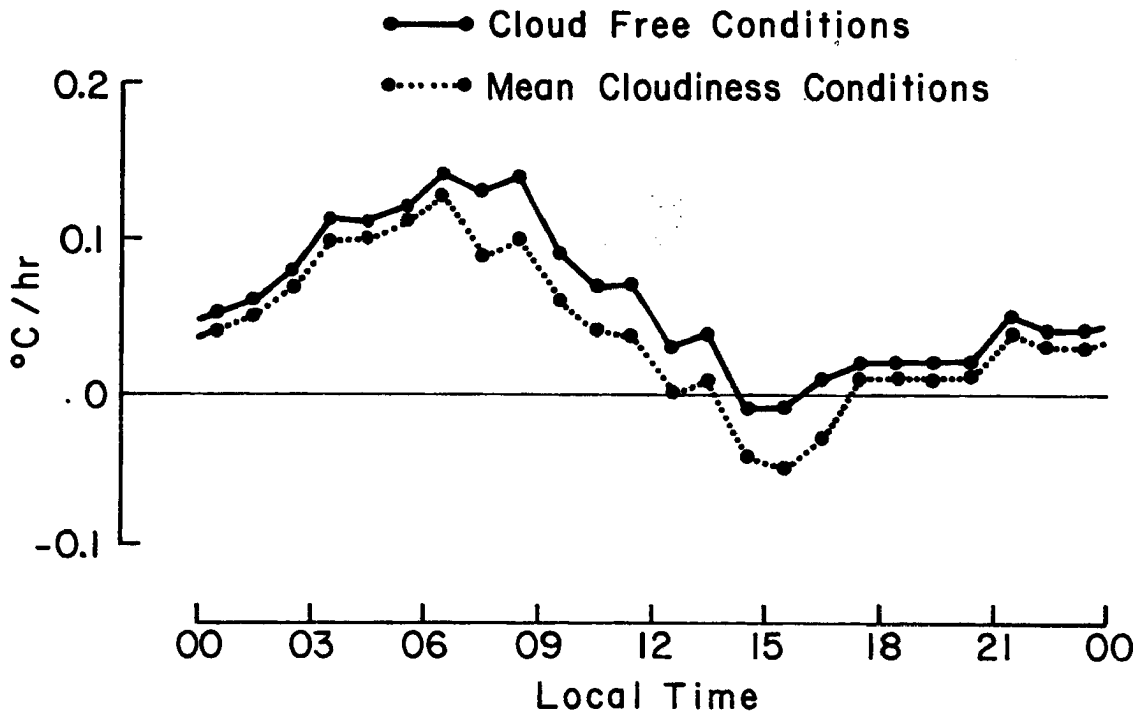


Fig. 5.16. Mean required warming for the five tropical experiments.

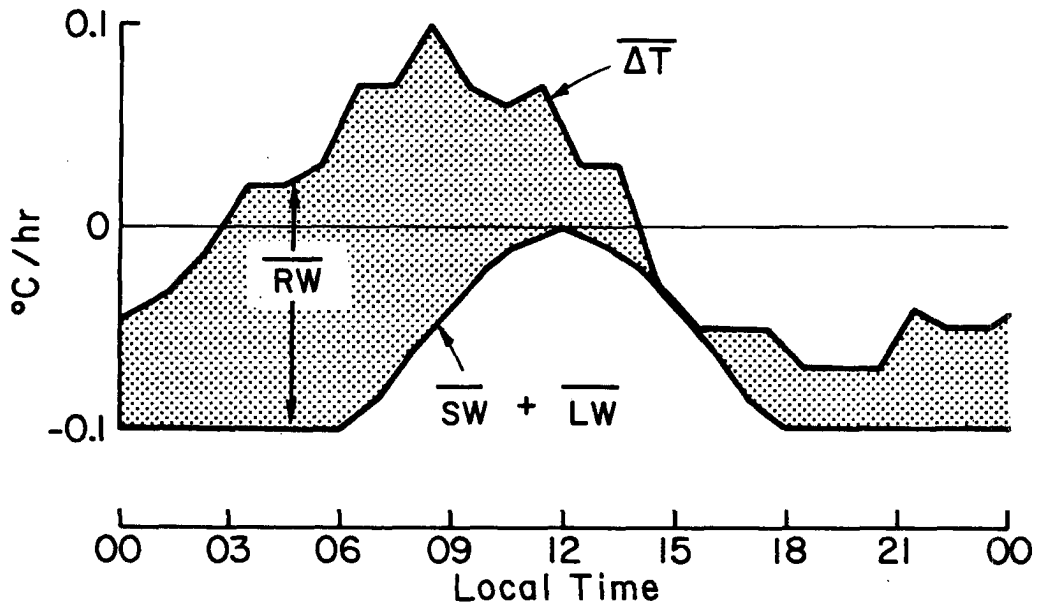


Fig. 5.17. Required warming ($\overline{\text{RW}}$ - dotted area) for the five tropical experiments determined from the hourly rate of temperature change ($\overline{\Delta T}$) and net radiative cooling ($\overline{\text{SW}} + \overline{\text{LW}}$) in the 850-300 mb layer (BOMEX data 850-450 mb).

6. SUMMARY

6.1 Results and Conclusions

It is apparent from the analysis of the Northern Hemispheric 12-hour data set, the 3-hour resolution data from GATE, and the other 3 and 6 hour resolution tropical experiment data that there is a large diurnal cycle in the tropospheric warming required to compensate for the continual net radiative cooling in the troposphere. These calculations of required warming support the contention that there is a large (approximately 2:1) morning maximum and late afternoon-early evening minimum in the tropospheric warming mechanism. As the tropical experiment data is of higher time resolution than the Northern Hemispheric 12-hour observations, it increases confidence in the early morning maximum found in the 12-hour data set. This diurnal variation of required warming is pervasive in its areal scope and appears to be a global phenomenon.

Figures 6.1 and 6.2 exhibit the warming required during various 12-hour intervals from data collected from all the tropical projects and upper-air stations located from 0° to 20°N in summer and winter. The maximum required warming unmistakably occurs during the early morning hours in both seasons. It is also important to note the diurnal consistency in the $\overline{\text{RW}}$ computation between the special experiments and the regular data sets.

In order to demonstrate the global aspects of this tropospheric process, Figs. 6.3 and 6.4 show the diurnal variation in required 12-hour interval warming at every island and ship included in this study from 0 - 60°N for summer and winter. Again, the morning maximum and late

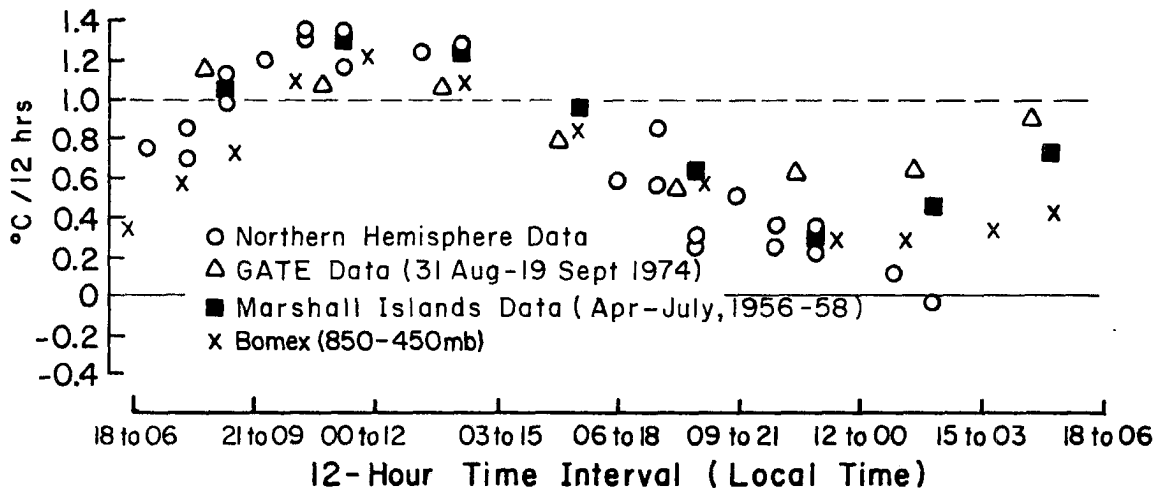


Fig. 6.1. Required warming in the 850-300 mb layer during 12-hour intervals from data collected for tropical experiments and upper air stations 0-20°N - Summer.

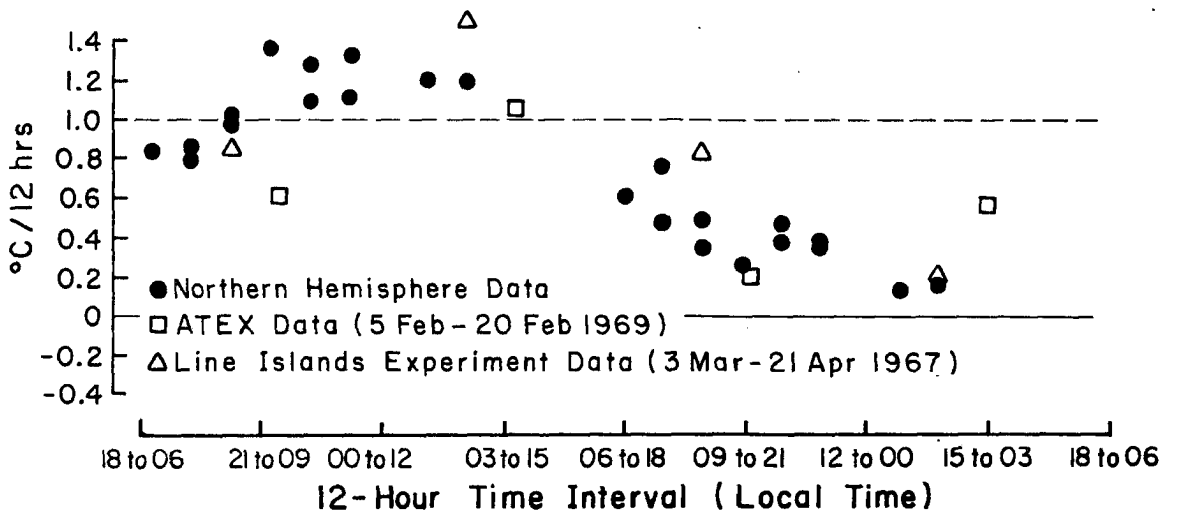


Fig. 6.2. Required warming in the 850-300 mb layer during 12-hour intervals from data collected for tropical experiments and upper air stations 0-20°N - Winter.

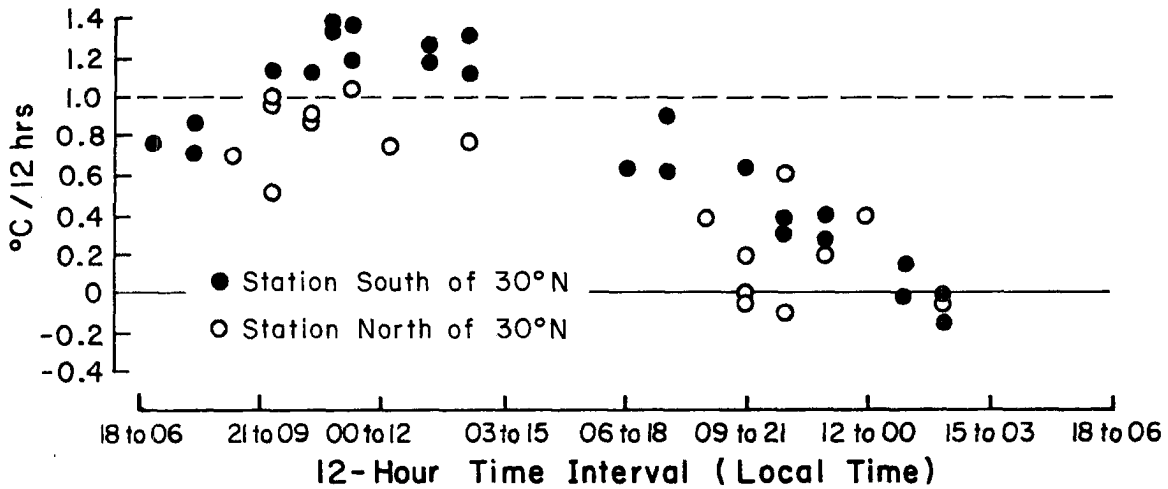


Fig. 6.3. 12-hour required warming at all ships and islands - equator to 60°N - for the 850-300 mb layer during the summer.

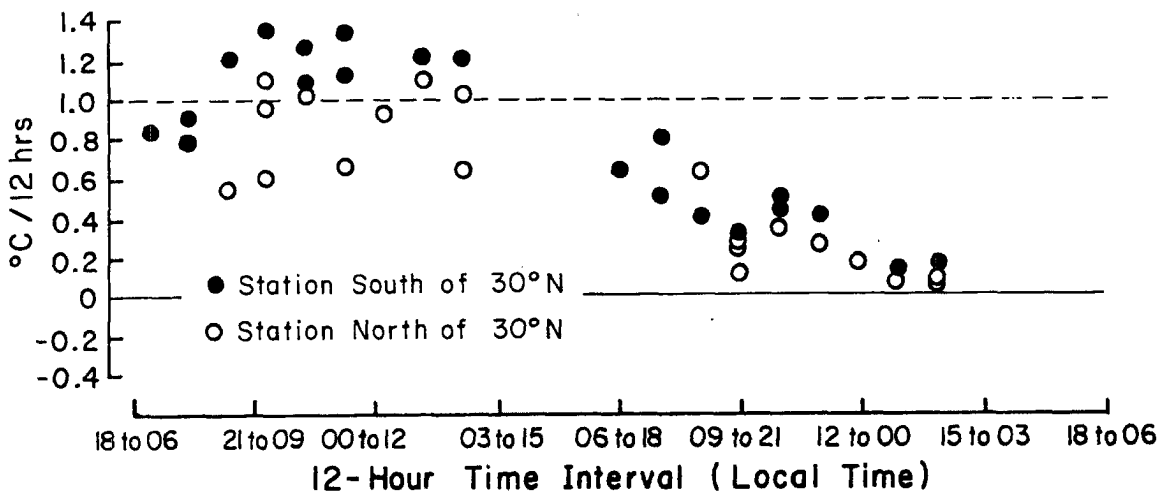


Fig. 6.4. 12-hour required warming at all ships and islands - equator to 60°N - for the 850-300 mb layer during the winter.

afternoon minimum of required warming are evident. The fact that no data collected over continental land areas is included (thereby minimizing the effect of turbulent transfers of sensible heat) indicates that this warming is mainly a result of the release of latent heat of condensation, probably occurring in the form of surrounding cloud and clear region subsidence.

A more obvious manifestation of this early morning warming maximum is seen in the early morning increases in temperature during all of the tropical experiments prior to the time when solar heating becomes significant (Fig. 6.5). This 0200 to 0800 LT observed temperature increase should not be a result of instrument error. The absorption of solar radiation by the thermistor element in the first two hours after sunrise in the 850-300 mb layer is minimal due to the low elevation angle of the sun and the adequate ventilation of the sensor in the middle troposphere. This unexpected temperature increase can be attributed to a tropospheric warming mechanism operating on a diurnal cycle.

Riehl (1947) ascribed an observed warming in the middle troposphere between 0130 and 0430 (local time) over the Caribbean ocean to increased sinking motion during these hours. Also, in a study of 7 days of BOMEX data which were representative of undisturbed weather (Nitta and Esbensen, 1974) it was determined that there was a definite diurnal cycle in the vertical motion field with the maximum downward motion near 08 LT. These findings support the conclusion that there is a diurnal variation in tropospheric required warming and that increased morning subsidence is responsible.

A more specific analysis of the diurnal variation of required warming in the 0-10°N latitude belt is shown in Fig. 6.6. This region was

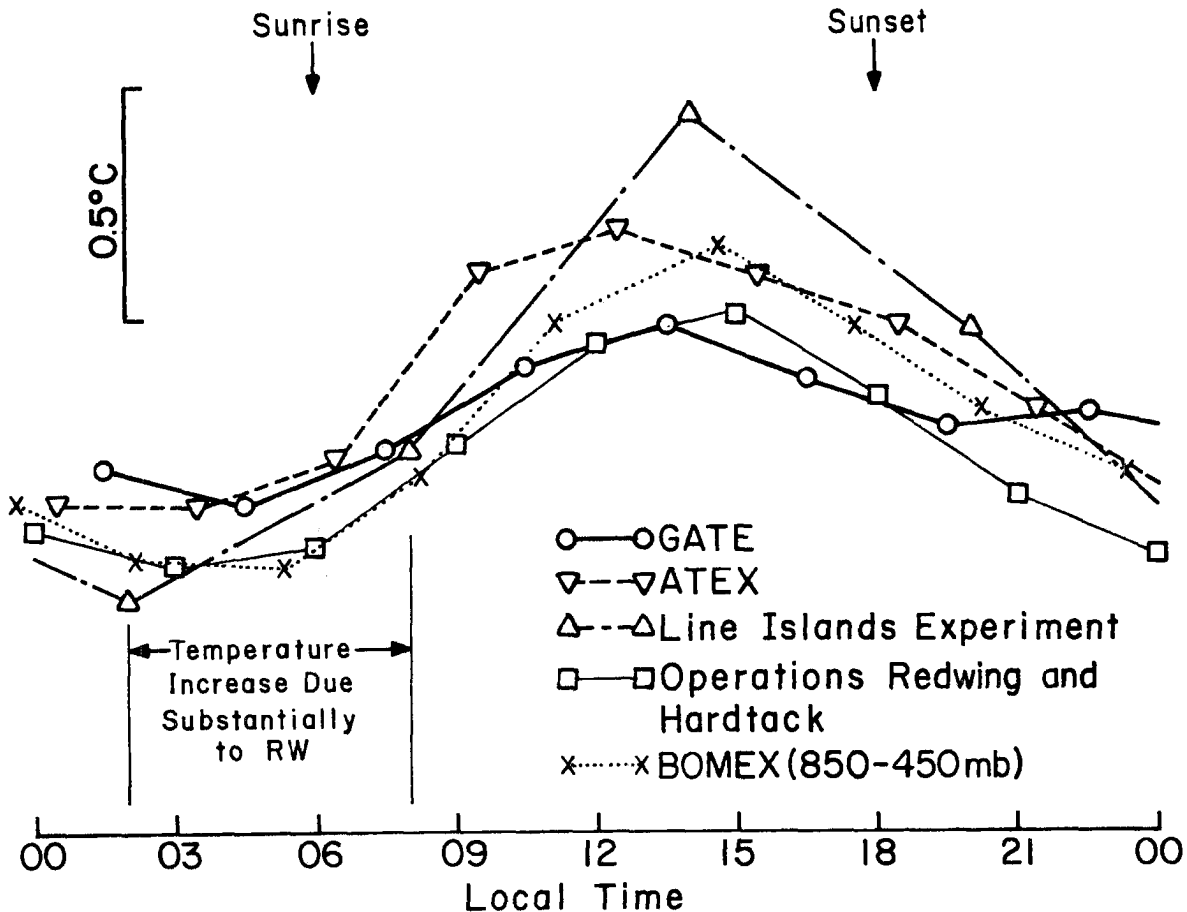


Fig. 6.5. Diurnal temperature variation of the 850-300 mb layer for special tropical experiments.

chosen due to the concentration of 3-hour time resolution data. This figure depicts hourly values of all the energy components of the 850-300 mb heat budget for cloud-free conditions (diagram a) and for mean cloud conditions from Dopplick (1970), (diagram b). It is shown that the minimum mean temperature of the 850-300 mb layer occurs near 0500 (local time) and the maximum near 1400 or 1500. During the summer, the sun rises a few minutes before 0600 and sets shortly after 1800. The use of mean cloudiness (Dopplick, 1970) radiation values (diagram b) does not appreciably alter the shape of the required warming curve. It does, however, reduce the magnitude of required warming at all hours.

Rate of Observed
Warming, $[\overline{\Delta T}]$

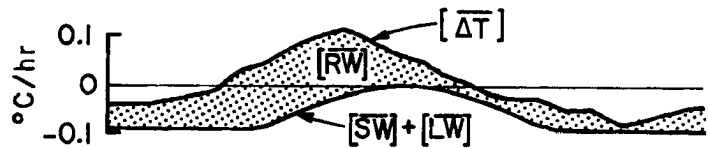


1. Cloud Free

Rate of Net Radiative
Cooling, $[\overline{SW}] + [\overline{LW}]$



$[\overline{\Delta T}] = [\overline{SW}] + [\overline{LW}] + [\overline{RW}]$



Rate of Required
Warming, $[\overline{RW}]$

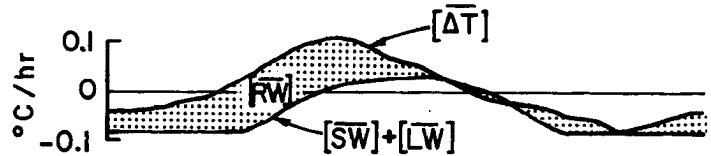


b. Mean Cloudiness

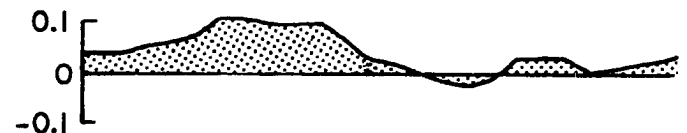
Rate of Net Radiative
Cooling, $[\overline{SW}] + [\overline{LW}]$



$[\overline{\Delta T}] = [\overline{SW}] + [\overline{LW}] + [\overline{RW}]$



Rate of Required
Warming, $[\overline{RW}]$



00 03 06 09 12 15 18 21 00
Local Time

Fig. 6.6. 0-10°N required warming (\overline{RW}) model. a) cloud free, b) mean cloudiness based on Dopplnick (1970).

Warming Mechanism. From the discussion in Chapter 1, it was determined that the tropospheric required warming term (\overline{RW}) represents four different tropospheric processes. Those processes are: 1) turbulent transfer of sensible heat from the surface, 2) horizontal temperature advection (ADV), 3) release of latent heat (LH), and 4) vertical motion (VM).

Each term will be considered as to its probable contribution to the diurnal variation of \overline{RW} .

- 1) Turbulent transfer of sensible heat - Since the Bowen ratio over oceanic regions is 10-20:1, very little sensible heat is transferred from the sea surface to the atmosphere. It can be considered negligible in the 850-300 mb layer over the ocean. It can become significant over land in the summer where the Bowen ratio is high (see Fig. 2.3). However, the time of maximum sensible heat transfer does not coincide with the time of maximum \overline{RW} . Therefore SH cannot be the cause of the morning maximum of \overline{RW} .
- 2) Horizontal temperature advection - This term ($V \cdot \nabla T$) was analyzed both in the tropics and in the mid-latitudes over central North America. The analysis was performed for the 12-hour intervals separating standard observation times. V represents the vector difference of the mean winds in the 850-300 mb layer at 00GMT and 12GMT. A paper by Wallace and Hartranft (1970) provided information on the 00GMT-12GMT tropical wind fields. A value of ~ 1 m/sec is assumed for V and the average temperature gradient is approximated by $0.5^\circ\text{C}/1000$ km. This yields a result of $.02^\circ\text{C}/12$ hrs for the most extreme situation when the wind is blowing parallel to the temperature gradient. Based on this result the horizontal temperature advection, although large at individual times, is small for a large statistical average in the tropics. The most dramatic diurnal variations in the mean wind field occur at low levels over Central North America in the summertime. From the U.S. Standard Atmosphere Supplements the mean summer time temperature gradient (850-300 mb layer) is about 4° between 30°N and 45°N . Hering and Borden (1962) show the 12 hour mean wind speed variation (850-300 mb) to be about 2 m/sec. The horizontal advective term is about 0.2°C under maximum conditions when the wind difference vector is perpendicular to the temperature gradient. This is relatively small when compared to the diurnal variability of the other terms in the energy balance. Therefore, even under the most extreme conditions, long term, large space scale values of this term should be quite small.

- 3) Release of latent heat (LH). Since latent heat release occurs with upward vertical motion and adiabatic cooling, it usually produces only very small or negligible amounts of sensible temperature change. Most of the condensation heat so released goes to expansion and potential energy gain. The temperature of the rising and condensing air parcel typically deviates only a small amount from the environmental lapse-rate. Upward vertical motion and the release of latent heat of condensation typically do not bring about significant cooling or warming (Gray, 1973). Thus, the diurnal variations in RW do not necessarily occur at the times and places of latent heat release. This term is not directly related to sensible heat gain and can be largely discounted as a direct source for the required warming, although the potential energy gain from the condensation produces sinking warming at other locations.
- 4) Vertical motion - Downward vertical motion acts to warm the environment (except in selective locations of heavy rainfall with evaporating downdrafts). In the tropics virtually all upward motion occurs in convective clouds and does not heat or cool the air directly (see process 3). Although this is less true at middle latitudes, most upward vertical motion still results in condensation and little direct sensible temperature change by the environment. Thus, the net influence of the total up-moist and down-dry vertical motion process is one of tropospheric warming. Dry adiabatic subsidence occurring in response to cumulus convection, is believed to be the primary physical mechanism which acts to balance the radiational cooling and produce the diurnal range in required warming.

Hastenrath and Steinberg (1971) examined diurnal variations of temperature and performed calculations concerning the diurnal variability of the tropospheric heat budget between 1000-100 mb over the Western Tropical Pacific. From data collected for April-July 1956 and 1958, mean soundings for 3-hour intervals were computed. A distinct nocturnal warming (occurring near 03 LT) was documented. The authors chose to examine the four constituents of the required warming mechanism; namely, heating due to condensation of water vapor, heating due to turbulent transfer of sensible heat, horizontal advection, and heating from vertical motion. They determined that the heating contribution from sensible heat transfer and from horizontal advection were negligible. Thus, only heating from latent heat and vertical motion remained. They

performed an extensive analysis of the rainfall over the 8 stations included in the study and calculated the amount of precipitation in the tropospheric column (1000-100 mb). All of this precipitation was assumed to directly warm the air by the release of latent heat. As just discussed, this is not consistent with the ideas of Gray (1973) and Lopez (1973) who believe that sensible heat gain results from condensation-induced subsidence rather than from direct latent heat release. Hastenrath and Steinberg then computed the amount of heating from vertical motion as a residual in the heat budget formula and concluded:

"Accordingly, two processes could be primarily responsible for the observed nocturnal warming of the tropospheric column as a whole:

- (a) a rainfall maximum during the hours after midnight; and
- (b) (large scale) subsidence, the timing of which would indeed match a maximum of the semi-diurnal variation of lower-layer divergence borne out in an earlier study (Hastenrath, 1971)."

Hastenrath and Steinberg's analysis substantiates the diurnal variability of the \overline{RW} found in this study. However, their conclusion that direct latent heat release is a primary cause of this morning maximum does not fit our physical picture. We believe the required warming is a direct result of subsidence, but not necessarily a direct result of local condensation. This is an important difference.

Conclusion. The morning maximum and afternoon-evening minimum in RW is believed to be largely driven by the response of the troposphere to its diurnal radiation cooling and manifests itself in an enhanced morning and reduced afternoon-evening subsidence motion. This diurnal cycle in subsidence appears to be a pervasive phenomena of the entire global troposphere.

7. SUGGESTED PHYSICAL MECHANISM FOR DIURNAL CYCLE OF REQUIRED WARMING

by William M. Gray

Our observational studies of the last 7-8 years have strongly suggested that the condensation warming mechanism is a result of return flow subsidence and does not typically occur at the place of latent heat release. Heavily raining areas, or individual raining cumulus averaged over their life cycle, do not locally cause direct sensible temperature changes. The reports of Williams and Gray (1973), Lopez (1973) and Gray (1973) and Ruprecht and Gray (1976) offer supporting observational evidence and discussion of this point of view.

Latent energy typically goes to raise the potential temperature of the rising air parcel to that of the environment. Little or no significant sensible temperature increase results at the location of raining cumulus. The warming which results from cumulus rainfall occurs at the place of the compensating (return flow) subsidence. Some of this return flow subsidence occurs around the individual cumulus cloud, some at substantial distances from the convection as with the Hadley and Walker circulations and in anticyclones. Thus, the upper level mass source which feeds the subsidence may take place in the ITCZ region, along a frontal zone, or in a low pressure system at a distant location.

If one accepts this physical argument on the nature of the condensation warming mechanism, then, with the evidence of this paper, one is led to hypothesize a substantial diurnal variation in subsidence. We have, in fact, directly measured from composited rawinsonde data large 00Z (10 LT) vs. 12Z (22 LT) variations in clear region and cloud cluster divergence and vertical motion in the Western Pacific. Figure 7.1 shows the nearly two-to-one greater morning (00Z or 10 LT) subsidence occurring

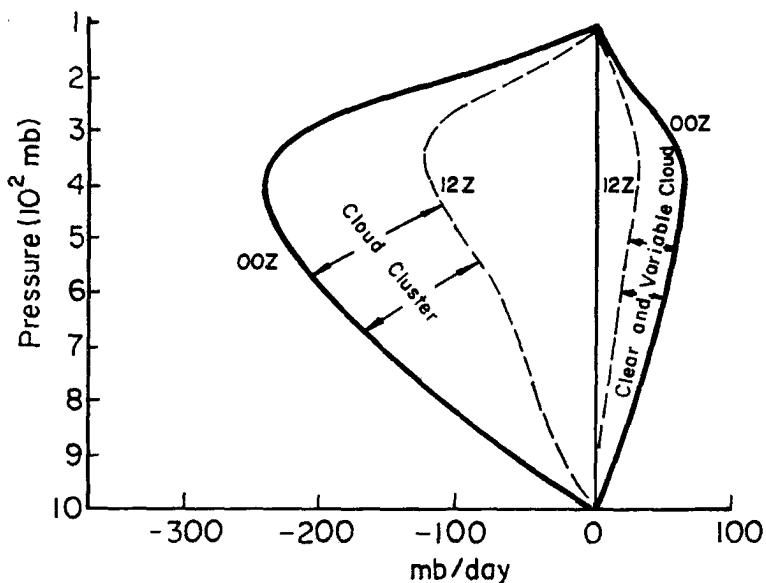


Fig. 7.1. Comparison of 00Z (10 LT) and 12Z (22 LT) vertical motion in satellite observed cloud clusters and in clear and variable cloud regions as determined from composited Western Pacific rawinsonde information.

in clear and variable cloud areas as compared with 12Z (or 22 LT) and the much larger morning cloud cluster vertical motion. This is more extensively discussed in the report by Jacobson and Gray (1976).

In regions with active morning deep cumulus convection, as in the Western Pacific, enhanced morning subsidence is occurring between the regions of more active morning cumulus convection. In cloud-free environments such as anticyclones, the enhanced morning subsidence must result from extra morning upper level convergence and low level divergence from continental scale circulations. Since diurnal variations in cumulus convection vary from region to region, this global morning subsidence maximum and afternoon-evening subsidence minimum can be either in-phase or out of phase with the local diurnal cumulus convection cycle. Thus, the upper level mass source that feeds the morning subsidence may be locally derived from enhanced morning deep cumulus convection or, in

cloud-free regions, result from upper level mass convergence produced by continental or hemispheric scale circulations.

The basic physical mechanism responsible for the initiation of the early morning tropospheric sinking and its maintenance through the morning is likely to be related to the relative radiational cooling of the nighttime troposphere in comparison with the daytime as indicated in Fig. 7.2. These radiational cooling differences produce pressure-thickness changes and relative upward-downward bulging of pressure surfaces. These changes in horizontal pressure gradient should cause wind accelerations and resulting diurnal differences in convergence-divergence and vertical motion. The regions of largest radiational cooling should be the places of largest upper level mass convergence, subsidence, and low-level divergence. Thus, the typical "before sunrise" initiation of tropospheric warming (Fig. 6.5) is probably a response of the troposphere to nighttime radiational cooling. This cooling manifests itself in a subsidence response which gradually grows stronger than the radiational forcing which initiated it.

As discussed in the previous chapter, the average required warming in the 12-hour period between 00-12 LT is $\sim .08^{\circ}\text{C}/\text{hr}$. During the hours of 12-24 LT, the typical required warming is only about one-quarter of this amount or $\sim .02^{\circ}\text{C}/\text{hr}$. Total daily required warming of the troposphere is thus:

00-12 LT	$.08^{\circ}/\text{hr.} \times 12 \text{ hr.}$	$\approx .96^{\circ}\text{C}$
12-24 LT	$.02^{\circ}/\text{hr.} \times 12 \text{ hr.}$	$\approx .24^{\circ}\text{C}$
00-24 LT		$\approx 1.20^{\circ}\text{C}$

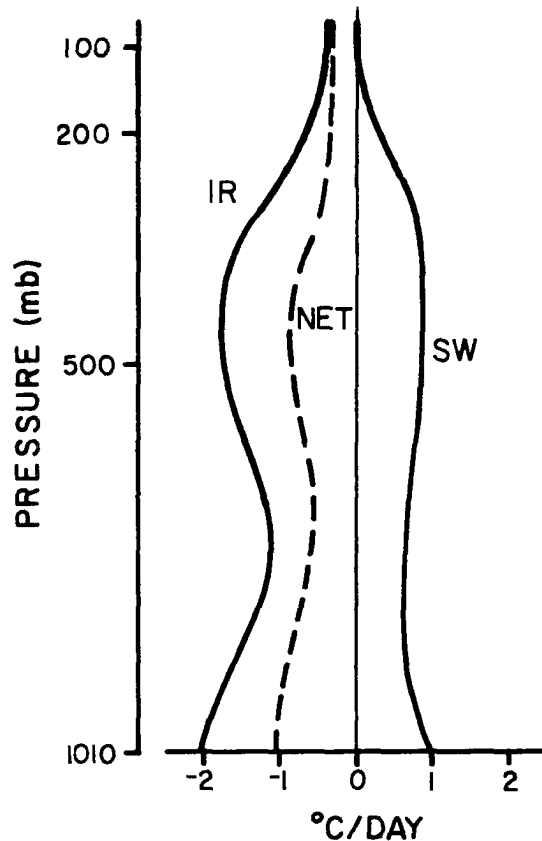


Fig. 7.2. Typical daily amount of tropical clear region infrared (IR) cooling and solar (or short wave) warming (SW) as derived by Cox (1975) and Dopplick (1974). The dashed curve gives the typical net daily radiation induced temperature change.

Given that tropospheric lapse rates are about two-thirds of the dry adiabatic lapse rate, the average tropospheric sinking motion required to account for the tropospheric radiational cooling is ~ 2 mb/hour between the hours of 00-12 LT and ~ 0.5 mb/hour between the approximate hours of 12-24 LT. Assuming a maximum of vertical motion at middle levels and no vertical motion at the surface and the tropopause, this requires middle tropospheric sinking motion to average ~ 4 mb/hour during the morning (00-12 LT) and ~ 1 mb/hour during the afternoon and early evening. Typical average upper and lower tropospheric divergences to match these vertical motions must thus be:

<u>Time</u>	<u>Level</u>	<u>Divergence (10^{-6}sec^{-1})</u>
00-12 LT	200-600 mb	~ -2.8
	600-1000 mb	~ +2.8
12-24 LT	200-600 mb	~ -0.7
	600-1000 mb	~ +0.7

Besides taking place in clear regions, this morning subsidence also occurs between and within cloudy areas and surrounding individual cumulus. Cloud groups and cloud clusters, even though possessing a mean upward circulation, also have a significant amount of extra "recycling" or downward motion (Gray, 1973; Lopez, 1973).

Since this morning maximum in subsidence appears to be a global phenomena, there are many locations where it cannot be directly associated with deep cumulus convection as it can in the tropical western Pacific (op.cit., Jacobson and Gray, 1976). Over the North American continent, for instance, cumulus convection is maximum in the afternoon and early evening, out of phase with the morning subsidence. Over the GATE region in the summer of 1974, a maximum of deep cumulus convection occurred between 10-20 LT, also out of phase with the morning subsidence. Thus, the upper tropospheric mass convergence that feeds this morning subsidence warming maximum is not necessarily regionally or locally derived as is the circulation illustrated in Fig. 7.3. A diurnal continental or hemispheric scale circulation must be occurring at a number of global locations. In their study of the diurnal variation of wind Wallace and Hartranft (1969) have demonstrated the existence of substantial 00Z minus 12Z differences in upper level winds on an oceanic or continental scale of motion (Fig. 7.4).

The upper tropospheric mass source to feed the global morning maximum and afternoon-evening minimum in subsidence appears to be a

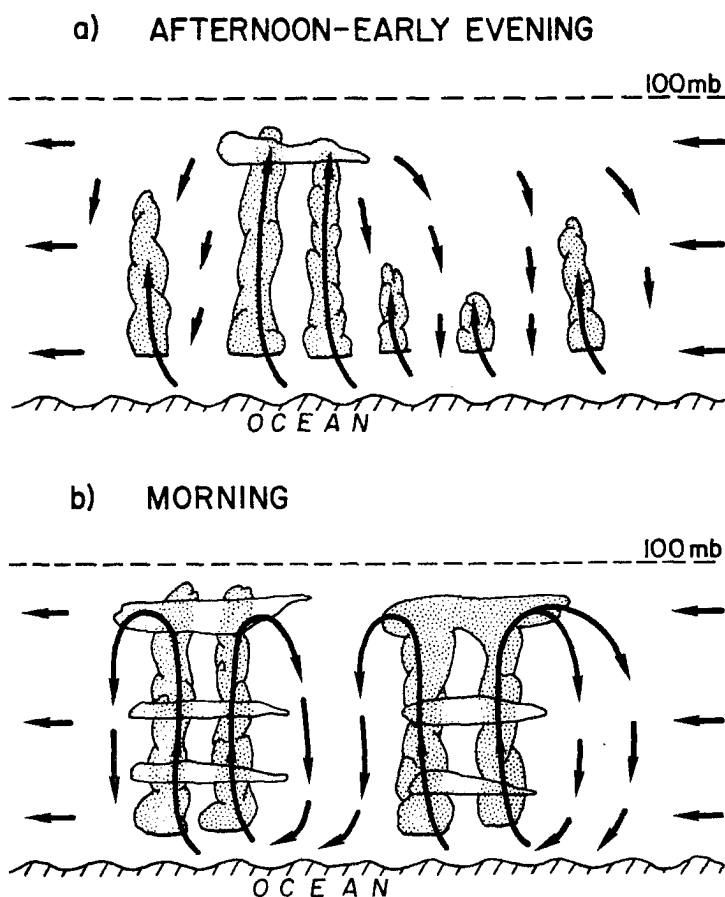


Fig. 7.3. Idealized illustration of a diurnal variation in subsidence due to a regional diurnal variation in deep cumulus convection. No regional diurnal variation in divergence need be present. A morning maximum and afternoon-early evening minimum in subsidence is present.

consequence of at least three different scales of circulation:

- a) A regional or local diurnal circulation driven by day vs. night differences in net radiational cooling and associated day-night differences in cloud and cloud-free regions as previously discussed by Jacobson and Gray (1976). Cloud and cloud-free radiation variations can produce diurnal divergence differences on the order of 10^{-6}sec^{-1} or greater. This is probably the dominant mechanism for the oceanic morning maximum of subsidence. Morning enhancement of deep cumulus convection within middle latitude meso-scale cloud systems due to cloud and cloud-free diurnal radiation differences can also be part of this scale of circulation.
- b) A continental-ocean circulation probably characteristic of North American and the surrounding ocean region - Fig. 7.5. Our study of the diurnal variation of winds and the study of

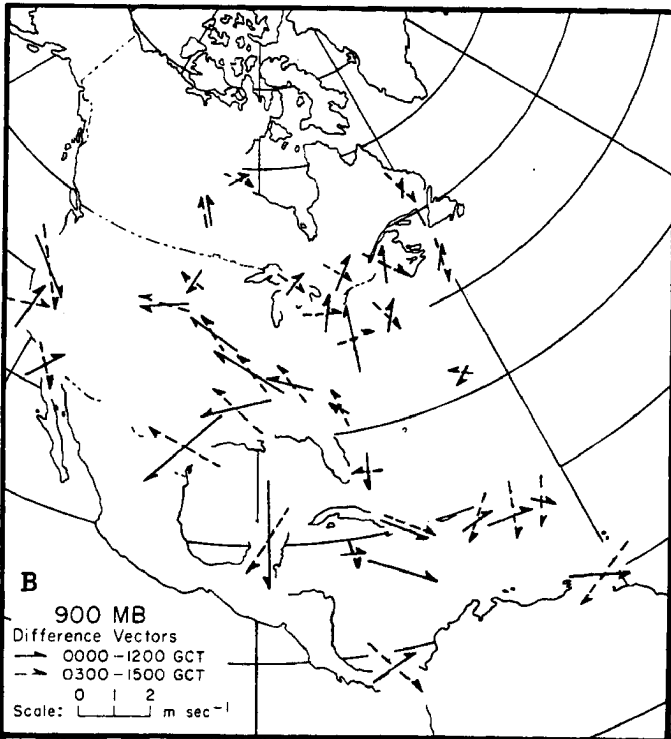
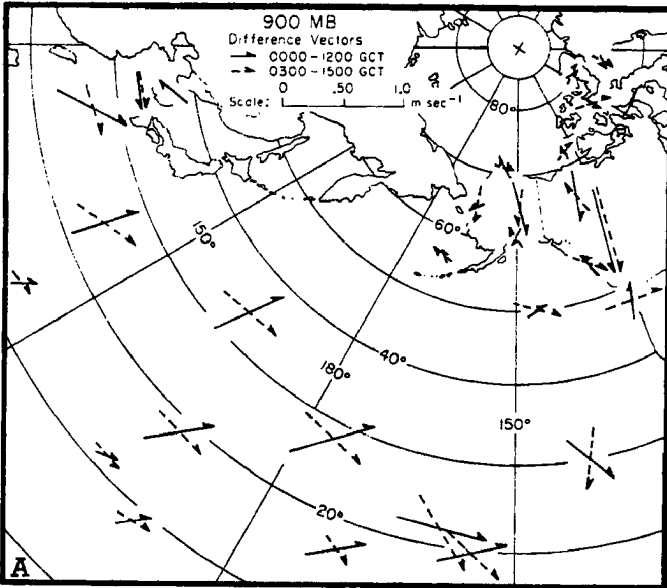


Fig. 7.4a. Annual average 0000-1200 GMT (solid) and 0300-1500 GMT (dashed) wind differences at 900 mb, plotted in vector form (from

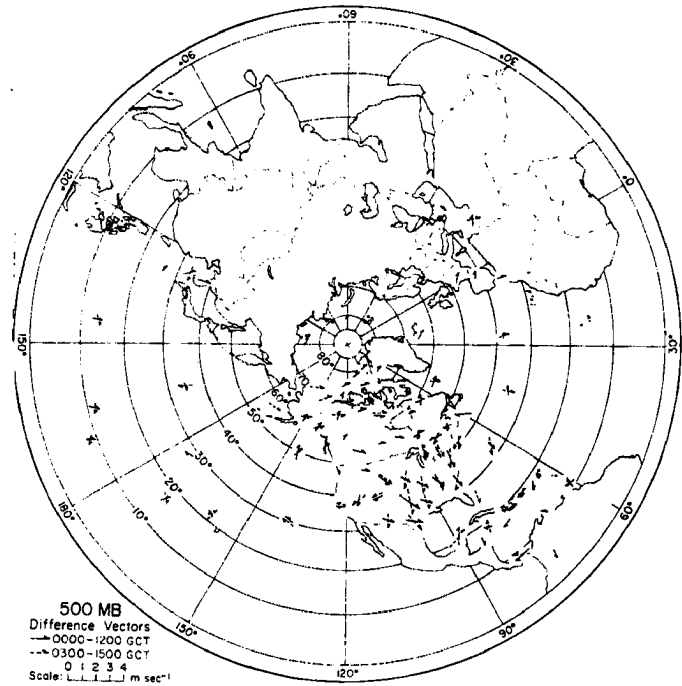


Fig. 7.4b. Same as Fig. a for 500 mb.



Fig. 7.4c. Same as Fig. a for 200 mb.

Fig. 7.4. Diurnal variation of wind as observed by Wallace and Hartranft (1969).

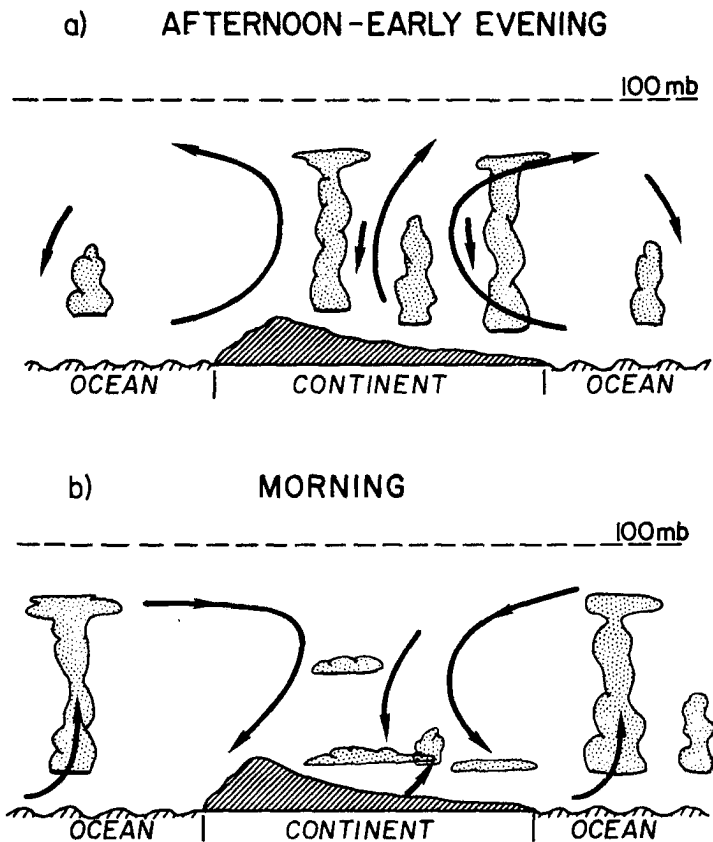


Fig. 7.5. Idealized illustration of diurnal ocean-continent circulation with a continental morning maximum of subsidence (diagram b) in comparison with a continental minimum of subsidence in the afternoon-early evening (diagram a). The oceanic subsidence is out of phase with the continental subsidence.

Wallace and Hartranft (1969) indicated that continental-ocean scale circulations can produce diurnal divergence changes of 10^{-6}sec^{-1} or more. It appears that circulations on this scale might substantially contribute to the morning maximum of continental subsidence which is out of phase with the continent afternoon maximum in deep convection. This type of continent-ocean diurnal circulation should also be present over other continents.

- c) A likely hemispheric tropospheric circulation driven by the mean $\sim 0.5-0.7^{\circ}$ net daytime minus nighttime tropospheric warming over nighttime value which this paper has documented. This requires the daytime tropospheric depth to be about 20-30 meters greater during the day than at night. Although impossible to measure, this hemispheric circulation (Fig. 7.6) may well exist and produce extra upper level divergence in the sun-free hemisphere. If this type of hemispheric circulation is in operation, the resulting upper and lower tropospheric divergence-convergences would be on the order of $\sim 10^{-7}\text{sec}^{-1}$. Although

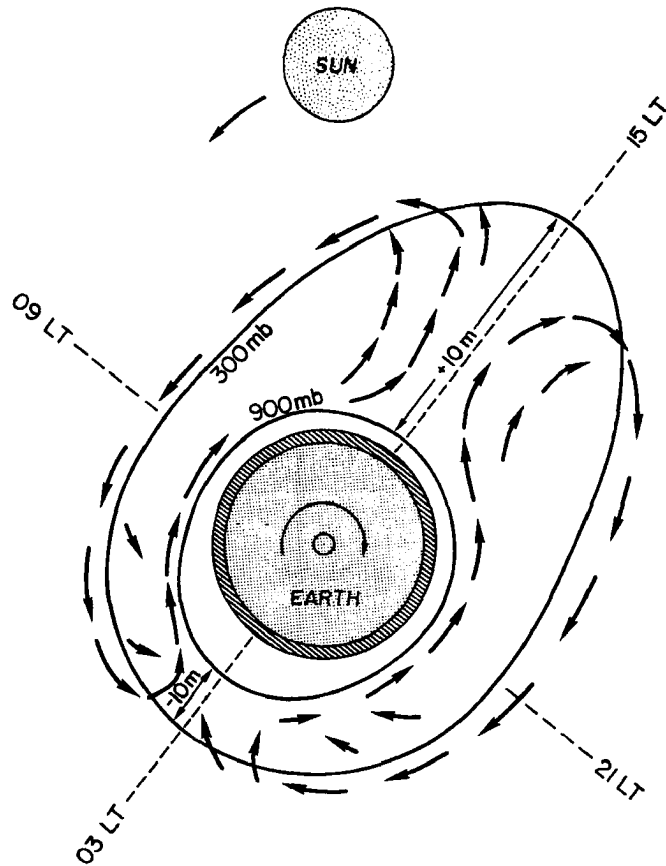


Fig. 7.6. Idealized illustration of how solar warming of the sunlit portion of the atmosphere in comparison with the sun-free portion of the globe could produce pressure level slopes and induce horizontal motions causing relative maximum of subsidence during the nighttime hours. For illustrative purposes the slopes of the pressure surfaces are greatly exaggerated.

these divergence values are too small to explain the diurnal differences in required subsidence, they do act to enhance morning subsidence. Were this hemispheric circulation to be concentrated in selective locations, it could be locally significant.

It is hypothesized that the nature of deep cumulus convection patterns in each region largely dictate that region's mode of diurnal subsidence response. Moist oceanic regions long distances from continents probably produce their morning subsidence maximum through mechanism a). The convection-free sub-tropical anticyclone regions will likely develop their enhanced morning subsidence through a combination of mechanisms

b) and c). Other regions will have other combinations. Mechanism c) may contribute in all areas.

Tropospheric subsidence is thus believed to be primarily produced by the net radiation energy deficit of the troposphere. This is analogous to the physical argument advanced by Charney (1975) on the probable subsidence response of a region to increased radiation loss from albedo change. The larger the radiation deficit the larger the subsidence. Assuming a 2-4 hour lag in adjustment time of wind to pressure-thickness changes, the nighttime radiation subsidence maximum may thus extend throughout the morning hours (up to about noon) and the solar radiation induced daytime subsidence minimum well into the evening hours (up to 22 LT or midnight) as discussed by Jacobson and Gray (op.cit.).

More observational and modeling studies of this diurnal tropospheric energy cycle are needed. Perhaps the coming First GARP Global Experiment (FGGE) measurements can be used to more explicitly tie down this apparent large diurnal variation in subsidence. It is implied that the Hadley, Walker, Ferrel, and other large circulation systems should possess a substantial diurnal cycle. It is a moot question whether global numerical weather prediction will require proper handling of this diurnal circulation.

ACKNOWLEDGEMENTS

The author would like to express his sincere gratitude to Professor William M. Gray for his guidance and enthusiastic approach to education. The author has also appreciated the use of Professor Stephen Cox's radiation model and for discussions on radiation theory. Many thanks also are due to Ms. Barbara Brumit and Ms. Dianne Schmitz for their untiring efforts in typing the manuscript and to Mr. Charles Solomon and Mr. Edwin Buzzell for their computer programming assistance. Dr. William M. Frank and Mr. William A. Fingerhut assisted with the final manuscript review. The author especially appreciates the patience and understanding of his wife, Janie.

This research has been sponsored by the National Science Foundation Grant Number OCD 75-01424.

BIBLIOGRAPHY

- Ballard, J. C., 1933: The diurnal variation of free-air temperature and the temperature lapse rates. Mon. Wea. Rev. 61, 61-80.
- Betts, A. K., 1972: A composite mesoscale cumulonimbus budget. Atmos. Sci. Research Paper No. 186, Colo. State Univ., Ft. Collins, CO, 43 pp.
- Brünner, B., F. Ostapoff, and H. Schmidt, 1973: Upper air soundings during Atlantic Trade-wind Expedition. National Oceanic and Atmospheric Administration, U.S. Gov't Printing Office.
- Carlson, G. C. and S. Hastenrath, 1970: Diurnal variation of wind, pressure and temperature in the troposphere and stratosphere over Eniwetok. Mon. Wea. Rev., 98, 408-416.
- Charney, J. G., 1975: Dynamics of deserts and drought in the Sahel. Quart. J. Roy. Meteor. Soc., 101, 193-202.
- Cox, S. K., 1969a: Observational evidence of anomalous infrared cooling in a clear tropical atmosphere. J. Atmos. Sci., 26, 1347-1379.
- Cox, S. K., 1969b: Radiation models of mid-latitude synoptic features. Mon. Wea. Rev., 97, 637-651.
- Cox, S. K. and S. Hastenrath, 1971: Radiation measurements over the equatorial central Pacific. Mon. Wea. Rev., 98, 823-832.
- Cox, S. K., T. Vonder Haar, K. J. Hanson and V. Suomi, 1973: Measurements of absorbed short wave energy in a tropical atmosphere. Solar Energy, 14, 169-173.
- Cox, S. K., 1974: Infra-red heating calculations with a water vapor pressure broadened continuum. Quart. J. Roy. Meteor. Soc., 99, 669-679.
- Davis, P. A., 1963: Analysis of the atmospheric heat balance. J. Atmos. Sci., 20, 5-22.
- Dopplick, T. G., 1970: Global radiative heating of the earth's atmosphere. Ref. No. 24, Planetary Circulation Project, Dept. of Meteorology, M.I.T., Cambridge, 128 pp.
- Finger, F. G., R. B. Mason and S. Teweles, 1964: Diurnal variation in stratospheric temperatures and heights reported by the U.S. Weather Bureau outrigger radiosonde. Mon. Wea. Rev., 92, 243-250.
- Finger, F. G. and R. M. McInturff, 1968: The diurnal temperature range of the middle stratosphere. J. Atmos. Sci., 25, 1116-1128.
- Gray, W. M., 1973: Cumulus convection and larger-scale circulations, Part I: Broadscale and meso-scale considerations. Mon. Wea. Rev. 101, 839-853.

BIBLIOGRAPHY (cont'd)

- Gray, W. M., 1976: Diurnal variation of oceanic deep cumulus convection, Part II: Physical Hypothesis. Atmos. Sci. Research Paper No. 243, Colo. State Univ., Ft. Collins, CO, 49-106.
- Hanson, K. J., T. Vonder Haar, and V. Suomi, 1967: Reflection of sunlight to space and absorption by the earth and atmosphere over the United States during spring 1962. Mon. Wea. Rev., 95, 354-362.
- Harris, M. F., 1959: Diurnal and semidiurnal variations of wind, pressure, and temperature in the troposphere at Washington, DC. J. Geophys. Res., 64, 983-995.
- Harris, M. F., F. G. Finger and S. Teweles, 1962: Diurnal variation of wind, pressure and temperature in the troposphere and stratosphere over the Azores. J. Atmos. Sci., 19, 136-149.
- Hastenrath, S., 1972: Daily wind, pressure and temperature variation up to 30 km over the tropical western Pacific. Quart. J. Roy. Meteor. Soc., 98, 49-59.
- Hastenrath, S. and M. Steinberg, 1971: On daily variations of temperature and heat budget in the tropical atmosphere. Arch. Met. Geoph. Biokl., Ser. A, 189-210.
- Hergesell, H., 1922: The daily change of temperature in the free atmosphere over Lindenberg. Arb. Preuss. Aeron. Obs. Lindenberg., 14, 1-4.
- Jacobson, R. W. and W. M. Gray, 1976: Diurnal variation of oceanic deep cumulus convection. Atmos. Sci. Research Paper No. 243, Colo. State Univ., Ft. Collins, CO, 106 pp.
- Kay, R. H., 1951: The apparent diurnal temperature variation in the lower stratosphere. Quart. J. Roy. Meteor. Soc., 77, 427-434.
- London, J., 1952: The distribution of radiational temperature change in the northern hemisphere during March. J. of Meteor., 9, 145-151.
- London, J., 1957: A study of the atmospheric heat balance. Final Report, Contract No. AF 19(122)-165, Dept. of Meteor. and Oceanography, NYU, 1957, 99 pp.
- Lopez, R. E., 1973: Cumulus convection and larger scale circulations. II: Cumulus and mesoscale interactions. Mon. Wea. Rev., 101, 856-870.
- Madden, R., E. Zipser, E. Danielsen, D. Joseph and R. Gall, 1971: Rawinsonde data obtained during the Line Islands Experiment, Vol. 1. NCAR Tech. Note, Nat'l Center for Atmos. Research, Boulder, CO.

BIBLIOGRAPHY (cont'd)

- Manabe, S. and R. F. Strickler, 1964: Thermal equilibrium of the atmosphere with a convective adjustment. J. Atmos. Sci., 21, 361-385.
- Nitta, T. and S. Esbensen, 1974: Diurnal variations in the western Atlantic trades during the BOMEX. J. Meteor. Soc. Japan, 52, 254-257.
- Ostapoff, F., W. W. Shimmers and E. Augstein, 1970: Some tests on the radiosonde humidity error. NOAA Tech. Report, ERL 194, AOML, 4, 24 pp.
- Pressman, J., 1955: Diurnal temperature variations in the middle atmosphere. Bull. Am. Meteor., 36, 220-223.
- Reynolds, D. W., T. H. Vonder Haar and S. K. Cox, 1975: The effect of solar radiation absorption in the tropical troposphere. J. Appl. Meteor., 14, 433-444.
- Riehl, H., 1947: Diurnal variation of pressure and temperature aloft in the Eastern Carribean. Bull. Amer. Meteor. Soc., 28, 311-318.
- Rogers, C. D., 1967: The radiative heat budget of the troposphere and lower stratosphere. MIT, Dept. of Meteor., Planetary Circulations Project, Report No. A2, 99 pp.
- Ruprecht, E., 1975: Diurnal temperature corrections for rawinsonde humidity sensors. Mon. Wea. Rev., 103, 352-355.
- Ruprecht, E. and W. M. Gray, 1976: Analysis of satellite-observed cloud clusters. Paper I and II. Tellus, 391-425.
- Sellers, W. D., 1965: Physical Climitology. Univ. of Chicago Press, 272 pp.
- Sparrow, J. G., 1967: Note on the diurnal cycle in the equatorial stratosphere. J. Appl. Meteor., 6, 441-444.
- Teweles, S. and F. G. Finger, 1960: Reduction of diurnal variation in the reported temperatures and heights of stratospheric constant-pressure surfaces. J. Meteor., 17, 177-194.
- U.S. Standard Atmosphere Supplements, 1966: ESSA, U.S. Gov't Printing Office, 289 pp.
- Wallace, J. M. and F. R. Hartranft, 1969: Diurnal wind variations, surface to 30 kilometers. Mon. Wea. Rev., 97, 446-455.

BIBLIOGRAPHY (cont'd)

- Wallace, J. M. and D. B. Patton, 1970: Diurnal temperature variations: surface to 25 kilometers. Mon. Wea. Rev., 98, 548-552.
- Williams, K. T. and W. M. Gray, 1973: Statistical analysis of satellite observed trade wind cloud clusters in the western north Pacific. Tellus, 25, 313-336.
- Wulf, O. R., M. W. Hodge, and S. J. Obloy, 1946: The meteorological conditions in the upper reaches of the radiosonde flights over the United States, II diurnal effects in temperature and pressure. Dept. of Meteor., Univ. of Chicago, Misc. Report No. 21, 44 pp.

APPENDIX A

CHARACTERISTICS OF RADIOSONDE INSTRUMENTATION

For many years the basic radiosonde instrument used by the U.S. Weather Bureau was of the duct or channel type. The measured properties were taken of air passing through a centered protected portion of the instrument. The absorption of solar radiation in the upper atmosphere by this type of sonde caused a temperature error which increased with altitude. The primary reason for this problem was that the thermistor element was not ventilated properly and the sensor reached equilibrium with the warmer instrument housing surrounding it. One of the main reasons why the duct-type instrument continued to be used was that the thermistor and hygistor were protected from hydrometeors. Early in 1960, however, the U.S. Weather Bureau instituted a program to replace the duct-type radiosonde instrument with one having an outrigger construction ("X" series radiosondes) for the temperature sensing element. This unit employed a white coated rod thermistor of 50 mil³ diameter. This element reflects approximately 94 percent of the incident solar radiation (Teweles and Finger, 1960). Brasefield (1948) determined that the outrigger radiosonde has a radiational error at upper levels only about one-tenth as large as the duct-type sonde. By the end of 1960 most Weather Bureau radiosonde stations were equipped with this new instrument. By contrast, the U.S. military radiosonde, (AR/AMT-AA) has had an externally mounted 33 - mil diameter thermistor since before 1956.

³₁ mil = .001 inch

The U.S. Weather Bureau "X" Series Radiosondes. The "X" designation refers to radiosondes having an outrigger type construction for the temperature sensing unit. This type sonde was utilized at all USWB, Mexican, and Canadian radiosonde stations during the period examined in the Northern Hemispheric portion of this study. From the Federal Meteorological Handbook No. 3: Radiosonde Observations (1969), the temperature of the free atmosphere is measured by a thermistor whose electrical resistance is a function of temperature. As the sonde ascends, the thermistor is switched sequentially (alternating with the hygristor) into the modulator circuit by the baroswitch and the information is transmitted to the receiving station. The U.S. supported radiosonde stations together with the Mexican and Canadian stations utilize sondes operating on a nominal carrier frequency of 1680 MH or 403 MHZ. Thus the radiosonde identifier, WB-1680-X or WB-403-X, indicates the transmitting frequency of the sonde (1680 MHZ or 403 MHZ) and the fact that an externally mounted thermistor is employed (X). Table A1 lists the various types of radiosondes utilized in this study. Figures A1 and A2 show the basic sonde design and more specifically the construction of the temperature sensing system.

TABLE A1

Types of Radiosondes Used In Collecting

Data For This Study

	<u>Type of Radiosonde Used</u>
1. Northern Hemisphere operational program (1966-1969)	WB - 403 - X WB - 1680 - X

TABLE A1 (cont'd)

	<u>Type of Radiosonde Used</u>
2. Operations Redwing and Hardtack	AN/AMT - 4A
3. Line Islands Experiment	WB - 403 - X
4. Atlantic Tradewinds Experiment	WB - 403 - X
5. Barbados Oceanographic and Meteorological Experiment	WB - 403 - X WB - 1680 - X
6. GARP Atlantic Tropical Experiment	WB - 403 - X (with modi- fied hygistor system)

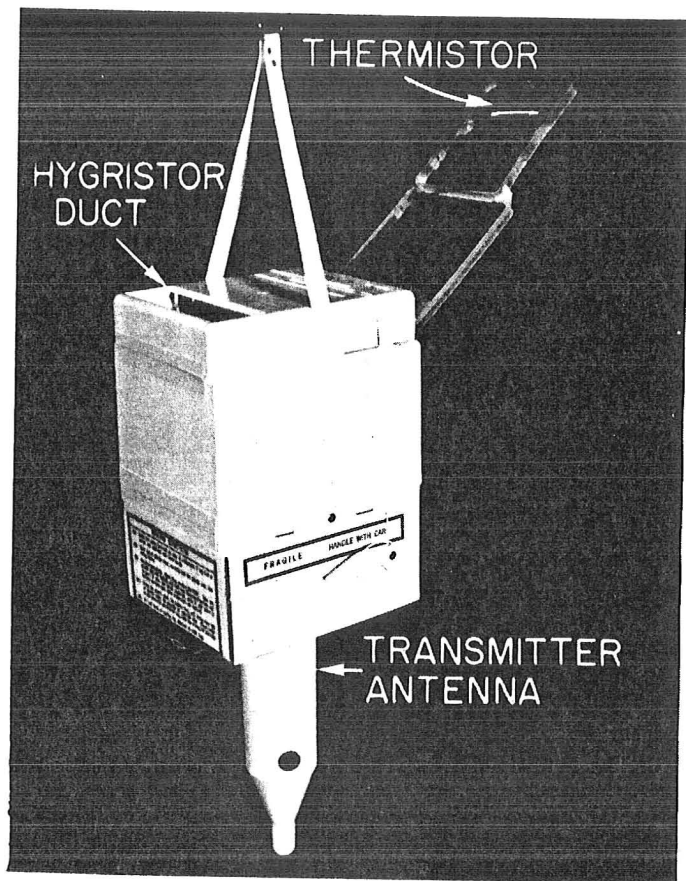


Fig. A.1. Standard Radiosonde utilized during the Northern Hemispheric portion of this study.

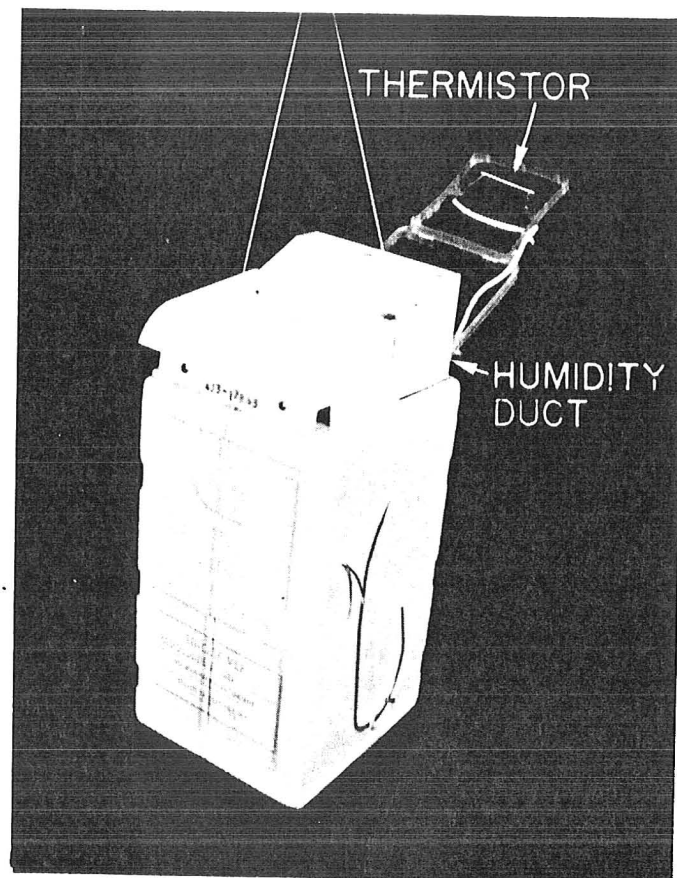


Fig. A.2. Radiosonde used during GATE.

APPENDIX B

INSTRUMENTAL ERRORS IN THE TEMPERATURE OBSERVATIONS

The absorption of solar radiation by the temperature sensing element on the radiosonde has long been the nemesis of scientists studying the upper atmosphere (Harris, 1959; Teweles and Finger, 1960; Wallace and Patton, 1970; and others). Attempts have been made to employ observational data for the purpose of verifying various theoretically derived results of the diurnal variation in the troposphere and stratosphere. However, these efforts have been hampered by a rather limited knowledge of radiationally induced error. It is of particular importance in this study that a suitable understanding of the tropospheric radiation error be attained. The primary question is one of separating the magnitude of the spurious and true components of the diurnal temperature variation. While a detailed correctional scheme used for radiation induced errors is beyond the scope of this study, a discussion of the approximate magnitude of this error will be made. Four basic types of errors affect the temperature observation. They are: 1) solar radiation error, 2) infrared radiation error, 3) baseline check error, and 4) lag error.

The error due to solar radiation absorption increases with altitude. This occurs partly because less solar energy has been depleted due to gaseous scattering and absorption but primarily because the ventilation of the radiosonde thermistor element in the rarified air decreases as a function of density. At stratospheric levels this ventilation is quite small. The problem is minimized when only data collected below 300 mb is utilized. Infrared

radiation from the earth-atmosphere system also has some affect on the accuracy of the measurement. By examining values computed for upward and downward flux of infrared radiation from the IR cooling model, the conclusion was reached that in the troposphere the infrared radiational flux can essentially be considered constant throughout daylight and darkness. (See Figs. D6 - D9). This conclusion is based on satellite observations that indicate that the diurnal variation in total cloudiness is not large (Winston, 1976; Gruber, 1975). Following Finger and McInturff (1968), the diurnal temperature variation can be represented as

$$[T(00) - T(12)]_{\text{observed}} = T(00) + T_i + T(\alpha_1) - [T(12) + T_i + T(\alpha_2)]$$

where $T(00)$ and $T(12)$ - actual temperatures

T_i - error due to infrared radiation

$T(\alpha)$ - error due to solar radiation which is dependent on the solar elevation angle and altitude

Because it has no diurnal function, T_i can be eliminated from this equation requiring the observed diurnal temperature variation to be comprised of only two parts - actual variation and error induced by solar radiation.

Several studies have attempted to bypass the inherent error in the temperature sensing element of the radiosonde by applying an independent method of using wind observations to calculate pressure variations which in turn can be converted to temperature variations through the hydrostatic and geostrophic relationships. This method has made use of a model based on a linearized form of the equations of motion and the assumptions of frictionless flow and a simple westward progressing wave (Harris 1959).

The magnitude of solar radiational error has been determined for a layer between 250 mb and 125 mb at eight stations in the Northern Hemisphere (Finger, Harris & Teweles, 1965) by employing the computational procedure similar to that described for Harris (1959). The systematic radiationally induced error found was $.12^{\circ}\text{C}$, and this is consistent with National Weather Service specifications. The NWS has used the same temperature sensing device since 1960 and has laboratory tested the instrument in relation to random and systematic errors due to radiation and determined that the observations are valid within $.2^{\circ}\text{C}$ in the mid-latitude troposphere (A. Mellick).⁴ Badgley (1957) also performed laboratory experiments with white-coated rod thermistors of 0.027 in (0.069 cm) diameter. He determined that at 5 km, with 13.5% of the radiative flux from the sun depleted, the solar radiationally induced temperature error was $.15^{\circ}\text{C}$. He performed the same test at a simulated 10 km and found that with 10% of the solar radiative flux depleted the error was $.19^{\circ}\text{C}$. These calculations were made with the assumption that the long axis of the thermistor rod was perpendicular to the solar rays. He used a ventilation speed of 305 m/min which is consistent with NWS specifications. It should be realized that this magnitude of error is not present in all daytime observations and that this error increases to its maximum as the time of observation approaches local noon. The error increases in magnitude with higher altitude reaching rather exorbitant values (on the order of a degree) in the upper stratosphere.

⁴Personal communication, Art Mellic, Radiosonde Development Office, 30 March 1976.

Therefore, it is assumed that although there probably is a small error in the diurnal variation of temperature in the 300-850 mb layer, it does not alter the basic conclusions arrived at in this paper. However, since the exact magnitude and distribution of error relative to the solar elevation angle is currently unknown, the results must be interpreted with this inherent problem in mind.

Inaccurate radiosonde temperature-baseline techniques (Cox, Maynard, and Suomi, 1968) can also cause an error in the temperature observation. An analysis of radiosonde measurements made during the Line Islands Experiment indicated that the conventional preflight procedures utilized by the average observer may cause a slight underestimate of upper level temperatures. This occurs because the baseline check prior to sonde release is made at relatively high temperatures in the tropics, and this part of the temperature-frequency curve is rather insensitive; i.e., for a given frequency value, an error of $\pm .67^{\circ}\text{C}$ in temperature could result because of the flat slope of the curve.

While the baseline check problem is recognized as affecting the absolute temperature measurements of the troposphere, it does not vary diurnally and therefore should have no effect on the rate of change of the hourly temperature. It should not affect the results of this study.

A "lag" error can also be present. This is due to variations of ambient temperature with time which the thermistor element cannot precisely follow. Again this error affects the absolute magnitude of the temperature for a pressure level, but as long as the data is treated consistently (either lag corrected or left as originally observed) this type of error will have no effect on determining variations of temperature for a daily cycle.

Summary. Solar radiationally induced error, infrared error, baseline temperature calibration error, and lag error are the major types of error affecting the temperature observation. Of these four error sources, only solar absorption error has any significant effect. However, it is relatively small (generally less than $\sim 0.2^{\circ}\text{C}$) in the 850-300 mb layer. Therefore, the observed temperature variations are considered to be essentially real and not merely a result of instrument error.

APPENDIX C

COMPARISON OF RADIOSONDE ASCENTS
MADE IN DARKNESS AND DAYLIGHT

A number of studies analyzing the diurnal variations of temperature in the lower stratosphere and troposphere have utilized a data base consisting of upper air soundings taken only twice a day. Some ingenious schemes have been devised to examine the diurnal temperature variation. Teweles and Finger (1960) conducted an empirical study of the diurnal changes in temperature computed from successive radiosonde observations taken only in daylight and only in darkness and related their results to the variation of solar elevation angle. They attempted to evaluate the spurious portion of the diurnal temperature variation for several types of radiosondes and solar elevation angles. With the aid of a previous paper by Badgley (1957) on radiosonde instrumentation, Teweles and Finger determined that the radiosonde temperature error in darkness is due to incident long wave radiation only and is quite small when compared to the solar radiation error experience during daylight hours. This solar error occurs on the temperature sensing element (thermistor) due to absorption of incoming solar radiation causing an inflated daytime temperature. They showed that the daytime temperature error was a function of the solar elevation angle.

Utilizing the information that the sunrise line in relation to the 1200GMT observation and the sunset line in relation to the 0000GMT observation migrate annually across North America, they were able to collect successive ascent data taken at both 00GMT and 1200GMT in darkness only and in sunlight only. An example of the annual movement of the 0000GMT sunset and 1200GMT sunrise lines at the 300 mb level

pertinent to this study can be seen in Fig. C.1. The first day of the month was selected to represent the mean sunrise and sunset time for the entire month. Data collected only in darkness or in daylight when the solar angles are approximately the same can be considered relatively free from solar radiationally induced error.

Teweles and Finger also examined data from successive sonde ascents in which one was in darkness and one was in daylight. Because of the movement of the sunrise and sunset lines relative to standard observation times, stations in the eastern portion of North America release sondes in daylight in the morning and in darkness in the evening while in the west the daylight runs occur in the afternoon while the morning observations are in darkness. This series of events allowed the authors to compare 12-hour temperature differences at a specific level for the same solar elevation angle, one group of morning daylight minus darkness soundings, the other afternoon daylight minus darkness soundings. This procedure yielded what Teweles and Finger considered to be a close approximation to the diurnal variation of temperature, especially in the stratosphere where temperature variations are tied directly to radiational processes. This technique was used in subsequent papers by Finger, Mason and Teweles (1964) and Finger and McInturff (1968) to specify a typical model of the diurnal march of temperature at specific stratospheric levels and latitudinal bands. Although these papers were confined to the stratosphere their methods and conclusions are also applicable to studies examining the diurnal variability of tropospheric temperature.

While the method used by Teweles and Finger is applicable to ascertaining the temperature variations at a specific level (for example,

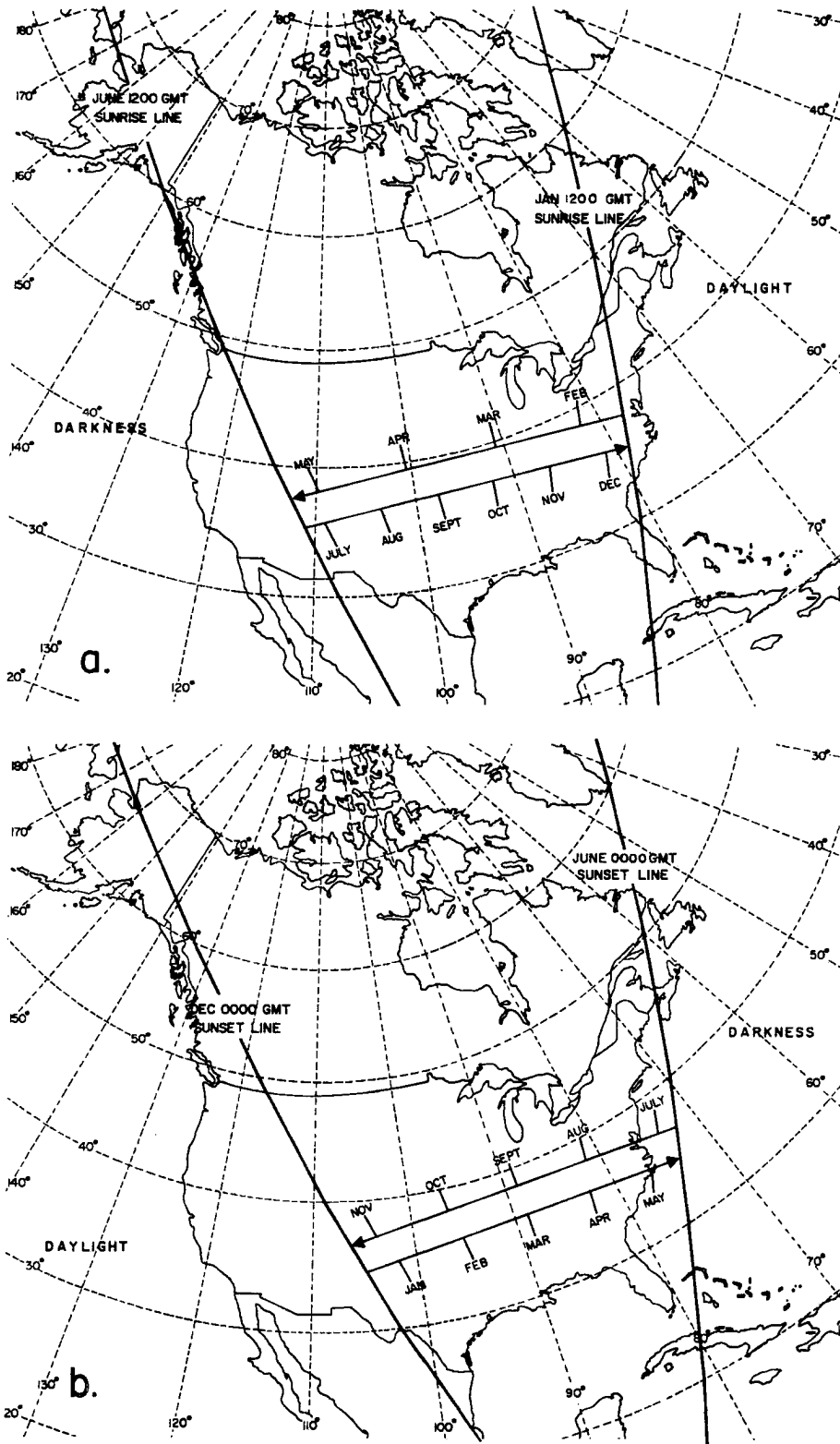


Fig. C.1. Annual migration of 12GMT sunrise line (a) and 00GMT sunset line (b) at 300 mb. Arrow indicates direction of movement for lines between extremes (From Finger, and McInturff, 1968).

100 mb), it must be modified in order to isolate entire sonde ascents from 850 mb to 300 mb in darkness or daylight. The purpose of this procedure is to identify the radiosonde stations which are located in regions where successive radiosonde ascents from 850-300 mb will be made totally in darkness or totally in sunlight.

In order to determine whether the radiosonde ascent is in darkness or daylight for runs made near local sunrise, the sunrise time at 300 mb during the winter and summer must be known. If the sun has not risen at 300 mb above the radiosonde station by the time that the sonde passes through that level, the run has been made in darkness and the temperatures will not be affected by incident solar radiation. If the sonde passes through 300 mb after sunrise, however, solar radiation may have influenced the thermistor. The solar elevation angle for sunrise at 300 mb is approximately -3.0° . Assuming that the sonde ascent was essentially vertical, the sunrise time at 300 mb on the equator was calculated to be about 8 minutes earlier than the sunrise at the upper-air station on the surface. This time difference is affected by the latitude of the radiosonde station and the season. The sunrise time at 300 mb relative to the surface sunrise below is computed utilizing the solar elevation angle at sunrise, the azimuth angle at sunrise, and the fact that the sun moves through 1° of longitude in four minutes. In Fig. C.1 (a) the line through the eastern portion of the continent is a manifestation of this calculation for the first of January and the line through the western portion of the country was computed for June 1st. These lines relate the mean solar time at 1200GMT to the local time of sunrise at 300 mb. The following assumptions were made in order to carry out this calculation:

(a) a balloon ascent rate of 305 m (1,000 ft.) per min.; and (b) a release time of 30 minutes prior to the standard observation time, as per NWS requirements. Therefore, the sonde was considered to pass through the 300 mb level at 00GMT and 12GMT as it takes about a half an hour to ascend from the surface to 300 mb.

The sunset calculation is somewhat simpler. If a sonde is released just after sunset, the entire ascent is made in the absence of incident solar radiation. Therefore, the surface sunset time relative to 0000GMT delineates the daylight/darkness lines shown in Fig. C.1. (b).

Winter. The lines designating the region where successive radio-sonde ascents were made in darkness are shown in Fig. C.2. These lines represent the latest time of the 300 mb sunrise and the earliest sunset time during December and January. Table C.1 lists all stations which are located in this region and their mean 850-300 mb temperature difference.

The temperature differences shown in Table C.1 indicate that there is actually a diurnal variation in the mean temperature of the 850-300 mb layer. The solar error component has been eliminated. The $\overline{\Delta T}$ values for the southern-most stations are the greatest in magnitude.

Summer. From previous studies (Teweles and Finger, 1960; Finger, Mason, and Teweles, 1964; others) it is known that the error due to solar radiation absorption is a direct function of the solar elevation angle. The error reaches its maximum when the solar elevation angle is greatest (local noon). To eliminate as much solar radiationally induced error as possible, the solar elevation angle at stations in central North America were calculated at 15 minutes prior to 0000GMT and 1200GMT for January 10 for the winter season and July 10 for the

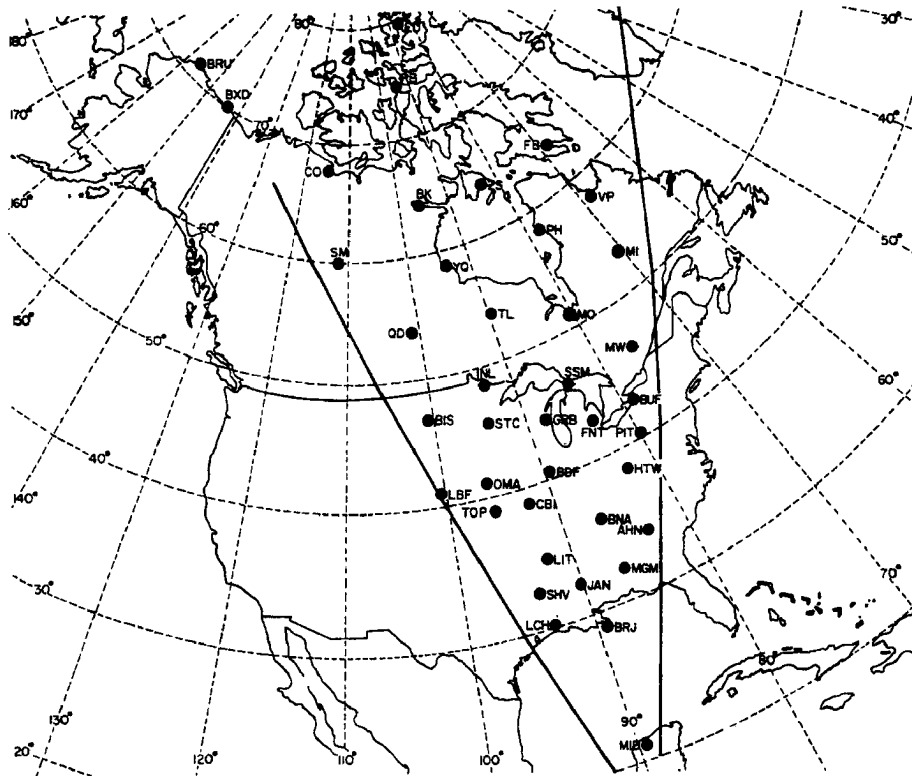


Fig. C.2. Stations included in region where both 00GMT and 12GMT radiosonde ascents are made in darkness during the winter (December and January.).

summer season. These dates were considered to represent the mean elevation angle conditions for their respective seasons. The following relationship was used for the calculation.

$$\cos z = \sin \phi \sin \delta + \cos \phi \cos \delta \cos t$$

where z - zenith angle

ϕ - latitude of station

δ - declination angle

t - hour angle of sun

and θ (solar elevation angle) = $90^\circ - z$

TABLE C1

Stations Included in Region Where Both 00GMT and 12GMT
Observations are in Darkness During the Winter Season

<u>Station</u>	<u>WMO#</u>	<u>[ΔT]</u>	<u>Station</u>	<u>WMO#</u>	<u>[ΔT]</u>
20-30°N			40-50°N (cont'd)		
Merida	76644	.33	S.S. Marie	72734	.16
Boothville	72232	.34	Int'l Falls	72747	.16
			Maniwaki	72722	.16
30-40°N			50-60°N		
Lake Charles	72240	.20	Inoucdjovac	72907	.09
Shreveport	72248	.27	Trout Lake	72848	.07
Jackson	72235	.39	Churchill	72913	.05
Montgomery	72226	.34	The Pas	72867	.25
Little Rock	72340	.18			
Nashville	72327	.22	60-70°N		
Huntington	72425	.07	Frobisher Bay	72909	.14
Columbia	72445	.31	Coral Harbor	72915	.13
Topeka	72456	.25	Baker Lake	72926	.17
40-50°N			Ft. Smith	72934	.10
Pittsburgh	72520	-.02	Coppermine	72938	.06
Peoria	72532	.24	70-80°N		
Omaha	72553	.32	Eureka	72917	.04
North Platte	72562	.13	Resolute	72924	.11
Buffalo	72528	.02	Pt. Varrow	70026	.22
Flint	72637	.14	Barter Is.	70086	.05
Green Bay	72645	.22			
St. Cloud	72655	.00			
Bismarck	72764	.00			

These computations were performed for 15 minutes prior to 0000GMT and 1200GMT because the sonde was assumed to be released thirty minutes prior to the standard observation time and in fifteen minutes the sonde would have ascended halfway to 300 mb.

When the solar elevation angles for 0000GMT and 1200GMT at a single station are approximately equal, the temperature difference (ΔT) can be considered essentially free from solar absorption error. Stations where this occurs are listed in Table C.2 and shown in Fig. C.3.

TABLE C2

Stations Included in Region Where the Solar Elevation
Angle is Approximately Equal at 00 GMT and 12 GMT

Summer Season

Latitude Belt	Station	WMO#	00GMT Solar Elevation Angle	12GMT Solar Elevation Angle	$[\Delta T]$
20-30°N	Boothville	72232	7.1°	7.1°	.76
30-40°N	Lake Charles	72240	13.5°	8.6°	.70
	Montgomery	72226	8.2°	15.4°	.47
	Jackson	72235	11.8°	11.8°	.68
	Shreveport	72248	14.2°	9.5°	.90
	Nashville	72327	10.7°	15.3°	.60
	Little Rock	72340	13.7°	11.4°	.82
	Columbia	72445	16.1°	11.7°	.73
	Topeka	72456	18.4°	9.5°	.65
40-50°N	Peoria	72534	14.4°	14.4°	.72
	Omaha	72553	19.0°	10.4°	.55
	Flint	72637	10.9°	19.3°	.49
	Green Bay	72645	14.5°	16.5°	.56
	St. Cloud	72655	12.8°	18.9°	.36
	S.S. Marie	72734	12.1°	20.1°	.53
	Int'l Falls	72747	18.6°	14.7°	.60
50-60°N	Trout Lake	72848	17.9°	17.9°	.57
	Churchill	72913	21.3°	16.8°	.45
60-70°N	Coral Harbor	72915	17.6°	22.7°	.31
	Baker Lake	72926	23.0°	18.6°	.42
70-80°N	Resolute	72924	22.8°	20.4°	.13
	Eureka	72917	21.3°	22.9°	-.08

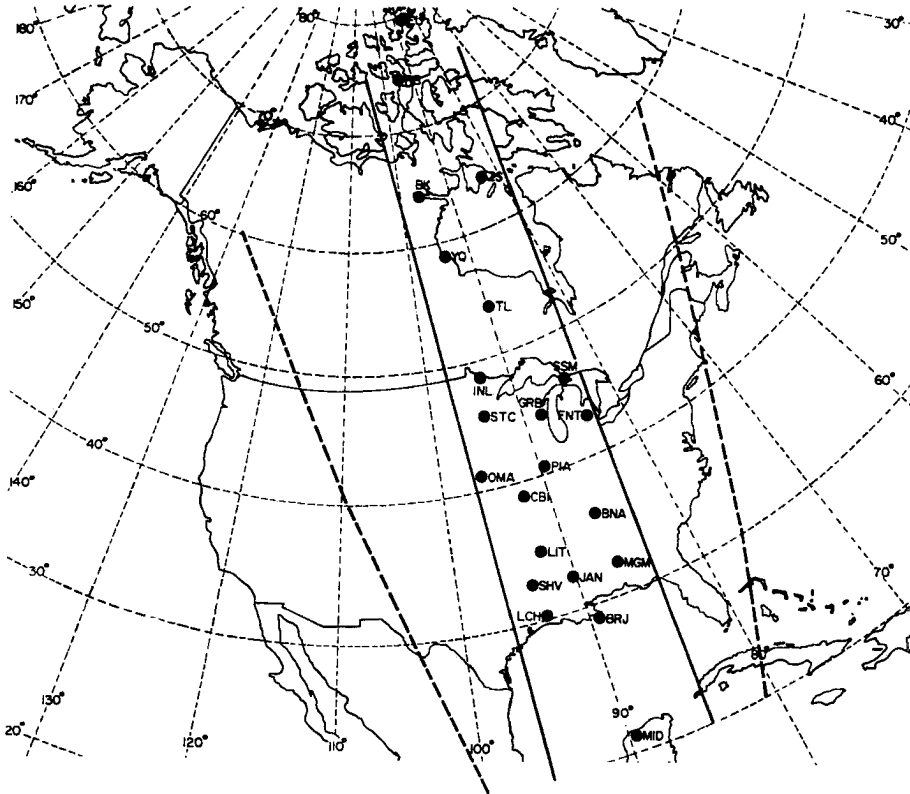


Fig. C.3. Region where successive 00GMT and 12GMT sonde ascents are made in sunlight (dashed lines). Stations included in region where mean solar elevation angle (θ) for the summer (June and July) is approximately equal (solid lines).

It is important to note that when the solar elevation angles at 00GMT and 12GMT are equal, they are never high angles and occur about 2 hours after sunrise and 2 hours prior to sunset. Thus, the values for $\overline{\Delta T}$ are not taken at the times when the maximum difference would be expected. Mean temperature differences for the 850–300 mb layer taken in the absence of solar radiationally induced error conform favorably to the general diurnal variability trend. There is definitely a diurnal variation in the mean temperature of the middle tropospheric layer as it appears in observations where there is no inherent solar radiational error.

Summary. Solar radiationally induced instrument error was eliminated from the data collected by radiosondes released from upper air

stations in central North America in both summer and winter. The temperature differences ($\overline{\Delta T}$) were of significant magnitude and substantiate the belief that the diurnal variation of temperature in the middle troposphere is real and not a product of instrument error.

APPENDIX D

SHORT AND LONG WAVE RADIATION MODELS

Determination of Heating Due to Solar Radiation Absorption. It is generally accepted (first suggested by Mügge and Möeller, 1932) that the amount of energy absorbed in an atmospheric layer is a function of the effective optical depth of the layer itself, the effective optical depth of the layers above, and the amount of energy incident upon the atmosphere from the sun. This, then was the basis for the model from Manabe and Strickler (1964) model which was used to calculate the heating due to short wave radiation. The atmospheric constituents used in the calculations were water vapor, carbon dioxide, and ozone. Clouds were not included as it would be very difficult to determine mean cloud distribution for each of the geographical blocks. However, Dopplick (1970) has determined heating and cooling due to short and long wave radiation using mean cloudiness and geographically varying radiative parameters (temperature, humidity, CO_2 , O_3) for each 10 degrees of latitude. His values are used as a comparison with this study's cloud free calculations.

A determination is first made of the effective optical depth of water vapor, CO_2 , and ozone by summing downward from the top of the atmosphere through the optical path of each layer.

The effective optical path for the entire atmosphere is then determined by summing for all layers in the atmosphere and correcting for the zenith angle of the sun. From the effective optical path the effective pressure of each constituent is computed, and subsequently the absorptivity values proposed by Manabe and Strickler (1964) can

be determined. The amount of short wave absorption ($\overline{\Delta a}$) in the 850-300 mb layer is determined by summing and averaging the individual level absorbances. The rate of solar radiation induced temperature change ($\frac{dT}{dt}$) is specified by:

$$\frac{dT}{dt} = \frac{g}{C_p} \frac{\Delta a}{\Delta p} \quad (D.1)$$

where T - temperature

t - time over which the change occurs

g - acceleration of gravity

C_p - specific heat of air at constant pressure

$\overline{\Delta a}$ - calories of short wave absorption which occurs in the layer

Δp - layer thickness

This model also has the capability of calculating the heating rate for small increments of time between sunrise and sunset (see Fig. 4.1).

The distribution of heating vs. time of day can thus be obtained.

This allows one to determine the amount of solar heating for any time increment during the solar heating period.

Long Wave Cooling. The basis for this computation is the radiative transfer equation which has been simplified somewhat by the assumption that all scattering processes can be neglected as the wavelength dimension is large compared to that of the scattering particles in a cloud-free atmosphere. The calculation of net long wave flux divergence in finite difference is given by

$$\begin{aligned}
 H(P) = & \sum H_i \left[\Delta \epsilon_{i_{H_2O}} + \Delta \epsilon_{i_{CO_2}} + \Delta \epsilon_{i_{O_3}} \right] + \\
 & H_o \left[1 - \sum \Delta \epsilon_{i_{H_2O}} - \sum \Delta \epsilon_{i_{CO_2}} - \sum \epsilon_{i_{O_3}} \right]
 \end{aligned}
 \tag{D.2}$$

where $H(P)$ is the irradiance at the specified pressure level P .

H_o is the irradiance emitted by the background to the atmosphere, i.e., this represents the σT_o^4 radiant energy for the earth's surface when computing the upward flux. H_o is equal to zero for the downward flux calculation as it is assumed that there is no infrared radiation entering the earth's atmosphere from above. The term containing H_i represents the emitted irradiance from the atmosphere itself arriving at pressure level P . $H_i = \sigma T_i^4$ where T_i is the average temperature of the layer i .

$\Delta \epsilon_{i_{H_2O}}$, $\Delta \epsilon_{i_{CO_2}}$, and $\Delta \epsilon_{i_{O_3}}$ are changes in emissivity through layer i from water vapor, carbon dioxide, and ozone, respectively. These flux emissivities are a function of the optical depth of the constituent (Staley & Jurica, 1970). Emissivity values were taken from sources compiled by Cox, Polifka, Rockwood, and Griffith, (1976). The effects of collision broadening are also incorporated in the computation. After the upward and downward irradiances are calculated and the net flux divergence for each layer is determined, the following equation is employed to compute the rate of long wave induced temperature change in the layer:

$$\frac{dT}{dt} = \frac{g}{(c_p)} \frac{(\Delta H_{net})}{\Delta p}
 \tag{D.3}$$

where ΔH_{net} - net long wave flux convergence (watts m^{-2})
and all other symbols are as previously defined
in equation (D.1).

Input Data. These radiation models require input data consisting of the vertical profiles of temperature, water vapor, carbon dioxide, and ozone. Mean 00GMT and 12GMT soundings for each geographical block for each season are used as input data for the radiational models. The radiosonde observational specific humidity data was supplemented at upper levels with frost point hygrometer data (Mastenbrook, 1968). Mastenbrook's data was collected in the West Indies, Washington, D.C., and Thule, Greenland and it was applied to the 0-30°N, 30-60°N, and 60-80°N latitudinal belt soundings, respectively. The ozone content of the atmosphere at various latitudes was taken from the Handbook of Geophysics and Space Environment.

In general, the daytime observation was used as the input sounding for the short wave model. However, in the cases when successive ascents were made in darkness or in daylight the afternoon sounding was utilized. It has been documented by several individuals (Ostapoff, Shinnars, and Augstein, 1970; Ruprecht, 1975; and others) that solar radiation incident on the hygistor (humidity sensing element) causes error in the reported values of relative humidity. The observed daytime relative humidity is less than actual because the humidity element senses an erroneously high temperature which produces a higher saturation vapor pressure than actual conditions prescribe. Thus the relative humidity (e/e_s) value is often 5-10% less than actual as is the specific humidity value calculated for input into the model.

This problem caused concern in attempting to accurately determine the heating from solar radiation based on erroneous humidity values.

Ruprecht (1975) determined that the nighttime relative humidity values for the lower troposphere, where the error is most significant, are a good estimate of humidity values for the entire day. Therefore, computations were performed with the short wave model utilizing daytime temperatures in combination with nighttime specific humidity values. The computations were made for several representative locations in an effort to determine the variation of total solar heating in the 850-300 mb layer (700-300 mb layer for elevated regions) due to instrument induced specific humidity variations. Figures D1 through D5 demonstrate the results. Obviously the specific humidity variations have very little effect on the computed heating values. In light of these results the daytime sounding will be used as input data for the solar heating calculation.

The nighttime sounding was used as input data for the infrared cooling model except in the case when successive ascents were in darkness or daylight and then the morning sounding was utilized. The variation of IR cooling between day and night was examined in an effort to determine whether a constant cooling rate for the entire 24 hour period could be assumed. Also the effect of specific humidity errors in the daytime soundings on the cooling rate was considered. Three different soundings were used as input for the long wave model cooling calculations:

1. Nighttime temperature and nighttime humidity.
2. Daytime temperature and daytime humidity (specific humidity less than actual due to instrument error).

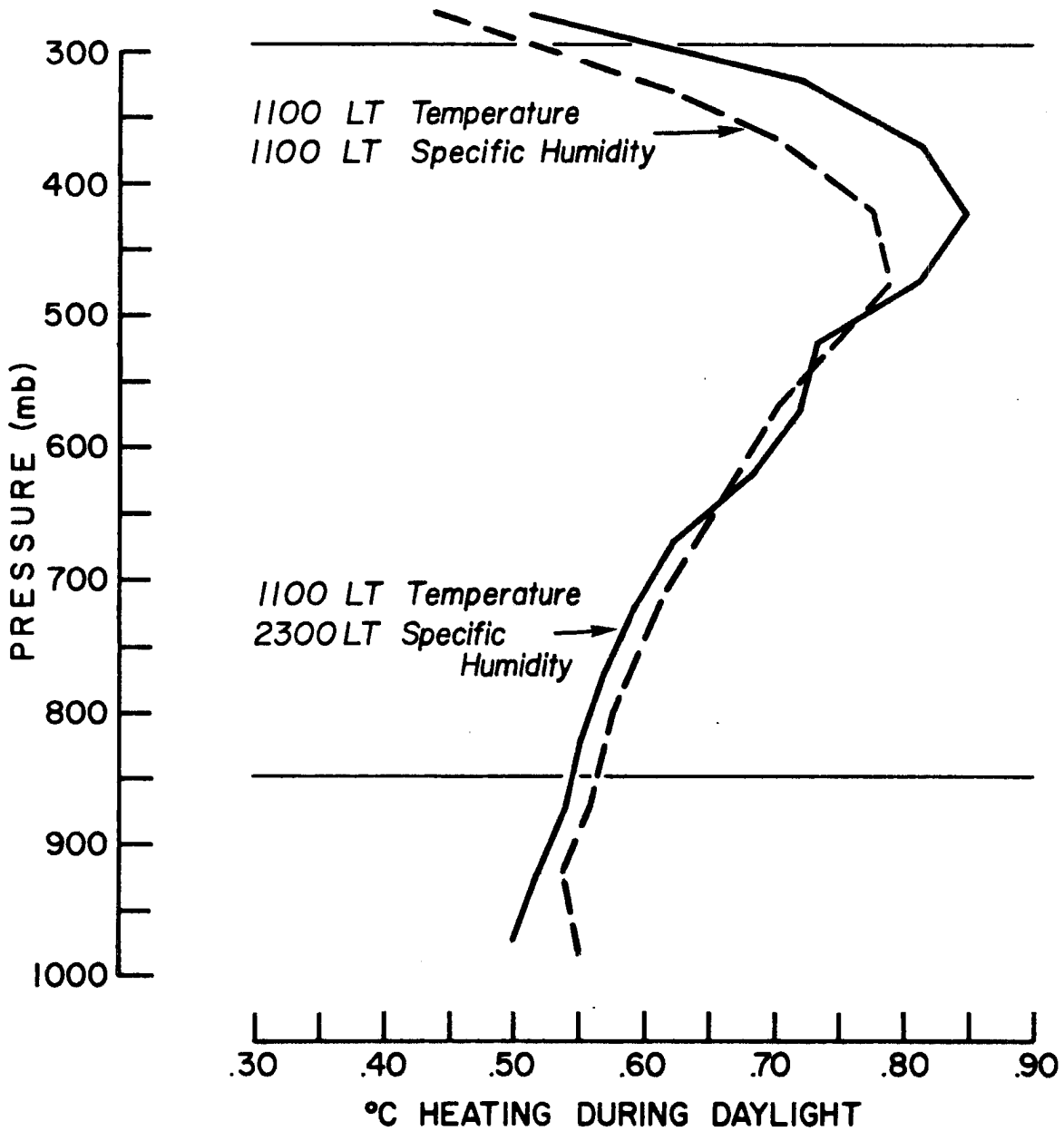


Fig. D.1. Variation in solar heating at a tropical location (Ponape) utilizing different input soundings. Mean solar heating in 850-300 mb layer was calculated to be $.70^{\circ}\text{C}$ with 1100 LT temperature and 2300LT specific humidity and $.67^{\circ}\text{C}$ with 1100LT temperature and 1100 specific humidity.

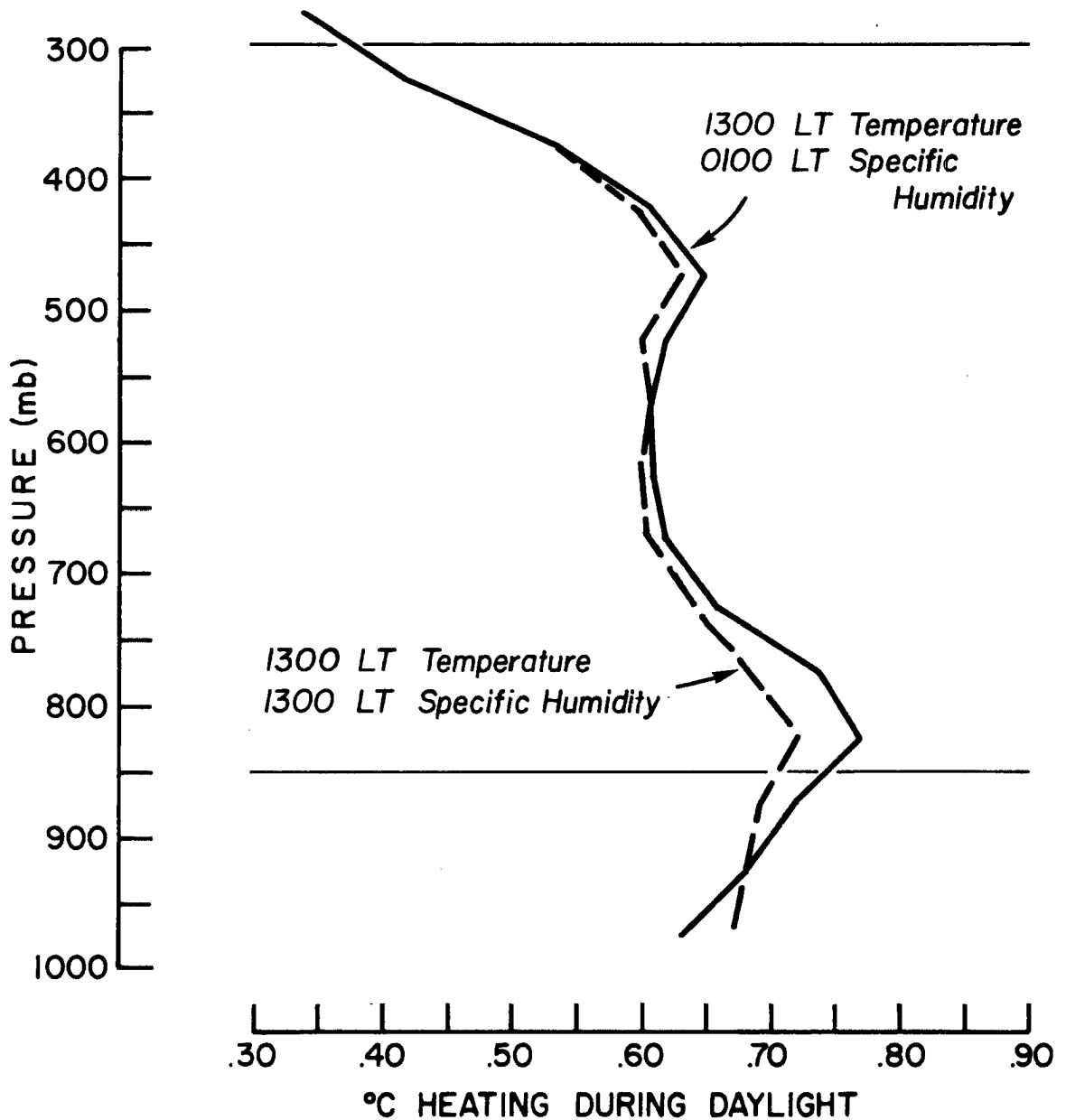


Fig. D.2. Variation in solar heating at a subtropical location (Johnston Island) utilizing different input soundings. Mean solar heating in 850-300 mb layer was calculated to be $.62^{\circ}\text{C}$ with 1300LT temperature and 0100LT specific humidity and $.61^{\circ}\text{C}$ with the 1300LT temperature and 1300LT specific humidity.

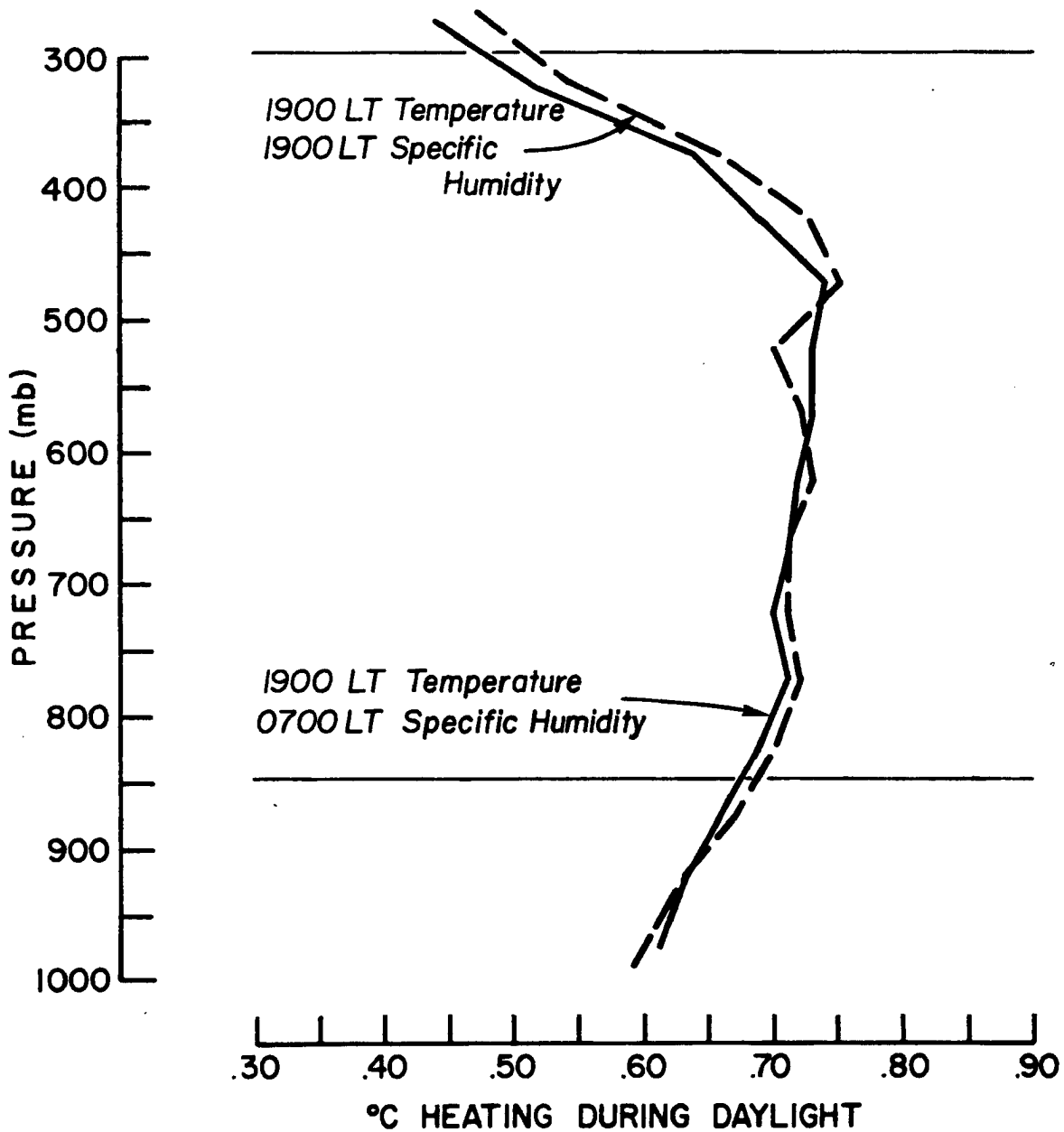


Fig. D.3. Variation in solar heating at a mid-latitude coastal location (Washington, D.C.) utilizing different input soundings. Mean solar heating in 850-300 mb layer was calculated to be $.69^{\circ}\text{C}$ with 1900LT temperature and 0700LT specific humidity and $.69^{\circ}\text{C}$ with 1900LT temperature and 1900LT specific humidity.

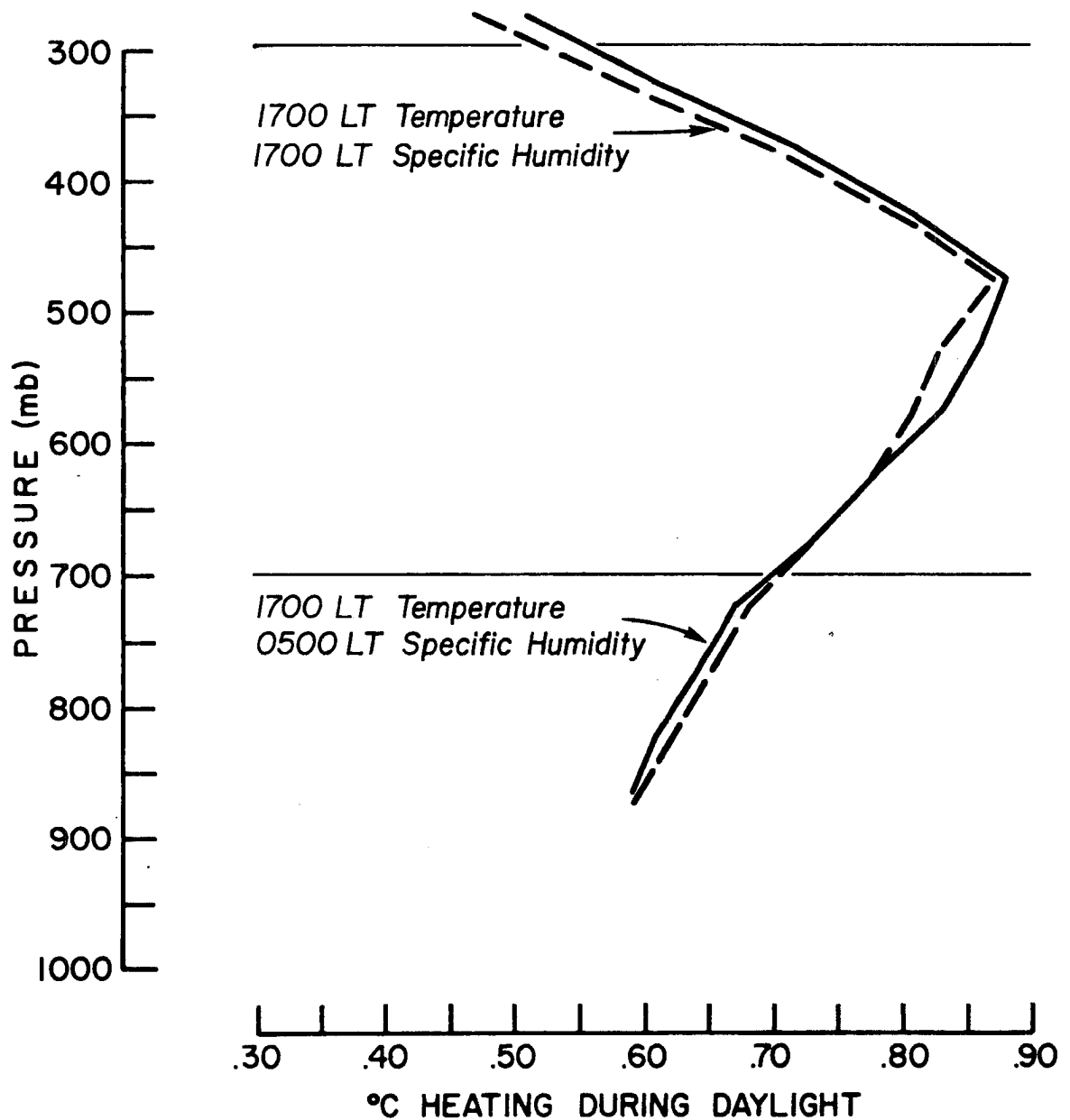


Fig. D.4. Variation in solar heating at a mid-latitude elevated location (El Paso, Texas) utilizing different input soundings. Mean solar heating in 700-300 mb layer was calculated to be $.78^{\circ}\text{C}$ with 1700LT temperature and 0500LT specific humidity and $.76^{\circ}\text{C}$ with 1700LT temperature and 1700LT specific humidity.

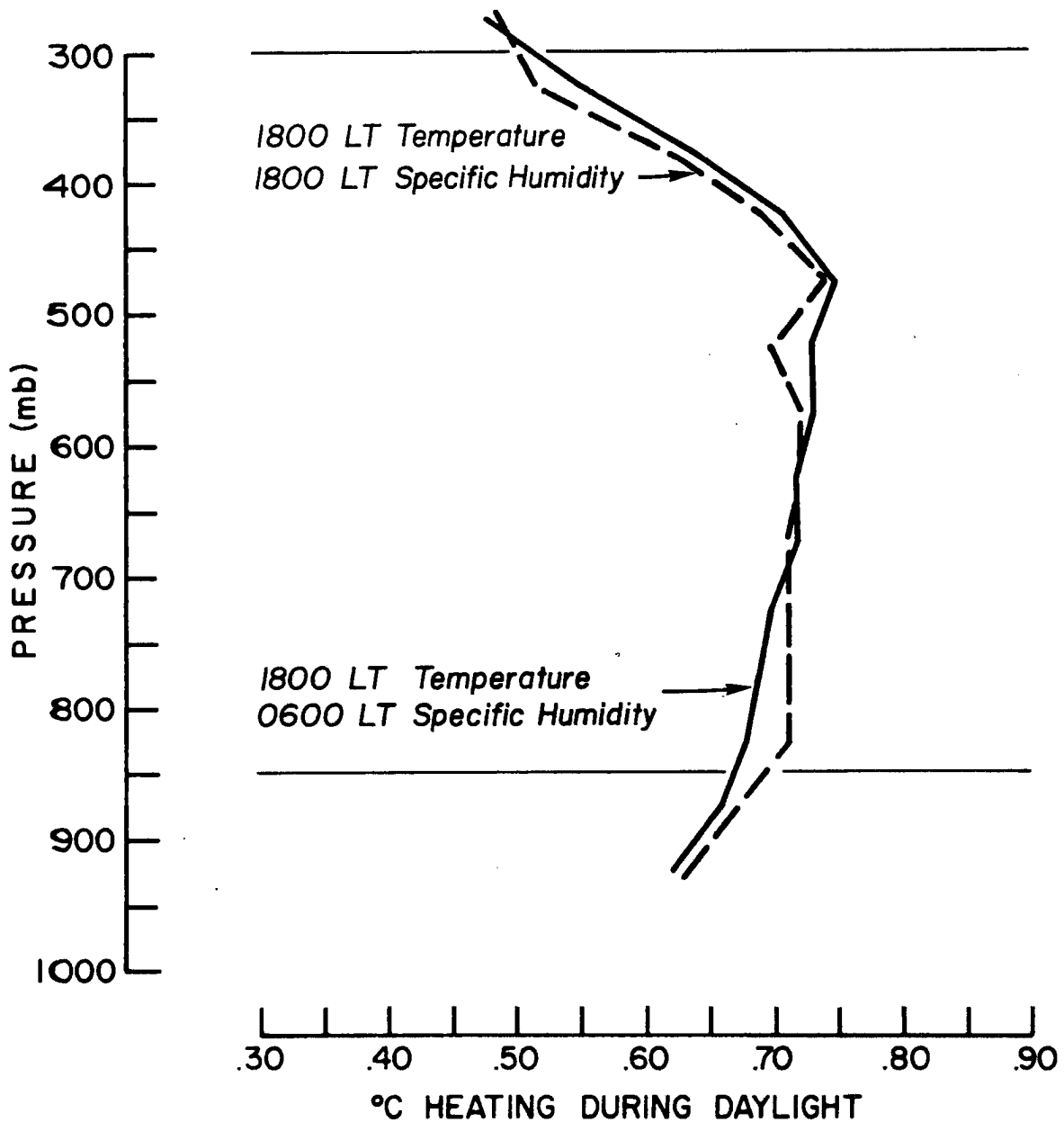


Fig. D.5. Variation in solar heating at a mid-latitude continental location (Peoria, Illinois) utilizing different input soundings. Mean solar heating in 850-300 mb layer was calculated to be $.69^{\circ}\text{C}$ with 1800LT temperature and 0600LT specific humidity and $.69^{\circ}\text{C}$ with 1800LT temperature and 1800LT specific humidity.

3. Daytime temperature and nighttime humidity (most realistic representation of daytime moisture conditions).

The computations were performed at several locations, and the results are displayed in Figs. D6 through D10. In the tropics and subtropics, the mean cooling rates for the 850-300 mb layer from the input soundings described for calculations (1) and (3) vary insignificantly and support the assumption of a constant cooling rate throughout the day. In the mid-latitudes the early morning cooling rate in the middle tropospheric layers is somewhat larger than the afternoon cooling rate. However, this difference becomes quite small when the 24 hour cooling rate is divided in half in order to compute the required warming for a twelve hour period. The maximum variation is only $.08^{\circ}\text{C}/12\text{ hr}$, (Fig. D9). Therefore, the nighttime sounding was used as input data for the calculation of the infrared cooling rate throughout the day.

Summary. The short and long wave radiation models computed the radiation induced temperature changes for the 850-300 mb layer (700-300 mb over elevated regions). From these calculations the values of $\overline{\text{SW}}$ and $\overline{\text{LW}}$ were obtained. The daytime relative humidity error had a negligible affect on the $\overline{\text{SW}}$ and $\overline{\text{LW}}$ computations, and the long wave cooling rate was assumed constant throughout the day.

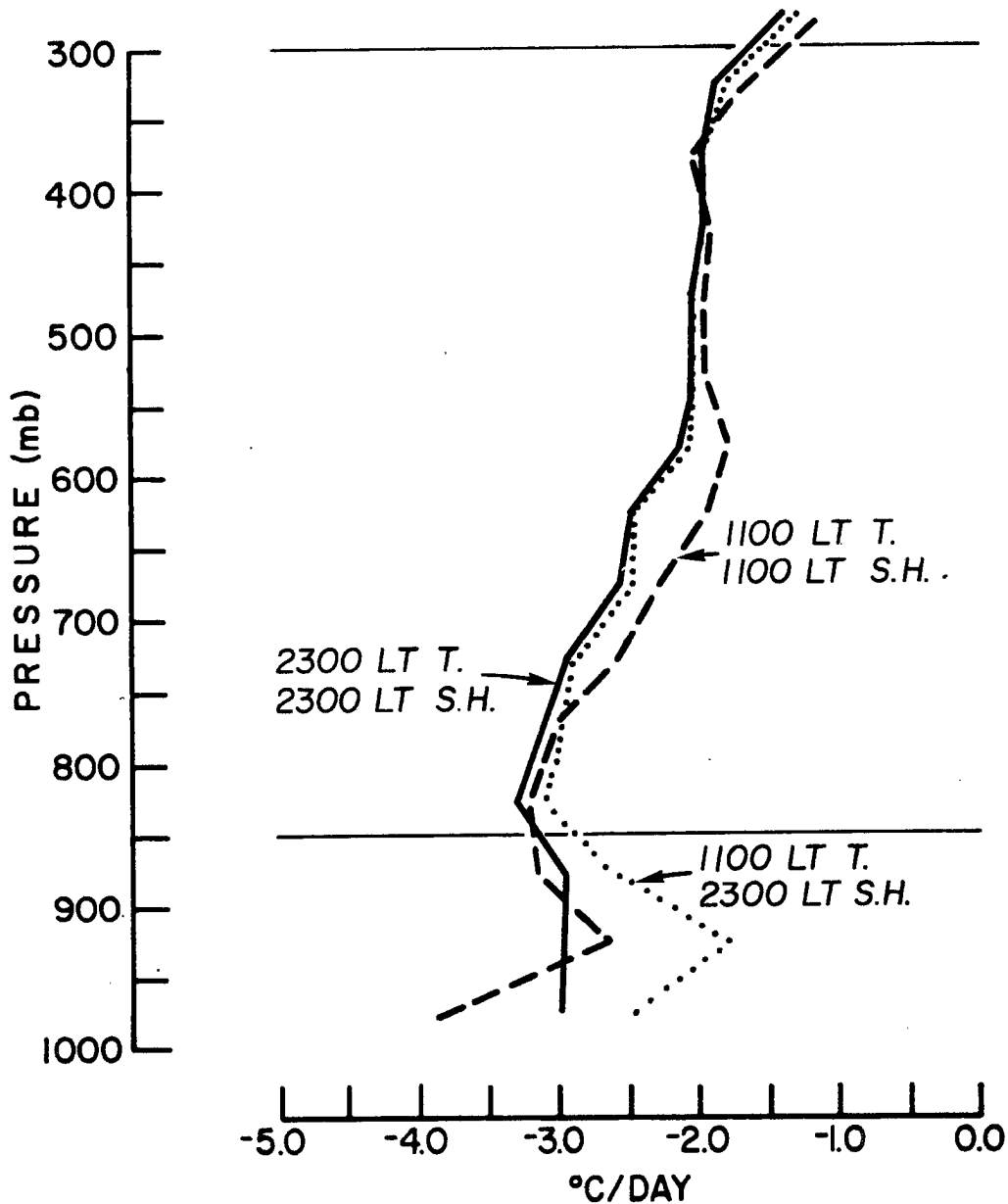


Fig. D.6. Variation in IR cooling at a tropical location (Ponape) utilizing different input soundings. Mean IR cooling rate in the 850-300 mb layer was calculated to be $-2.20^{\circ}\text{C}/\text{day}$ with 1100LT temperature and 1100 specific humidity, $-2.36^{\circ}\text{C}/\text{day}$ with 1100LT temperature and 2300LT specific humidity, and $-2.37^{\circ}\text{C}/\text{day}$ with 2300LT temperature and 2300LT specific humidity.

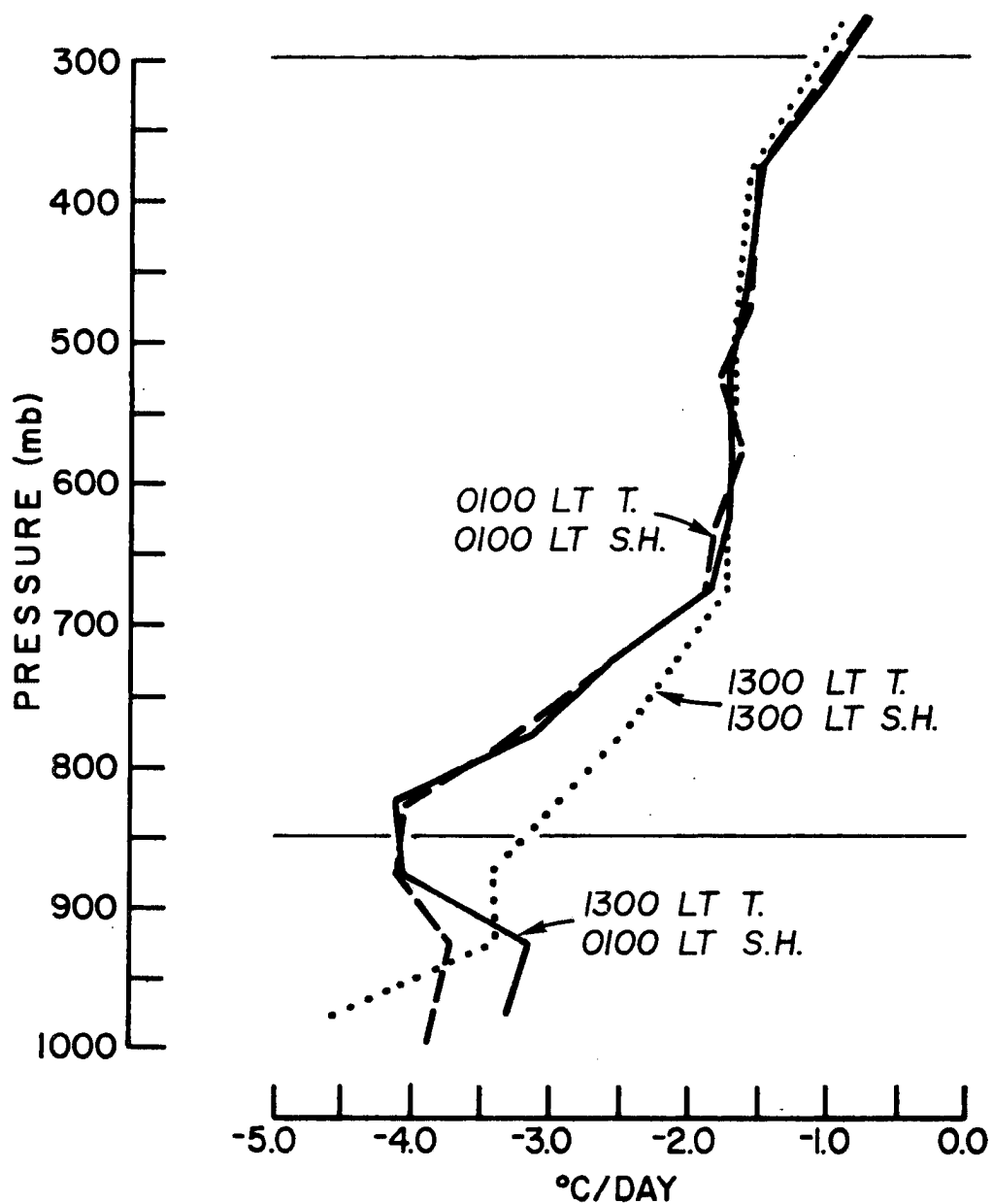


Fig. D.7. Variation in IR cooling at a subtropical location (Johnston Island) utilizing different input soundings. Mean IR cooling rate in the 850-300 mb layer was calculated to be $-1.96^{\circ}\text{C}/\text{day}$ with the 1300LT temperature and 0100LT specific humidity, $-1.84^{\circ}\text{C}/\text{day}$ with the 1300LT temperature and 1300 LT specific humidity, and $-2.02^{\circ}\text{C}/\text{day}$ with the 0100LT temperature and 0100LT specific humidity.

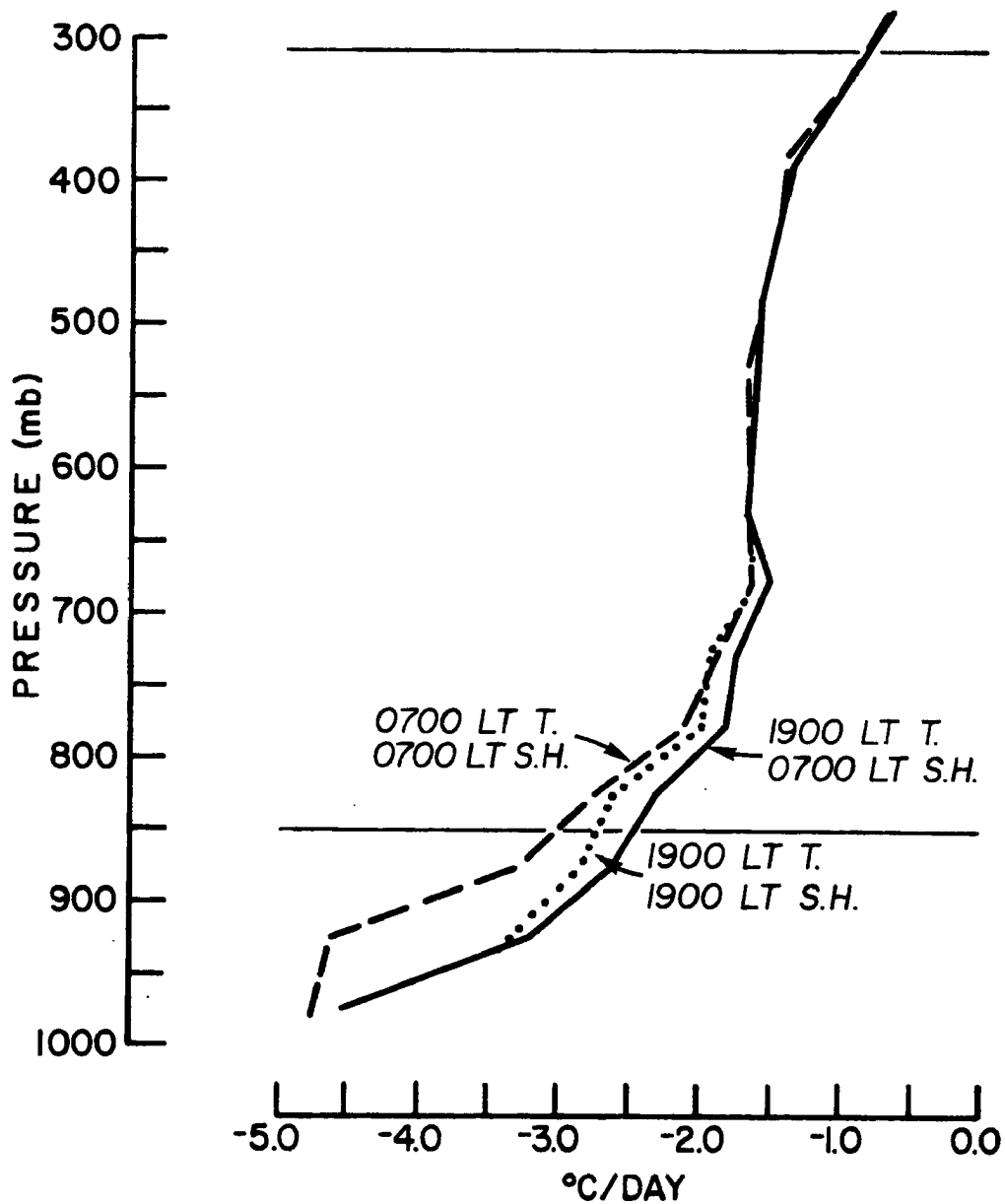


Fig. D.8. Variation in IR cooling at a mid-latitude coastal location (Washington, D.C.) utilizing different input soundings. Mean IR cooling rate in the 850-300 mb layer was calculated to be $-1.62^{\circ}\text{C/day}$ with 1900LT temperature and 0700LT specific humidity, $-1.72^{\circ}\text{C/day}$ with 0700LT temperature and 0700LT specific humidity, and $-1.67^{\circ}\text{C/day}$ with the 1900LT temperature and 1900LT specific humidity.

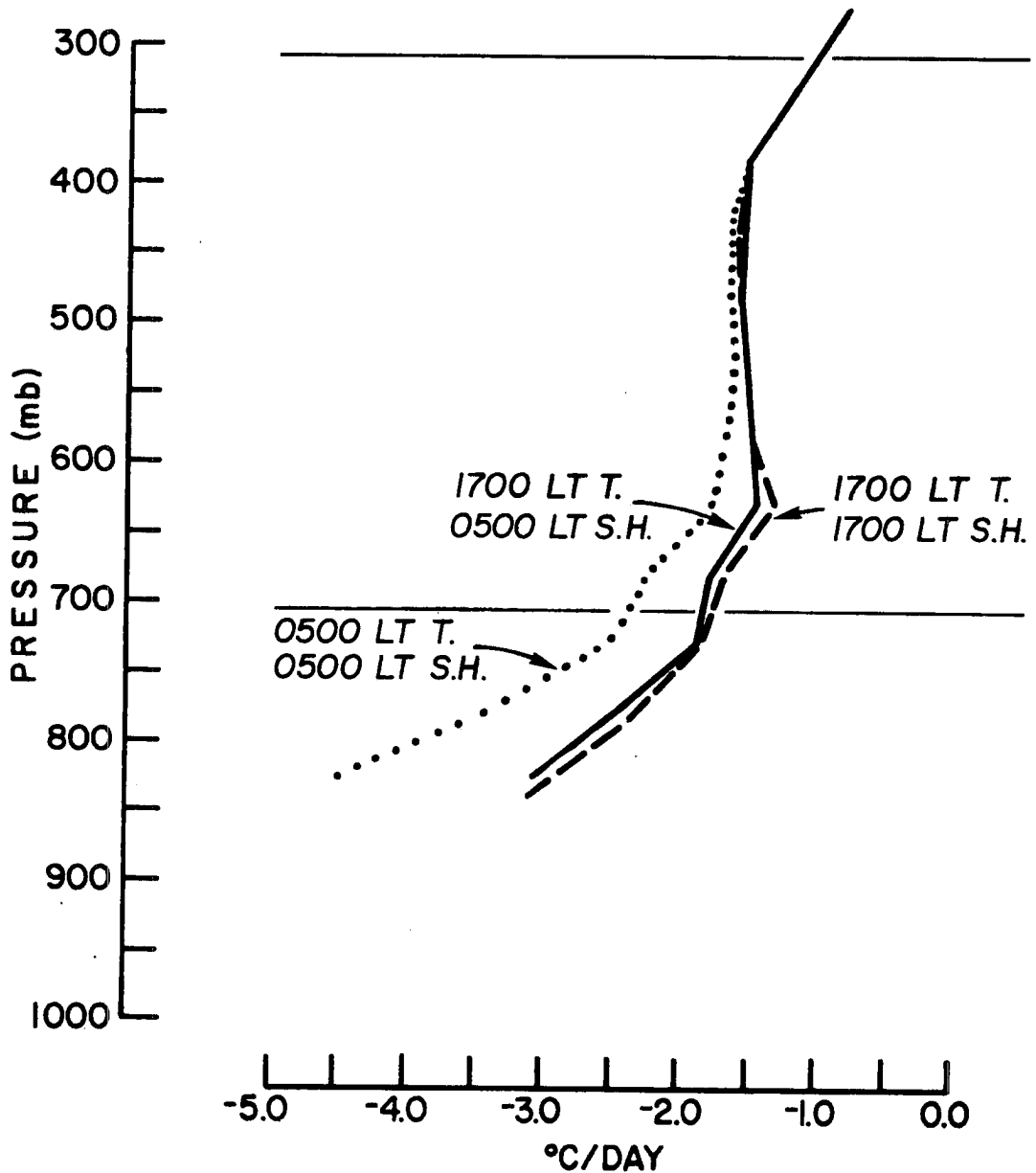


Fig. D.9. Variation in IR cooling at a mid-latitude elevated location (El Paso, Texas) utilizing different input soundings. Mean IR cooling rate in the 700-300 mb layer was calculated to be $-1.53^{\circ}\text{C}/\text{day}$ with 1700LT temperature and 0500LT specific humidity, $-1.50^{\circ}\text{C}/\text{day}$ with 1700LT temperature and 1700LT specific humidity, and $-1.69^{\circ}\text{C}/\text{day}$ with 0500LT temperature and 0500LT specific humidity.

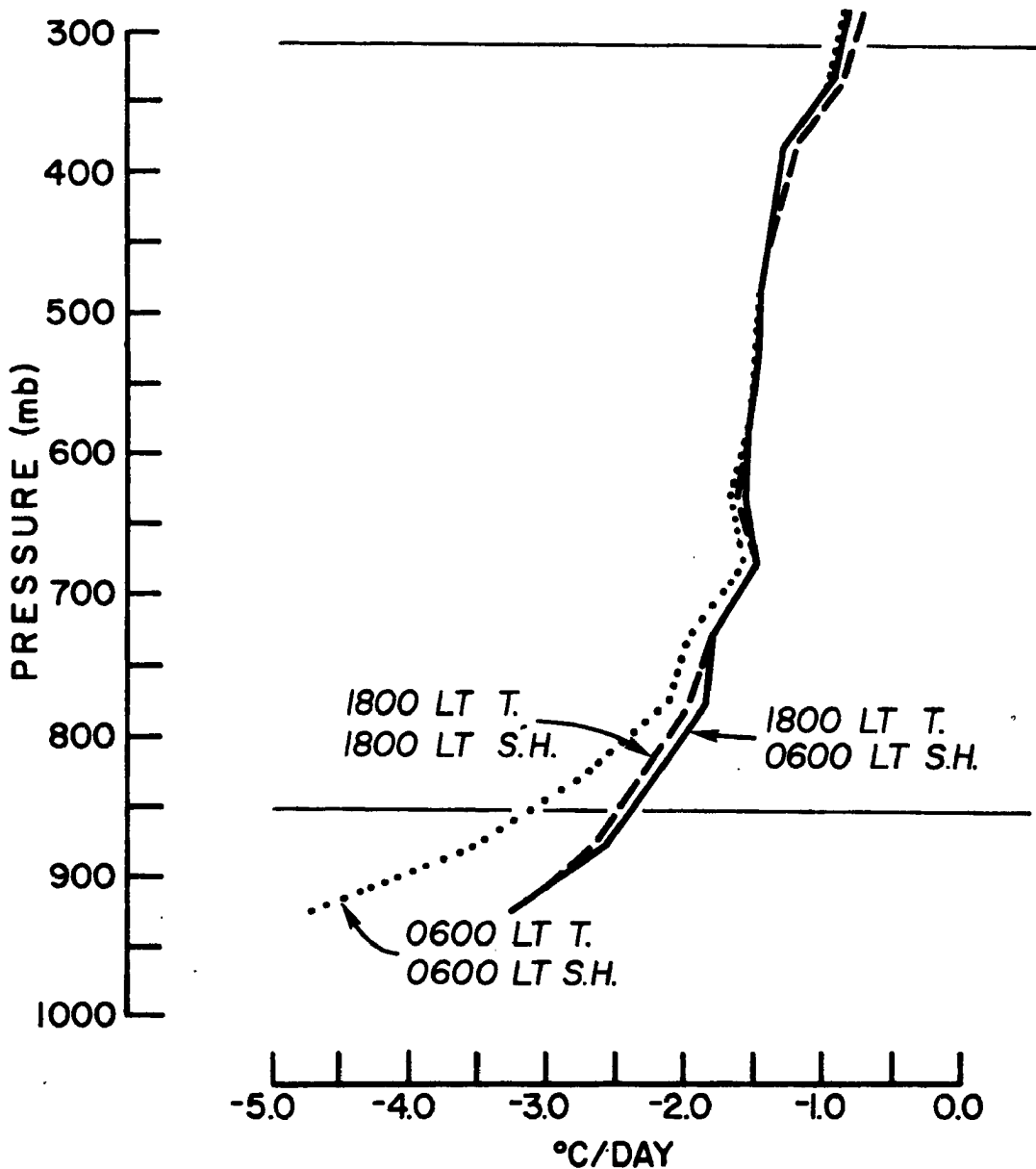


Fig D.10. Variation in IR cooling at a mid-latitude continental location (Peoria, Ill.) utilizing different input soundings. Mean IR cooling rate in the 850-300 mb was calculated to be $-1.58^{\circ}\text{C}/\text{day}$ with 1800LT temperature and 0600LT specific humidity, $-1.58^{\circ}\text{C}/\text{day}$ with 1800LT temperature and 1800 LT specific humidity, and $-1.68^{\circ}\text{C}/\text{day}$ with 0600LT temperature and 0600LT specific humidity.

APPENDIX BIBLIOGRAPHY

- Badgley, F. I., 1975: Response of Radiosonde Thermistors. The Rev. of Sci. Instruments,
- Brasefield, C. J., 1947: Measurement of air temperature in the presence of solar radiation. J. Meteor., 5, 147-151.
- Cox, S. K., J. A. Maynard, and V. E. Suomi, 1968: Radiosonde temperature baseline inaccuracy. J. Appl. Meteor., 7, 691-696.
- Cox, S. K., C. Polifka, A. Rockwood, and K. Griffith, 1976: Radiation transfer computational routines for atmospheric science applications. Atmos. Sci. Research Paper, Colo. State Univ., Ft. Collins, CO.
- Federal Meteorological Handbook No. 3: Radiosonde Observations, 1969, U.S. Gov't. Printing Office, Wash., D.C.
- Finger, F. G., M. F. Harris, and S. Teweles, 1965: Diurnal variation of wind, pressure, and temperature in the stratosphere. J. Appl. Meteor., 4, 632-635.
- Gruber, A., 1975: The diurnal variation of cloudiness over the GATE B area (outer hexagon). NOAA HESS, MSL Paper, 13 pp.
- Handbook of Geophysics and Space Environments, 1965, A. F. Cambridge Research Laboratories, McGraw Hill Book Co., Inc.
- Mastenbrook, H.J., 1968: Water vapor distribution in the stratosphere and high troposphere. J. Atmos. Sci., 25, 299-311.
- Mellick, A., 1976: Personal communication.
- Mügge, R., and F. Möller, 1932: Zur Berechnung von Strahlungsströmen und Temperaturänderungen in Atmosphären von Beliebigen Aufbau. Zeitschr. Geophysik, 8, 53-64.
- Staley, D. O. and G. M. Jurica, 1970; Flux emissivity tables for water vapor, carbon dioxide and ozone. J. Appl. Meteor., 9, 365-372.
- Winston, J., 1975: Personal communication with William M. Gray.

W. M. GRAY'S FEDERALLY SUPPORTED RESEARCH PROJECT REPORTS SINCE 1967

CSU Dept. of
Atmos. Sci.
Report No.

Report Title, Author, Date, Agency Support

104	The Mutual Variation of Wind, Shear, and Baroclinicity in the Cumulus Convective Atmosphere of the Hurricane (69pp). W. M. Gray. February 1967. NSF Support.
114	Global View of the Origin of Tropical Disturbances and Storms (105pp). W. M. Gray. October 1967. NSF Support.
116	A Statistical Study of the Frictional Wind Veering in the Planetary Boundary Layer (57pp). B. Mendenhall. December 1967. NSF and ESSA Support.
124	Investigation of the Importance of Cumulus Convection and Ventilation in Early Tropical Storm Development (88pp). R. Lopez. June 1968. ESSA Satellite Lab. Support.
Unnumbered	Role of Angular Momentum Transports in Tropical Storm Dissipation over Tropical Oceans (46pp). R. F. Wachtmann. December 1968. NSF and ESSA Support.
Unnumbered	Monthly Climatological Wind Fields Associated with Tropical Storm Genesis in the West Indies (34pp). J. W. Sartor. December 1968. NSF Support.
140	Characteristics of the Tornado Environment as Deduced from Proximity Soundings (55pp). T. G. Wills. June 1969. NOAA and NSF Support.
161	Statistical Analysis of Trade Wind Cloud Clusters of the Western North Pacific (80pp). K. Williams. June 1970. ESSA Satellite Lab. Support.
---	A Climatology of Tropical Cyclones and Disturbances of the Western Pacific with a Suggested Theory for Their Genesis/Maintenance. W. M. Gray. NAVWEARSCHFAC Technical Paper No. 19-70 (225pp). November 1970. (Available from U.S. Navy, Monterey, CA). U.S. Navy Support.
179	A Diagnostic Study of the Planetary Boundary Layer over the Oceans (95pp). W. M. Gray. February 1972. Navy and NSF Support.
182	The Structure and Dynamics of the Hurricane's Inner Core Area (105pp). D. J. Shea. April 1972. NOAA and NSF Support.
188	Cumulus Convection and Larger-Scale Circulation, Part I: A Parametric Model of Cumulus Convection (100pp). R. E. Lopez. June 1972. NSF Support.

CSU Dept. of
Atmos. Sci.
Report No.

Report Title, Author, Date, Agency Support

- 189 Cumulus Convection and Larger-Scale Circulations, Part II: Cumulus and Meso-Scale Interactions (63pp). R. E. Lopez. June 1972. NSF Support.
- 190 Cumulus Convection and Larger-Scale Circulations, Part III: Broad-scale and Meso-Scale Considerations (80pp). W. M. Gray. July 1972. NOAA-NESS.
- 195 Characteristics of Carbon Black Dust as a Tropospheric Heat Source for Weather Modification (55pp). W. M. Frank. January 1973. NSF Support.
- 196 Feasibility of Beneficial Hurricane Modification by Carbon Black Seeding (130pp). W. M. Gray. April 1973. NOAA Support.
- 199 Variability of Planetary Boundary Layer Winds (157pp). L. R. Hoxit. May 1973. NSF Support.
- 200 Hurricane Spawned Tornadoes (57pp). D. J. Novlan. May 1973. NOAA and NSF Support.
- 212 A Study of Tornado Proximity Data and an Observationally Derived Model of Tornado Genesis (101pp). R. Maddox. November 1973. NOAA Support.
- 219 Analysis of Satellite Observed Tropical Cloud Clusters (91 pp). E. Ruprecht and W. M. Gray. May 1974. NOAA-NESS Support.
- 224 Precipitation Characteristics in the Northeast Brazil Dry Region (56pp). R. P. L. Ramos. May 1974. NSF Support.
- 225 Weather Modification through Carbon Dust Absorption of Solar Energy (190pp). W. M. Gray, W. M. Frank, M. L. Corrin, and C. A. Stokes. July 1974.
- 234 Tropical Cyclone Genesis (121pp). W. M. Gray. March 1975. NSF Support.
- Tropical Cyclone Genesis in the Western North Pacific (66pp). W. M. Gray. March 1975. U.S. Navy Environmental Prediction Research Facility Report. Technical Paper No. 16-75. (Available from the U.S. Navy, Monterey, CA). Navy Support.
- 241 Tropical cyclone Motion and Surrounding Parameter Relationships (105pp). J. E. George. December 1975. NOAA Support.

CSU Dept. of
Atmos. Sci.
Report No.

Report Title, Author, Date, Agency Support

- 243 Diurnal Variation of Oceanic Deep Cumulus Convection.
Paper I: Observational Evidence, Paper II: Physical
Hypothesis (106pp). R. W. Jacobson, Jr. and W. M. Gray.
February, 1976. NOAA NESS Support.
- 257 Data Summary of NOAA's Hurricane Inner-Core Radial Leg
Flight Penetrations 1957-1967, and 1969 (245pp). W. M.
Gray and D. J. Shea. October, 1976. NSF and NOAA Support.
- 258 The Structure and Energetics of the Tropical Cyclone
(180 pp). W. M. Frank. October, 1976. NOAA (NHEML),
NOAA (NESS) and NSF Support.
- 259 Typhoon Genesis and Pre-typhoon Cloud Clusters (79pp).
R. M. Zehr. November, 1976.
- Unnumbered Severe Thunderstorm Wind Gusts (81pp). G. W. Walters.
December, 1976. NSF Support.

BIBLIOGRAPHIC DATA SHEET	1. Report No. CSU-ATSP-262	2.	3. Recipient's Accession No.
4. Title and Subtitle Diurnal Variation of the Tropospheric Energy Budget		5. Report Date November, 1976	6.
7. Author(s) Gary S. Foltz (P.I. William M. Gray)		8. Performing Organization Rep. No. CSU-ATSP-262	
9. Performing Organization Name and Address Atmospheric Science Department Colorado State University Fort Collins, CO 80523		10. Project/Task/Work Unit No.	11. Contract/Grant No. OCD-75-01424
12. Sponsoring Organization Name and Address National Science Foundation Washington, D.C. 20550		13. Type of Report & Period Covered Project Report	
15. Supplementary Notes		14.	
16. Abstracts The tropospheric energy balance is examined in an effort to ascertain the diurnal variation of its components. The mean local diurnal temperature change in the 850-300 mb layer was observationally determined utilizing upper air data collected at 142 Northern Hemisphere radiosonde stations. Temperature data from GATE, ATEX, BOMEX and LIE Experiments, and Operations Redwing and Hardtack in the Tropical West Pacific were also analyzed. Diurnal radiative cooling values are computed for specific geographical regions and the magnitude of the required diurnal warming for each region is determined. A large morning maximum and late afternoon-early evening minimum of tropospheric required warming is found in all the data sets. This is hypothesized to result from enhanced morning subsidence produced by larger nocturnal radiational cooling.			
17. Key Words and Document Analysis. 17a. Descriptors Tropospheric Energy Balance Diurnal Variation			
17b. Identifiers/Open-Ended Terms			
17c. COSATI Field/Group			
18. Availability Statement		19. Security Class (This Report) UNCLASSIFIED	21. No. of Pages 140
		20. Security Class (This Page) UNCLASSIFIED	22. Price